

# **Simulation studies of plasma wakefield acceleration**

A thesis submitted to the University of Manchester for the degree of  
Doctor of Philosophy  
in the Faculty of Science and Engineering

2017

Kieran Hanahoe

School of Physics and Astronomy

# Contents

<b>List of figures</b>	<b>6</b>
<b>List of tables</b>	<b>9</b>
<b>Abstract</b>	<b>10</b>
<b>Declaration</b>	<b>11</b>
<b>Copyright</b>	<b>12</b>
<b>Acknowledgements</b>	<b>14</b>
<b>List of symbols</b>	<b>15</b>
<b>1 Introduction and motivation</b>	<b>17</b>
1.1 Background . . . . .	19
1.2 Advanced RF accelerators . . . . .	21
1.3 Laser plasma accelerators . . . . .	25
1.3.1 Laser acceleration of ions . . . . .	29
1.4 Beam-driven plasma wakefield accelerator . . . . .	30
1.4.1 Proton beam driver . . . . .	33

1.5	Motivation . . . . .	36
1.6	Outline . . . . .	37
<b>2</b>	<b>Physics of plasma wakefield acceleration</b>	<b>40</b>
2.1	Properties of a plasma . . . . .	41
2.1.1	Plasma frequency . . . . .	42
2.1.2	Debye length . . . . .	45
2.2	Mechanism of plasma wakefield acceleration . . . . .	48
2.3	Linear theory of plasma wakefield acceleration . . . . .	51
2.3.1	Transformer ratio . . . . .	63
2.4	Ponderomotive force . . . . .	66
2.5	Nonlinear regime . . . . .	67
2.6	Summary . . . . .	69
<b>3</b>	<b>Particle-in-cell simulation of plasma wakefield acceleration</b>	<b>70</b>
3.1	Why carry out simulations? . . . . .	70
3.2	Particle-in-cell simulation . . . . .	71
3.2.1	Dimensionality . . . . .	74
3.2.2	Instabilities . . . . .	76
3.3	PIC simulations using VSim . . . . .	77
3.4	Summary . . . . .	80
<b>4</b>	<b>Beam-driven plasma wakefield acceleration</b>	<b>82</b>
4.1	The CLARA accelerator . . . . .	82
4.2	Plasma sources . . . . .	85

4.2.1	Alkali metal vapour source . . . . .	85
4.2.2	Gas jet source . . . . .	88
4.2.3	Discharge source . . . . .	89
4.3	PWFA with a single bunch . . . . .	90
4.3.1	CLARA Front End . . . . .	92
4.4	PWFA with two Gaussian bunches . . . . .	98
4.5	Shaped bunches . . . . .	101
4.5.1	Longitudinally shaped drive bunch . . . . .	102
4.5.2	Longitudinally shaped witness bunch . . . . .	107
4.6	Summary . . . . .	110
<b>5</b>	<b>Study of plasma lens effect</b>	<b>112</b>
5.1	Focusing in particle accelerators . . . . .	112
5.2	Plasma focusing . . . . .	116
5.2.1	Active and passive plasma lens . . . . .	116
5.2.2	Mechanism of passive plasma focusing . . . . .	120
5.3	Aberrations . . . . .	123
5.4	Plasma focusing with VELA . . . . .	126
5.4.1	Emittance growth . . . . .	129
5.5	Simulation results . . . . .	133
5.5.1	Plasma density . . . . .	135
5.5.2	Plasma length . . . . .	137
5.5.3	Plasma lens experimental setup . . . . .	141
5.6	Summary . . . . .	143

<b>6 Study of plasma beam dump</b>	<b>144</b>
6.1 Challenges in high-energy beam dumps . . . . .	144
6.1.1 Noble gas beam dump . . . . .	146
6.2 Plasma beam dump . . . . .	147
6.2.1 Plasma and conventional beam dump compared .	151
6.3 Varying plasma density . . . . .	154
6.3.1 Energy recovery from a plasma beam dump . .	160
6.4 Simulation results . . . . .	161
6.5 Summary . . . . .	168
<b>7 Conclusion</b>	<b>171</b>
<b>A Parameters for simulations presented in this thesis</b>	<b>175</b>
<b>List of publications</b>	<b>177</b>
<b>Bibliography</b>	<b>180</b>

# List of Figures

1.1	Kilpatrick breakdown limit . . . . .	22
2.1	Diagram showing plasma oscillations . . . . .	44
2.2	Diagram of mechanism of PWFA . . . . .	50
2.3	Plasma response to a point charge . . . . .	57
3.1	Flowchart showing particle-in-cell simulation scheme . . .	73
4.1	CLARA/PARS layout . . . . .	83
4.2	Tunnelling ionization rate for Li and Rb . . . . .	87
4.3	Electric field and plasma density response to CLARA beam	92
4.4	Longitudinal phase space for CLARA-FE bunch at different initial energies . . . . .	94
4.5	Dependence of average gradient on initial beam energy for CLARA-FE . . . . .	95
4.6	Longitudinal phase space for realistic CLARA-FE bunch	96
4.7	CLARA-FE field and bunch from 3D simulation . . . .	97
4.8	Electric field and bunch density for realistic CLARA-FE bunch . . . . .	98
4.9	Effect of degree of beam loading on witness bunch energy	100

4.10	Effect of degree of beam loading on longitudinal electric field . . . . .	101
4.11	Pseudocolour plot of wakefields for Gaussian drive and witness bunches . . . . .	101
4.12	Longitudinal electric field for ramped drive bunches . . . . .	105
4.13	Drive and witness bunch longitudinal phase space for ramped drive bunch . . . . .	106
4.14	Longitudinal electric field for ramped witness bunch . . . . .	110
5.1	Geometry of particle focusing . . . . .	115
5.2	Azimuthal magnetic field of a Gaussian bunch . . . . .	123
5.3	Diagram of effect of longitudinal aberration . . . . .	127
5.4	Test particle phase space showing spherical aberration . . . . .	130
5.5	Emittance growth due to longitudinal aberration . . . . .	132
5.6	Particle tracking phase space showing longitudinal aberration . . . . .	133
5.7	VELA phase space before and after plasma focusing . . . . .	134
5.8	Pseudocolour plot of plasma focusing fields . . . . .	135
5.9	Effect of plasma density on emittance and focusing strength	136
5.10	CLARA-FE bunch size variation due to plasma focusing	137
5.11	Bunch rms size evolution for different plasma lengths . . . . .	138
5.12	Variation of focal length with plasma length . . . . .	139
5.13	Variation of emittance growth with plasma length . . . . .	140
5.14	Diagram of VELA plasma experiment setup . . . . .	142
6.1	Diagram of noble gas beam dump . . . . .	148

6.2	Diagram of defocusing due to plasma density change . . .	155
6.3	Stepped and gradient plasma density profiles . . . . .	157
6.4	Re-acceleration length for different plasma density profiles	159
6.5	Energy loss for different plasma density profiles . . . .	163
6.6	Fields and plasma density in a plasma beam dump . . .	165
6.7	Longitudinal phase space comparison between uniform and gradient plasma density profiles . . . . . . . . . . .	166
6.8	Transverse phase space comparison between uniform and gradient plasma density profiles . . . . . . . . . . .	166
6.9	Evolution of longitudinal phase space for linear gradient plasma . . . . . . . . . . . . . . . . . . . . . . .	167
6.10	Re-accelerated charge for different plasma density profiles	167
6.11	Energy spectrum change for linear plasma density profile	168

# List of Tables

1	List of constants . . . . .	15
2	List of variables . . . . .	16
1.1	Common RF frequencies and band designations . . . . .	23
1.2	Summary of plasma wakefield experiments . . . . .	36
4.1	CLARA beam modes and parameters . . . . .	84
5.1	VELA and CLARA-FE bunch parameters . . . . .	128
6.1	Decelerating gradients for different plasma density profiles	164
A.1	Simulation parameters . . . . .	176

# Abstract

Plasma-based accelerators offer the potential to achieve accelerating gradients orders of magnitude higher than are typical in conventional accelerators. A Plasma Accelerator Research Station has been proposed using the CLARA accelerator at Daresbury Laboratory. In this thesis, theory and the results of particle-in-cell simulations are presented investigating experiments that could be conducted using CLARA as well as the preceding VELA and CLARA Front End.

Plasma wakefield acceleration was found to be viable with both CLARA and CLARA Front End, with accelerating gradients of  $\text{GV m}^{-1}$  and  $100 \text{ MV m}^{-1}$  scale respectively. Drive-witness and tailored bunch structures based on the CLARA bunch were also investigated. Plasma focusing of the VELA and CLARA Front End bunches was studied in simulations, showing that substantial focusing gradient could be achieved using a passive plasma lens.

A plasma beam dump scheme using varying plasma density is also presented. This scheme allows the performance of a passive plasma beam dump to be maintained as the bunch is decelerated and has some advantages over a previously proposed method.

# **Declaration**

No portion of the work referred to in this thesis has been submitted in support of an application for another degree or qualification of this or any other university or other institute of learning.

# Copyright

The author of this thesis (including any appendices and/or schedules to this thesis) owns certain copyright or related rights in it (the “Copyright”) and s/he has given The University of Manchester certain rights to use such Copyright, including for administrative purposes.

Copies of this thesis, either in full or in extracts and whether in hard or electronic copy, may be made only in accordance with the Copyright, Designs and Patents Act 1988 (as amended) and regulations issued under it or, where appropriate, in accordance with licensing agreements which the University has from time to time. This page must form part of any such copies made.

The ownership of certain Copyright, patents, designs, trademarks and other intellectual property (the “Intellectual Property”) and any reproductions of copyright works in the thesis, for example graphs and tables (“Reproductions”), which may be described in this thesis, may not be owned by the author and may be owned by third parties. Such Intellectual Property and Reproductions cannot and must not be made available for use without the prior written permission of the owner(s) of the relevant Intellectual Property and/or Reproductions.

Further information on the conditions under which disclosure, publication and commercialisation of this thesis, the Copyright and any Intellectual Property and/or Reproductions described in it may take place is available in the University IP Policy (see <http://documents.manchester.ac.uk/DocuInfo.aspx?DocID=24420>), in any relevant Thesis restriction declarations deposited in the University Library, The University Library's regulations (see <http://www.library.manchester.ac.uk/about/regulations/>) and in The University's policy on Presentation of Theses.

# Acknowledgements

Thanks to my supervisor Guoxing Xia for his support and advice.

Thanks also to colleagues at the University of Manchester and the Cockcroft Institute especially Oznur Mete-Apsimon, Yangmei Li and Yelong Wei for their friendship and many useful discussions. I also owe thanks also to colleagues from the University of Strathclyde and DESY with whom we collaborated on the VELA experiment. Although the results weren't altogether successful I learned a lot about the experimental side of the field.

My gratitude also to Jonathan Smith from Tech-X UK ltd for helping me get started using VSim, getting the software working on remote machines and showing a great deal of patience as I bombarded him with e-mails when things didn't work as I expected.

I gratefully acknowledge the computing time granted as part of projects HHH20 and HHH36 on the supercomputers JUROPA and JURECA at Jülich Supercomputing Centre (JSC).

# List of symbols

Table 1: List of constants

Symbol	Quantity	Value	Unit
$k_B$	Boltzmann constant	$1.380 \times 10^{-23}$	$\text{J K}^{-1}$
$e$	Elementary charge	$1.602 \times 10^{-19}$	C
$m_e$	Electron mass	$9.109 \times 10^{-34}$	kg
$m_e c^2$	Electron mass-energy	0.511	MeV
e	Exponential constant	$\approx 2.718$	–
$\alpha$	Fine-structure constant	$\approx 1/137$	–
$\mu_0$	Permeability of free space	$4\pi \times 10^{-7}$	$\text{H m}^{-1}$
$\varepsilon_0$	Permittivity of free space	$8.854 \times 10^{-12}$	$\text{F m}^{-1}$
$\hbar$	Reduced Planck constant	$1.055 \times 10^{-34}$	J s
$c$	Speed of light in a vacuum	299 792 458	$\text{m s}^{-1}$

Table 2: List of variables

Symbol	Quantity	Unit
$q$	Electric charge	C
$Q$	Total electric charge	C
$\rho$	Charge density	$\text{C m}^{-3}$
$I$	Electric current	A
$j$	Current density	$\text{A m}^{-2}$
$E$	Electric field	$\text{V m}^{-1}$
$n_e$	Electron number density	$\text{m}^{-3}$
$\phi$	Electric scalar potential	V
$B$	Magnetic field	T
$A$	Magnetic vector potential	$\text{T m}$
$N$	Particle population	—
$n_0$	Background plasma density	$\text{m}^{-3}$
$n_1$	Perturbed plasma density	$\text{m}^{-3}$
$\lambda_D$	Debye length	m
$\omega_p$	(Electron) plasma frequency	$\text{rad s}^{-1}$
$\lambda_p$	Plasma wavelength	m
$k_p$	Plasma wavenumber	$\text{rad m}^{-1}$
$\gamma$	Lorentz factor	—
$\beta$	Relativistic $\beta = v/c$	—
$T$	Kinetic energy	J
$T$	Temperature	K
$A$	Relative atomic mass	—
$Z$	Atomic number	—

# Chapter 1

## Introduction and motivation

Plasma accelerators offer the potential to achieve orders-of-magnitude improvements in performance compared to conventional accelerators. However, the increased performance of plasma accelerators is accompanied by new challenges in achieving high beam quality, efficiency and consistency. Continued experimental tests of plasma wakefield acceleration are necessary to develop techniques to make plasma acceleration a viable tool in applied accelerators.

When considering experiments in plasma acceleration, simulations are a very important method of testing concepts both in a shorter timescale and at lower cost than a full experiment. Simulation results can be used to validate ideas prior to carrying out experiments. The purpose of the simulations presented in this thesis was to demonstrate the viability of plasma wakefield experiments using the accelerators at Daresbury Laboratory. The aim of experiments at Daresbury would be to develop experience in plasma wakefield acceleration, study in detail previously

demonstrated concepts, achieve experimental results for concepts that have only been studied by simulation, and to test new concepts developed in theory and simulations.

Studies of plasma wakefield acceleration, using beam parameters for the planned CLARA Front End and CLARA accelerators at Daresbury Laboratory, demonstrated the suitability of the accelerators for plasma accelerator research. The potential for acceleration of a separate witness bunch using CLARA was investigated. Modified CLARA beam parameters were used to study tailored bunch profiles in order to achieve improved performance. Two-dimensional particle-in-cell simulations of a linearly ramped bunch profile in the linear regime showed that such a scheme could achieve a marked increase in witness bunch energy and acceleration over extended lengths compared to a symmetrical bunch distribution.

Plasma focusing, and the emittance growth that results from aberrations in a plasma lens, were studied by particle tracking and particle-in-cell simulation. The effect of plasma density and length was studied in detail for an electron bunch representative of those produced by the VELA accelerator at Daresbury Laboratory. Particle tracking was used to study the effect on emittance growth of plasma density over a large density range.

Following on from studies of beam-driven plasma acceleration, a passive plasma beam dump was modelled using particle-in-cell simulation. The passive plasma beam dump was found to be able to achieve a high initial decelerating gradient while having a density orders of magnitude

smaller than that of a conventional beam dump. A new method of addressing a major limitation of the passive plasma beam dump, the reacceleration of a portion of the beam after it has been decelerated to non-highly-relativistic velocity, by modifying the beam dump plasma density was validated. This would allow for an extended length plasma beam dump to be constructed without resorting to the use of conventional materials, as has been previously proposed.

## 1.1 Background

Over the past century, particle accelerators have been developed from electrostatic devices operating over a few hundred volts to a few giant energy frontier machines, hundreds of light sources and other research accelerators and many thousands of accelerators for industrial, medical and security applications. The wide range of applications for accelerators makes the development of new technologies a matter of great importance.

The two main external limits on accelerator performance are size and energy consumption, both of which are ultimately determined by cost. Although one-off particle physics machines may be huge and consume large amounts of energy, accelerators for industrial and medical applications must be economical to construct and operate. The performance that an accelerator can achieve given these limiting factors is determined by the technology that it employs. The earliest particle accelerators were electrostatic devices, accelerating particles linearly through a potential difference of up to a few tens of megavolts. The limitation of these ac-

celerators was initially the voltages that could be generated by van der Graaff generators. The need to isolate these high voltages from earth meant that as voltages increased the size of the accelerators also had to increase. One of the largest electrostatic accelerators was the Nuclear Structure Facility at Daresbury Laboratory, housed in a 70 m high tower [1].

A reduction in the size of accelerators was possible using radiofrequency (RF) acceleration. Instead of a single stage of a very large voltage drop, a smaller voltage is used repeatedly by synchronizing the accelerated particles with an oscillating electric field in an RF cavity. A circular RF accelerator is capable of passing a particle bunch through an accelerating voltage an arbitrary number of times, however there are still limits on the energy that can be achieved. In the case of an electron accelerator the limit is a result of synchrotron radiation: as the electron's trajectory is bent into a circular path it emits radiation and loses energy. At some point the radiated energy matches the energy supplied by the RF cavities and acceleration ceases. Although more energy can be supplied by increasing the RF power, the operating cost limits the maximum energy that can be maintained. The synchrotron radiation power  $P$  is given by the following formula [2]:

$$P = \frac{2}{3}\alpha\hbar c^2 \frac{\gamma^4}{\rho^2} \quad (1.1)$$

where  $\hbar$  is the reduced Planck's constant,  $\alpha$  is the fine structure constant and  $\rho$  is the bending radius. The dependence on the fourth power of  $\gamma$

means that for an electron/positron beam of the same energy as a proton beam, the radiated power is higher by a factor of  $10^{13}$ . One solution for a circular lepton accelerator is to increase the radius, but increasing size leads to increased construction costs. Another option is to use muons in place of electrons: the mass of the muon is 207 times that of the electron, so radiation losses are greatly reduced. As the muons are produced with high emittance it is necessary to cool them to achieve required luminosity, a significant challenge [3]. Bending losses in an electron accelerator can be eliminated by accelerating in a straight line, but this introduces a new limiting factor: accelerating gradient.

## 1.2 Advanced RF accelerators

Future linear accelerators need to achieve the highest possible accelerating gradient in order to minimize the length and hence construction cost of the accelerator, as well as the difficulty of finding a suitable location. The major limit on accelerating gradient in conventional metallic RF accelerators is the breakdown of the structure under large electric fields. Although breakdown of metallic structures is not perfectly understood, the semi-empirical Kilpatrick criterion indicates that the breakdown voltage  $E$  is proportional to the square root of the applied frequency  $f$ . The Kilpatrick criterion based on data from a number of structures, is given in Equation 1.2 [4]. Figure 1.1 shows a plot of the variation of the Kilpatrick limit on electric field as with frequency.

$$Ee^{-4.25/E} = 24.4 [f \text{ (GHz)}]^{(\frac{1}{2})} \text{ MV m}^{-1} \quad (1.2)$$

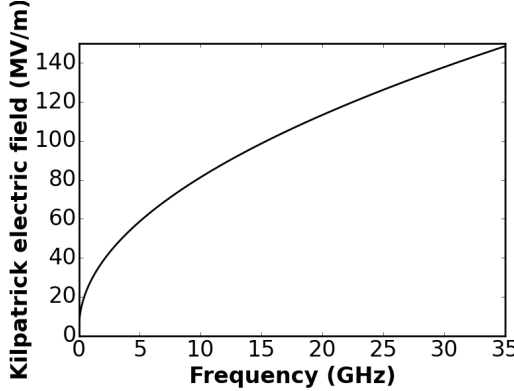


Figure 1.1: Plot of Kilpatrick criterion for breakdown electric field against frequency.

Hence, a method to achieve higher accelerating gradients in RF structures is to increase the frequency at which they operate. Frequencies are often referred to using the IEEE standard letters for radio-frequency bands, given in Table 1.1 [5]. The S-band has historically been a commonly used frequency for linear accelerators, such as the Stanford Linear Collider (SLC) at Stanford Linear Accelerator Center (SLAC) [6]. The SLC produced 50 GeV electron and positron beams over a total length including beam transport to the interaction region of approximately 4 km, with a main linear accelerator length of 2946 m and an accelerating gradient of  $20 \text{ MV m}^{-1}$ . This compares with the Kilpatrick limit for S-band of  $45 \text{ MV m}^{-1}$ . In practice RF accelerators operate with a field amplitude below the Kilpatrick limit, and with bunches sitting off the crest of the wave for stability reasons.

Table 1.1: IEEE standard designations for radio frequency bands, and the actual frequencies for each band that devices have been standardized at in Europe, and America.

Band	Frequency (GHz)	Europe (MHz)	America (MHz)
L	1-2	1300	1300
S	2-4	2998	2856
C	4-8	5996	5721
X	8-12	11992	11424
Ku	12-18	-	-
K	18-27	-	-
Ka	27-40	-	-
V	40-75	-	-
W	75-110	-	-

Two designs for future energy-frontier linear colliders are in an advanced state of preparation. The Compact Linear Collider (CLIC) is a novel, normal conducting, X-band design, while the International Linear Collider (ILC) is a more conventional, superconducting design operating in the L-band. Both ILC and CLIC have similar design goals: to achieve at least 500 GeV centre-of-mass energy and sufficiently high luminosity to study the Higgs boson in detail, to search for extended Higgs states and to make precision measurements of the properties of other fundamental particles [7, 8]. The planned accelerating gradient for the ILC is  $30 \text{ MV m}^{-1}$ , 50% higher than that of the Stanford Linear Accelerator. As a result of its relatively low gradient, ILC will be upwards of 30 km long for a centre-of-mass energy of 500 GeV. A technical design report for the ILC was published in 2010 [9]. CLIC is a novel normal-conducting accelerator design based on a two-beam design. A high current, low energy beam is accelerated and bunched and is used to drive electric fields

in RF cavities to accelerate lower charge bunches at high gradients. The operating principle is similar to a klystron. The accelerating gradient is considerably higher than the ILC, at  $100 \text{ MV m}^{-1}$ , and the technology is in principle capable of achieving gradients of greater than  $150 \text{ MV m}^{-1}$  [8].

In contrast to ILC and CLIC, which make use of similar technology to previous RF linacs, millimetre-wave accelerators operate at much higher frequencies and consequently are very different in design to previous machines. Millimetre-wave accelerators are expected to be capable of accelerating gradients in excess of  $100 \text{ MV m}^{-1}$ . A planar millimetre-wave accelerator was demonstrated in 2001 [10]. The structure consisted of parallel copper plates holding an alumina dielectric structure, with the beam propagating in the gap between the dielectric. The device was driven by a 300 MeV electron beam and operated in the W-band at 91.392 GHz, corresponding to a wavelength of 3.3 mm. It achieved an accelerating gradient of  $20 \text{ MeV m}^{-1}$  with no sign of breakdown occurring. Recently, a millimetre-wave structure consisting of grooved copper plates driven by a 65 MeV electron beam demonstrated an accelerating gradient of  $85 \text{ MeV m}^{-1}$  and an RF power of 4.8 MW, again operating in the W-band [11].

Although advances in RF accelerator technology can significantly increase the achievable gradient, to reach order-of-magnitude improvements the fundamental limit of metallic structures needs to be overcome. This is the breakdown of the structure under large electric fields. When breakdown occurs the structure is separated into its component elec-

trons and ions. A material consisting of free electrons and ions may be described as a plasma, depending on certain parameters. The controlled use of plasmas in accelerators escapes the breakdown limit as a plasma can support huge electric fields. Although the atomic species forming a plasma may be singly or multiply ionized after initial ionization has occurred, further breakdown is not possible as the plasma responds to electric fields in such a way as to neutralize them. Plasma accelerators can also be compared to conventional accelerators in the frequency at which they operate. Typical plasma wavelengths are  $\sim 0.5$  mm, corresponding to a frequency of 600 GHz. This frequency is much higher than that seen in conventional RF accelerators, though such frequencies are approached in millimetre wave accelerators.

### 1.3 Laser plasma accelerators

Early consideration of particle acceleration in a plasma medium resulted from attempts to explain the production of high energy cosmic rays, either in interstellar space [12] or within the solar system [13]. In 1979, Tajima and Dawson first proposed an accelerator based on a relativistic plasma wave driven by an intense laser pulse [14]. The excitation of the plasma wave is due to the ponderomotive force acting on the plasma electrons. This force is a result of the rapidly oscillating, non-uniform field of the laser pulse envelope. A time-averaged force acts on the plasma electrons and causes them to move in the direction of lower laser field amplitude, expelling them from the axis of the beam. Simulations showed

that a sufficiently high-intensity laser could generate unprecedented accelerating gradients. However, at the time, lasers with a sufficiently short pulse length were not available. It was noted that there was a way around this problem: the laser beat-wave accelerator. This operates by using two long-pulse lasers with frequencies differing by  $\omega_p$  which interfere generating a train of pulses with beat frequency equal to  $\omega_p$ . This train of pulses is able to resonantly drive a plasma wakefield.

Laser technology advanced dramatically in the late 1980s with the development of chirped-pulse amplification (CPA) allowing intensities five orders of magnitude higher than could previously be achieved [15]. An accelerating gradient of  $30 \text{ GeV m}^{-1}$  was demonstrated in 1995, using a 3 TW laser with a pulse length of 1 ps [16]. Also in 1995, the Vulcan laser at Rutherford Appleton Laboratory (RAL) demonstrated acceleration of electrons to a maximum of 44 MeV with a gradient of up to  $100 \text{ GV m}^{-1}$ . The laser used had a peak power of 25 TW and a pulse length of 0.8 ps [17]. These two experiments generated electrons with a range of energies from a few MeV up to the maximum reported. Such broad energy spectrum bunches would be of limited use in many of the common applications of accelerators. In 2004, the first experiments demonstrated the generation of quasi-monoenergetic electron beams from laser-plasma interactions. Using the Astra laser at RAL with a pulse length of 40 fs ( $12 \mu\text{m}$ ) an electron bunch with an energy spread of 3% could be generated. Due to variations in laser parameters, the central energy of the accelerated electrons varied by 30% [18]. The bunch charge reported was 22 pC. The low energy spread was made possible by the laser pulse

length being shorter than the plasma wavelength, while the plasma density remained high enough to achieve high accelerating gradients. Similar results were reported using a plasma channel to guide the laser pulse [19], and producing a quasi-monoenergetic bunch with a very high charge of 0.5 nC [20]. A major future laser wakefield accelerator experiment proposal is EuPRAXIA [21], which aims to demonstrate high-quality beam generation from laser wakefield acceleration of electrons, targeting energies of up to 5 GeV with energy spread of 1%. EuPRAXIA is currently in the early stages of planning.

The stability of laser wakefield accelerators has been a significant limitation on their practical application: it is difficult to use an accelerator if it is not known in advance what the properties of the beam will be. Shot-to-shot instability can be caused by instability of the laser pulse and amplification of fluctuations by the evolving laser pulse and injected electron bunch [22]. A significant improvement in shot-to-shot stability was reported in 2008, with the use of a capillary discharge plasma source in place of a laser-ionized gas jet [23]. The variation in energy was limited to 2.5% and in charge to 16%. Recent experiments have seen the maximum energy of laser wakefield accelerated electrons increased from the hundreds of MeV scale to multi-GeV levels [24, 25].

The major limitations of laser plasma accelerators are dephasing of the accelerated bunch with the laser pulse and depletion of the energy of the laser. Energy depletion is a result of the limited energy of a single laser pulse, and achieving increased pulse energy while maintaining high intensity is technically difficult. Dephasing, or phase slippage, occurs as

a result of the refractive index of the plasma. The laser phase velocity, and hence its group velocity, and the phase velocity of the plasma wave is significantly less than  $c$ . The accelerated electron bunch however quickly gains enough energy to become ultrarelativistic with a velocity very close to  $c$ . Over an extended propagation distance the electron bunch moves forward relative to the plasma wakefield phase and out of the accelerating region [26]. This limits the length over which the bunch can be accelerated. Simulations have shown that dephasing can be controlled by using a plasma density gradient, such that the plasma wavelength changes to match the advance of the accelerated bunch [27]. A staged laser wakefield accelerator can address both dephasing and depletion. Multiple plasma cells are used with a new laser pulse used to accelerate the same electron bunch over each stage. With each stage additional laser energy can be inserted, and the phase slippage of the electron bunch can be reset. Recently, acceleration over two stages was demonstrated for the first time [28]. Nonetheless, there are still major challenges in the development of laser wakefield acceleration. The low laser to bunch efficiency, coupled with the typically low wall-plug efficiency of lasers make the overall efficiency of such a system limited. Another difficulty is the synchronization of the hundreds of laser pulses that would be needed for an energy frontier accelerator based on the multi-stage LWFA scheme. Compared to the laser wakefield accelerator, in a beam-driven accelerator the drive and witness bunches may both have velocities close to  $c$  and phase slippage is less of an issue as long as the drive bunch remains ultrarelativistic. The energy input from a particle bunch can also be higher than for a laser

pulse as bunch charge and per-particle energy can be increased with relative ease compared to the technical difficulties of increasing laser pulse energy and intensity.

### 1.3.1 Laser acceleration of ions

Another application of laser plasma acceleration, though operating via a significantly different mechanism, is laser ion acceleration. An intense, short laser pulse incident on a thin foil is capable of generating extremely high accelerating gradients over a very short distance, and accelerating ions to several hundred MeV. There are three mechanisms by which laser ion acceleration occurs, with the dominant mechanism depending on the incident laser intensity and the target foil thickness. At lower laser intensities, Target-Normal Sheath Acceleration (TNSA) occurs. In this mechanism, a laser pulse is incident on a relatively thick target foil. A pre-pulse ionizes the rear surface of the foil, producing a plasma from which electrons are accelerated to MeV energy by the main pulse. These electrons travel through the foil and exit the far side, where they form a sheath which produces a very large electric field, similar in magnitude to the laser field, capable of ionizing and accelerating atoms in the surface of the foil [29]. At higher laser intensities and using thin foils, the Break-Out Afterburner (BOA) regime is reached [30]. In BOA the acceleration initially proceeds via the same mechanism as TNSA, producing an electron sheath that ionizes and accelerates particles from the surface of the foil. If the foil is sufficiently thin and the laser of sufficiently high

intensity, the laser pulse is able to penetrate the electron sheath and further accelerate the ions that have been ejected from the foil. This enables the BOA regime to achieve GeV ion energies. Radiation Pressure Acceleration (RPA) occurs in ultra-thin foils irradiated by ultra-intense circularly-polarized laser pulses [31]. In this regime acceleration occurs by the collective displacement of electrons and ions due to the radiation pressure of the driving laser pulse. In comparison to TNSA and BOA, RPA is capable of generating ultra-short ion pulses as acceleration occurs only over the duration of the laser pulse rather than over an extended period after the laser pulse has interacted with the foil.

## 1.4 Beam-driven plasma wakefield accelerator

The limitations of the laser wakefield accelerator, and the unavailability of sufficiently short, intense laser pulses at the time, led to the proposal by Chen *et al.* of a plasma wakefield accelerator (PWFA) driven by a charged particle beam [32]. The first experiment in beam-driven PWFA, the Advanced Accelerator Test Facility (AATF) at Argonne National Laboratory (ANL) in 1988 used a 21 MeV, up to 2.5 nC, multi-picosecond (i.e. mm-length) drive bunch, probed by a low-intensity witness [33]. Wakefield amplitudes of 1 to 2  $\text{MV m}^{-1}$  were inferred from witness beam energy changes of 50 keV. Deflection of the witness bunch by transverse wakefields was also observed. In 2000, the Argonne Wakefield Acceler-

ator (AWA) demonstrated plasma wakefield acceleration in the blowout regime, where the bunch density is higher than the plasma density [34]. An average accelerating gradient of  $25 \text{ MeV m}^{-1}$  was observed. In contrast to most other PWFA experiments, AWE made use of a very high charge (average of  $18 \text{ nC}$ , but with significant variation between shots) photoinjector bunch with relatively low energy of approximately  $15 \text{ MeV}$ , again with significant variation.

Experiments at SLAC National Accelerator Laboratory (formerly Stanford Linear Accelerator Center) were able to make use of a much higher energy beam, with much shorter bunch lengths, than was available to previous tests. Experiment E-157 used the 30 GeV Final Focus Test Beam (FFTB) and observed  $280 \text{ MeV}$  energy gain of electrons in the tail of the bunch over a  $1.4 \text{ m}$  plasma cell [35, 36]. The plasma source used was a lithium heat-pipe oven ionized by an ultraviolet laser. E-157 also demonstrated acceleration of positrons under similar conditions. Energy loss for the positron beam was observed at lower plasma densities, and energy gain was observed at the highest plasma densities as the tail of the bunch was able to sample the wakefield driven by the head [37, 38]. In the same experiment the transverse dynamics of the electron beam were studied and betatron oscillations as a result of the strong plasma focusing were observed [39].

Subsequently, experiment E-157 using FFTB showed up to doubling of the energy of particles in a  $42 \text{ GeV}$  electron beam over a plasma length of  $85 \text{ cm}$  giving a maximum accelerating field of  $52 \text{ GV m}^{-1}$  [40]. As this experiment used a single bunch the energy of the beam exiting the plasma

varied between less than the initial energy and up to nearly 100 GeV, although only a very small portion of the beam reached the maximum energy. In this experiment the plasma was produced by ionization of a lithium vapour by the electric field of the beam. Recently, FACET (Facilities for Accelerator science and Experimental Test beams) has replaced FFTB at SLAC. FACET includes the capability to produce a drive-witness bunch structure and, like FFTB, can provide both electron and positron beams [41]. In experiments at FACET, acceleration of a witness electron bunch was achieved with wake to bunch energy transfer efficiency as high as 30% and energy spread as low as 0.7% while achieving an accelerating gradient of  $4.4 \text{ GeV m}^{-1}$  [42]. The two-bunch structure was generated by dispersing a chirped electron beam through a bending structure and the central part of the bunch is scattered by a tantalum bar. The dispersion is then reversed giving two closely-spaced bunches while losing 40% of the initial bunch charge [42]. This process is referred to as beam notching. Experiments at FACET using a single positron bunch to drive and sample a plasma wakefield have shown the formation of a spectrally distinct peak with low energy spread, gaining 5 GeV over 1.3 m, while background particles in the bunch lose energy to drive the wakefield [43]. The charge contained in the peak was approximately 200 pC of the initial 2.24 nC bunch, allowing a high wake-to-bunch efficiency of 30%.

A new facility for the study of plasma accelerators is FLASHForward at DESY [44]. The facility receives the 1.25 GeV electron beam from the FLASH free electron laser (FEL), and is intended to demonstrate

injection of plasma electrons into the accelerating phase of the wakefield by use of a density down ramp, and by ionization, including laser-assisted ionization. In laser-assisted ionization, or the Trojan horse scheme, a gas containing a low-ionization energy component and a higher ionization energy component is used to form a plasma. The plasma wakefield is driven by a particle beam while a laser pulse is used to inject electrons by ionizing the high ionization energy component of the gas [45]. This method offers the possibility of generating ultra-short, low emittance, ultra-high brightness electron bunches with multi-GeV energy, and has recently been demonstrated at FACET as part of the E-210 experiment [46]. FLASH is also capable of providing a drive-witness bunch structure that can be preserved from the photocathode and accelerated in a single RF bucket, with a final energy of 700 MeV. It is also possible to produce drive-witness bunch structures using a beam scraper at the extraction section, where the bunch is transferred from the FLASH FEL beam-line to the FLASHForward section [47]. FLASHForward is also planned to demonstrate high transformer ratio acceleration using shaped drive bunches.

#### 1.4.1 Proton beam driver

As a result of the higher mass of the proton and the consequent reduction in radiation losses in a circular accelerator, the highest energy beams available are proton and heavy ion beams. The Large Hadron Collider (LHC) at CERN is capable of generating proton bunches with energy of

7 TeV and population of  $1.15 \times 10^{11}$  giving a charge per bunch of 18.4 nC [48]. The energy per bunch is thus 129 kJ compared to the energy of a 500 GeV ILC bunch of 1.6 kJ [9]. In practice a drive bunch for an electron beam driven PWFA would be of lower energy than the ILC bunch since the purpose of PWFA is to avoid the need to build such a large conventional accelerator. It was found by simulation that a 1 TeV proton bunch of length 100  $\mu$ m would be capable of accelerating a witness electron bunch with a gradient of 1.7 GeV m<sup>-1</sup> [49]. However, the length of the LHC proton bunch at maximum energy is approximately 8 cm [48]. This is not the case for the LHC bunch for a plasma of the required density. In order to drive a large plasma wakefield using a single proton bunch it would thus be necessary for the bunch length to be dramatically reduced. Compression of the proton bunches from the CERN Proton Synchrotron (PS) was found to be impractical as a large beamline geometry would be necessary to achieve sufficient bunch shortening, with smaller geometries leading to excessive loss of protons [50].

An alternative method to achieve large plasma wakefield amplitudes is the self-modulated proton-driven plasma wakefield accelerator. Self-modulation is the result of an instability that can occur when a long particle bunch propagates through a plasma. The small wakefield driven by the long bunch alternately focuses and defocuses the bunch behind the bunch head. As long as other instabilities are controlled, the loss of particles from the parts of the bunch in the defocusing region allows the self-modulation instability, and the wakefield driven by the increasingly modulated bunch to grow. When the instability saturates, the bunch

has been fully modulated into micro-bunches spaced at the plasma wavelength [50, 51]. Once a long proton bunch has undergone self-modulation the micro-bunches that result are ideally suited to resonantly drive a large-amplitude plasma wakefield. Electrons or positrons can then be externally injected into the appropriate accelerating phase of the wake-field. The high total energy of the modulated proton bunch means that the witness particles can be accelerated over a very large distance - hundreds of metres - without energy depletion of the drive bunch being a concern. Simulations have also shown that self-modulation can be observed in long electron and positron beams at FACET [52], with initial experimental results showing some evidence of this for electron beams [53]. Experiments in self-modulation have also begun at the PITZ experiment at DESY [54].

Self-modulated proton-driven plasma wakefield acceleration is currently being studied using the 400 GeV Super Proton Synchrotron (SPS) beam at CERN, the AWAKE experiment [51]. In AWAKE the self-modulation instability is seeded by a laser pulse that co-propagates at the longitudinal midpoint of the proton bunch. The seeding ensures that the self-modulation instability dominates over competing instabilities and shortens the plasma length required for the modulation to saturate. The plasma source used in AWAKE is a laser-ionized rubidium vapour [55, 56], which is capable of providing the uniform density (variation  $\sim 0.2\%$  [57]) that is required for self-modulation to occur. Initial experiments at AWAKE are aimed at studying the self-modulation of the proton bunches and do not include a witness electron beam. Modulation of the proton

bunches was recently observed [58, 59]. It is expected that when AWAKE operates with a witness electron beam an energy gain of 1.3 GeV over a 10 m plasma cell will be achieved [57].

Table 1.2: Summary of key parameters of plasma wakefield experiments. Parameters are for the drive bunch. Energy gain is for the witness bunch if present; in the case of AWAKE this is the electron bunch. \* indicates future experiments with expected parameters.

Experiment	Year	Drive species	$Q$ (nC)	$E$ (GeV)	$\sigma_z$ ( $\mu\text{m}$ )	$n_p$ ( $\text{m}^{-3}$ )	Acc. Grad. ( $\text{MeV m}^{-1}$ )	$\Delta E$ (MeV)
Argonne AATF	1988	$e^-$	2.5	0.021	2400	$10^{19}$	~2	0.05
Argonne AWA	2000	$e^-$	18	0.016	6600	$1.3 \times 10^{19}$	25	~3
FFTB E-157	2001	$e^-$	3.0	28.5	700	$10^{20}$	200	280
FFTB E-164	2003	$e^+$	1.9	28.5	720	$1.8 \times 10^{20}$	56	78
FACET E-210	2014	$e^-$	1.0	42	25	$5 \times 10^{22}$	4400	1600
AWAKE Run 1*	2018	p	48	400	120000	$1 \times 10^{20}$	~100	1000
AWAKE Run 2*	2021	p	48	400	120000	$7 \times 10^{20}$	> 500	$\sim 1 \times 10^4$
FLASHForward*	2018	$e^-$	0.5	1.25	3-150	$1 \times 10^{23}$	> 1000	350

## 1.5 Motivation

Exploiting the very high field strengths that a plasma can support offers a way forward in accelerator technology, with plasmas offering the potential to replace or augment conventional components not just in ultra-high gradient acceleration, but also in other applications in particle accelerators. However, the transient and tenuous nature of the plasmas used in accelerators presents a number of challenges when compared with conventional solid components. Fine-tuning of fields inside the plasma, and hence the output bunch parameters, is more difficult in a plasma accelerator than a metallic RF structure, for example. Studies of techniques that are applicable to plasma devices that push the frontiers of accelera-

tor technology need not be carried out only in these extreme conditions. Small scale tests of plasma technology using lower energy beams and lower density plasmas can provide insight into the means of achieving improved performance in larger scale machines. In addition to practical considerations, simulation studies of proposed experiments can also benefit from less extreme parameters. Larger bunch dimensions allow for lower simulation resolutions to be used, also allowing larger time-steps, and shorter overall lengths reduce the total runtime of simulations. The VELA (Versatile Electron Linear Accelerator) and later CLARA (Compact Linear Accelerator for Research and Applications) accelerators at Daresbury Laboratory provide a beam well suited to small scale testing of plasma accelerator techniques.

## 1.6 Outline

This thesis presents the results of simulations carried out in support of planned smaller-scale plasma wakefield experiments. The aim of the simulations is to demonstrate the viability of plasma wakefield acceleration under the proposed conditions and to demonstrate that useful and novel results can be achieved using relatively low-energy electron bunches with parameters achievable in the accelerators at Daresbury Laboratory. Chapter 2 describes important plasma parameters, and gives an outline of the linear theory of plasma wakefield acceleration. Chapter 3 discusses the simulation methods used in this thesis.

Chapter 4 presents results of simulation studies of plasma wakefield acceleration using the VELA and CLARA accelerators. A range of schemes are studied using single bunches, drive-witness bunch pairs and ramped drive and witness bunches to improve transformer ratio and accelerated bunch quality. An electron bunch from the full CLARA accelerator was shown to be capable of driving a plasma wakefield in excess of  $800 \text{ MV m}^{-1}$ . A realistic CLARA-Front End bunch was studied and compared to simulations using a Gaussian bunch, and results were found to be similar. It was found that a ramped drive bunch, with extended bunch length compared to the CLARA beam, and increased bunch charge, would be capable of achieving an increased transformer ratio compared to a Gaussian bunch and accelerating over an extended distance. An energy gain for a witness bunch of approximately  $1.3 \text{ GeV}$  over an accelerating length of  $4.8 \text{ m}$  was found to be possible.

Chapter 5 shows results of studies of plasma lensing. Plasma lensing was studied in order to validate the use of the VELA electron beam for plasma lensing experiments, aiming to study aberrations in plasma lensing with increased detail to past experiments. The effects of plasma focusing on bunch size and emittance are compared between theory and simulation. The effect of the longitudinal aberration was studied with particle tracking and particle-in-cell simulation and the emittance growth observed for both methods was compared and found to be similar, though not identical. An experimental setup for plasma lensing using a laser-ionized gas jet, which was demonstrated at Daresbury Laboratory is described.

In Chapter 6 the results of an investigation in a plasma-based beam dump are presented. A plasma beam dump offers the potential for improved compactness and reduced waste compared to a conventional beam dump, and relatively few studies of the scheme have been carried out previously. In this chapter, a new scheme for a passive dump is proposed, using a varying plasma density to address on the key drawbacks of the passive plasma beam dump, re-acceleration of the decelerated portion of the bunch. Particle-in-cell simulations are used to validate the scheme for bunch parameters representative of an ultra-short RF accelerated bunch or a conservative laser-wakefield generated bunch.

Chapter 7 concludes the thesis by summarizing the results and discussing further areas of study that could be developed to continue the work presented here.

# Chapter 2

## Physics of plasma wakefield acceleration

Theory and simulation studies of plasma wakefield acceleration are both necessary to efficiently obtain results that can be used to inform experimental design and further study. First, the basic properties of a plasma are described in this chapter. These properties determine what kinds of systems can be considered a plasma, and thus where the theory of plasmas can be used to make useful predictions. These properties also determine the parameters that can be used in simulations to ensure that the relevant physical behaviour of the system is captured.

There follows a description of the linear theory of plasma wakefield acceleration that can be used to predict the accelerating gradient in a beam driven plasma where the plasma density perturbation is small. The theoretical predictions can then be compared to simulation results: assuming good agreement, simulations validate the theoretical predictions

and the theory validates the simulation results. It has been found that although the linear theory of plasma wakefield acceleration is based on the assumption that the plasma density perturbation is small, its predictions remain valid beyond the limits of these assumptions. This makes the linear theory more applicable than the relatively narrow range of its assumptions would suggest. This also means that evolution of the beam parameters away from those consistent with the linear regime does not necessarily lead to dramatic changes in the properties of the wakefield. The linear regime also has limitations on the maximum energy gain and efficiency that can be achieved. The nonlinear regime, in which plasma perturbations are large compared to the background density has some advantages in these respects.

## 2.1 Properties of a plasma

A plasma is defined as a quasi-neutral medium consisting of free electrons, ions, and neutral particles which exhibits collective effects. Plasmas can exist in a huge range of temperatures, densities and length scales, however not all fully- or partially-ionized substances can be considered plasmas. An example is a metal at room temperature - although consisting of free electrons and ions its combination of low temperature and high density prevent it from showing the collective effects that define a plasma as the free electrons are too effective at screening charge imbalances. Among the important properties of plasmas are the Debye length  $\lambda_D$ , plasma frequency  $\omega_p$  and plasma wavelength  $\lambda_p$ .

The basic properties of a plasma can be used to determine its response to an excitation, and thus determine how a plasma behaves when used as an accelerating medium. The important factors for a plasma as an accelerating medium include the accelerating gradient, transverse fields, acceleration efficiency, and transformer ratio - the ratio of accelerating to decelerating field. These can all be calculated for the linear regime, when the plasma electron density perturbation is small. It becomes more difficult to predict these properties in the non-linear regime, where the density perturbation is large. However, predictions from the linear regime can still be of some use for the non-linear regime.

### 2.1.1 Plasma frequency

A typical plasma is quasi-neutral, meaning that the net charge of the free electrons and ions present is zero. The charges may however be displaced from one another e.g. by the excitation of the plasma by electromagnetic radiation. The displaced charge experiences a restoring force that depends on the plasma density  $n_p$ . The force can be calculated by considering a slab of plasma with number density  $n_p$ . If the plasma electrons are collectively displaced by a small distance  $\delta x$  they will create a surface charge density  $\sigma$  on one side of the slab, and a corresponding opposite charge will be generated by the ions on the opposite side of the slab (see Figure 2.1) [60]. The electric field  $E$  inside the slab can be

easily calculated using Gauss's law by virtue of the simple geometry:

$$E_x A = \frac{Q}{\varepsilon_0} = \frac{n_e e A}{\varepsilon_0} \delta x \quad (2.1)$$

where  $A$  is the area of the slab and  $\varepsilon_0$  is the permittivity of free space.

The area of the slab cancels and the equation of motion for each of the displaced electrons is given by:

$$\frac{d^2(\delta x)}{d(\delta x)^2} = \frac{e E_x}{m_e} = \frac{e^2 n_e}{\varepsilon_0 m_e} \delta x \quad (2.2)$$

where  $m_e$  is the electron mass. This is the equation of simple harmonic motion with a frequency of:

$$\omega_p = \left( \frac{e^2 n_e}{\varepsilon_0 m_e} \right)^{\frac{1}{2}}. \quad (2.3)$$

This is the plasma electron frequency. A plasma ion frequency can be defined in the same way, with the ion mass replacing the electron mass. The plasma ion frequency is hence lower than the electron frequency by a factor of around 40 for a hydrogen plasma and more than this for a plasma formed from heavier elements. The plasma period  $\tau = 1/\omega_p$  is the time scale over which plasma oscillations can be observed. If the lifetime of the system or the phenomenon being studied is less than or comparable to the plasma period for the applicable species (electrons or ions) plasma oscillations will not be observed, and treating the system as a plasma may not be appropriate. The plasma frequency gives rise to further quantities that are of use when studying plasma wakefield ac-

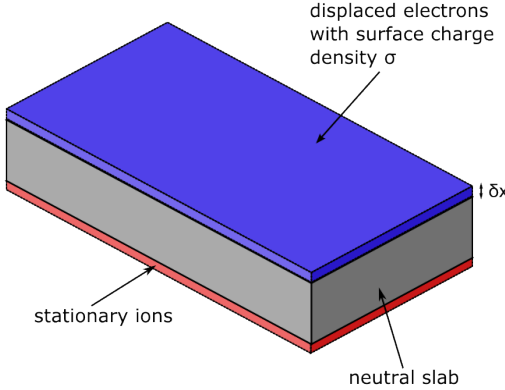


Figure 2.1: Displacement of electrons by a small distance  $\delta x$  generates a surface charge of  $\sigma$ , and the restoring force causes oscillations at a characteristic frequency that depends on the plasma density.

celeration. The plasma wavelength  $\lambda_p = 2\pi c/\omega_p$  is the wavelength of a plasma wave with frequency  $\omega_p$  and phase velocity of the speed of light  $c$ . This is the phase velocity for a plasma wave driven by a highly relativistic particle bunch. Likewise the plasma wavenumber  $k_p = 2\pi/\lambda_p$  is the corresponding angular wavenumber. It is convenient to use engineering formulae giving these quantities in terms of the plasma density. This is done by substituting in appropriate values for the constants in the formula for the plasma frequency (Equation 2.1) and introducing a scaling factor to make the unit size and constant convenient:

$$k_p = 1878 \sqrt{\frac{n_e}{10^{20}}} \text{ rad m}^{-1} \quad (2.4)$$

$$\lambda_p = 3.35 \left( \frac{n_e}{10^{20}} \right)^{-\frac{1}{2}} \text{ mm} \quad (2.5)$$

where the plasma density is specified in units of  $\text{m}^{-3}$ .

### 2.1.2 Debye length

The Debye length is the distance over which the free charged particles in a plasma screen a test charge placed in the plasma. A test charge  $Q$  can be represented by a Dirac  $\delta$ -function, with a plasma of density  $\rho = q(n - n_0)$ , where  $q$  is the charge of the species being considered,  $n_0$  is the background density and  $n$  is the density perturbed by the test charge. The potential  $\phi$  within the plasma at a large distance from the test charge can be described by Poisson's equation [60]:

$$\nabla^2\phi = \frac{1}{\varepsilon_0}[\rho + Q\delta(r)] . \quad (2.6)$$

The potential energy of the plasma particles is  $q\phi$ . If they follow a Boltzmann distribution, the density depends on the energy and can be written as:

$$n = n_0 \exp\left(-\frac{q\phi}{k_B T}\right) \quad (2.7)$$

where  $k_B$  is the Boltzmann constant and  $T$  is the temperature, which is assumed to be equal for electrons and ions. As we are considering the effect of the test charge at a large distance, the energy due to the potential will be much smaller than the thermal energy, and the density can be Taylor expanded as follows:

$$n = n_0 \left(1 - \frac{q\phi}{k_B T}\right) \quad (2.8)$$

and substituting into Equation 2.6, writing out the Laplacian operator and assuming radial symmetry we get:

$$\frac{1}{r^2} \frac{\partial}{\partial r} \left( r^2 \frac{\partial \phi}{\partial r} \right) = \frac{n_0 q^2}{\varepsilon_0 k_B T} \phi . \quad (2.9)$$

Rearranging Equation 2.9 in terms of  $r\phi$  gives the following:

$$\frac{\partial^2 (r\phi)}{\partial r^2} = \frac{1}{\lambda_D^2} r\phi \quad (2.10)$$

with the Debye length:

$$\lambda_D = \left( \frac{\varepsilon_0 k_B T}{n_0 q^2} \right)^{\frac{1}{2}} . \quad (2.11)$$

Under the boundary conditions that the potential falls to zero for large  $r$ , and matches the unshielded potential ( $\sim 1/r$ ) for a point charge at small  $r$ , the solution is:

$$\phi = \frac{Q}{r} \exp \left( -\frac{r}{\lambda_D} \right) \quad (2.12)$$

so the potential due to the test charge falls exponentially with characteristic distance of the Debye length. It is notable that unlike the plasma frequency,  $\lambda_D$  is independent of mass and as such is the same for electrons and singly-charged ions assuming thermal equilibrium. If the Debye length is so large that there is no significant screening of charge over the length scales being considered, the system cannot be considered to behave collectively and as such it is not useful to consider it to be a

plasma. The same applies to a system such as an electron bunch: since each electron sees the field of all other electrons in the bunch there is no screening and thus no Debye length to be defined. A plasma may have a net charge but it is necessary for charge balance to be sufficient for the Debye length to be small compared to the size of the system for the system to be considered a plasma [61].

The Debye length can also be derived from considering the distance travelled in one plasma period by a particle of the species being considered. The plasma period for a species of charge  $q$ , number density  $n$  and mass  $m$  is:

$$\tau = \frac{1}{\omega_p} = \left( \frac{\epsilon_0 m}{q^2 n} \right)^{\frac{1}{2}}. \quad (2.13)$$

The kinetic energy of a particle is  $k_B T/2$  per degree of freedom, so its velocity  $v$  in a given direction is on average  $\sqrt{k_B T/m}$ . The distance travelled by a particle in a plasma period is thus:

$$v\tau = \lambda_D = \left( \frac{\epsilon_0 k_B T}{q^2 n} \right)^{\frac{1}{2}}. \quad (2.14)$$

Since the plasma frequency and hence period is derived from considering the reaction of a plasma to a displacement of charge it is not surprising that the distance travelled in one plasma period is the same as the scale length for the screening of charges.

Typical parameters for a plasma wakefield accelerator are a density greater than  $10^{21} \text{ m}^{-3}$  and a temperature prior to excitation of no more than 1000 K. This gives a Debye length of 70 nm, which is smaller than

the typical length scales of a laser pulse or particle bunch, which are typically tens of  $\mu\text{m}$  or more.

## 2.2 Mechanism of plasma wakefield acceleration

When a charged particle bunch or laser pulse propagates in a plasma, the plasma electrons are displaced. Over time-scales much shorter than the ion plasma period, the plasma ions can be considered to be stationary. In the case of a charged particle bunch, the bunch may have a density greater than or less than the initial plasma electron density. For an electron driver bunch, the plasma electrons are expelled by the space charge force of the driver, leaving behind plasma ions which neutralize the driver's charge. The expulsion of plasma electrons continues until the plasma density perturbation matches the drive bunch density, or, if the drive bunch density is higher than the initial plasma density, until the plasma electrons in the vicinity of the drive bunch have been depleted. If the drive bunch density is much lower than the plasma density, the plasma density perturbation is small and the wakefield is linear, i.e. the wakefields from two or more drive bunches can be superimposed to obtain the resultant wakefield. If the bunch density is equal to or higher than the plasma density, the density perturbation is large and the wakefield is non-linear. In the case of a bunch density much higher than the plasma density, plasma electrons are completely expelled from a signifi-

cant volume behind the bunch: this is referred to as the blowout regime [62]. Compared to the linear regime, acceleration in the blowout regime allows for linear focusing and higher efficiency [63].

In the case of a laser driver, the relation between the driver properties and the plasma response is not as obvious. The non-linear regime is reached when the normalized vector potential of the laser,  $a_0 = eE_0/(m_e\omega_0c)$ , where  $E_0$  and  $\omega_0$  are the electric field amplitude and angular frequency of the laser, respectively, is greater than one [64]. When the laser driver is strong enough to expel electrons in a large volume, the term bubble regime is commonly used [62, 65]. This is essentially similar to the blowout regime in beam-driven plasmas. An advantage of the bubble regime in laser-plasma acceleration are that using a lower density plasma reduces dephasing between the laser and accelerated electrons, and allows for self-focusing of the laser pulse [26, 63].

The response of plasma electrons to a negatively charged driver bunch is to be accelerated away from the bunch's axis of propagation in the radial direction. The electrons then undergo oscillations around the axis with the restoring force provided by the net-positive-charge region of the plasma where, as the electrons are expelled while the ions remain stationary, the ion density is higher than the electron density. The amplitude of oscillation of an electron depends on its distance from the axis of the beam: an electron further from the beam sees a smaller electric field due to screening of the bunch charge by the plasma. The phase of the plasma electrons depends on the time at which the excitation occurred, and thus the phase velocity of the plasma wave is equal to the velocity

of the drive bunch. A diagram showing the motion of plasma electrons due to a negatively charged drive bunch is shown in Figure 2.2.

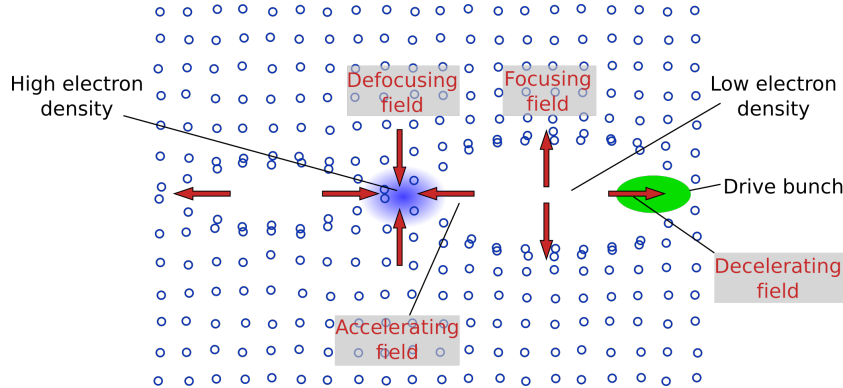


Figure 2.2: Diagram illustrating the mechanism of beam-driven plasma wakefield acceleration.

The oscillating plasma electrons create alternating regions of high and low electron density, while the ion density remains approximately constant. The imbalanced charges of the plasma give rise to an electric field that is (for particles of a given charge) alternately decelerating and accelerating, and focusing and defocusing. As the phase velocity of the plasma wake is equal to the velocity of the drive bunch, and this is very close to  $c$ , a witness bunch may be placed in the accelerating region of the wakefield. As long as the witness bunch is also highly relativistic, it can remain in the accelerating region and continue gaining energy for an extended period of time.

## 2.3 Linear theory of plasma wakefield acceleration

The linear theory of plasma wakefield acceleration can be derived by considering the plasma as a fluid, with the assumptions that the perturbation to the plasma density is small compared to the background density, and that plasma electrons remain non-relativistic. The following derivation is primarily based on references [66] and [67]. The continuity equation (Equation 2.15) defines the rate of change of density of a fluid in the absence of any sources or sinks. For a plasma this means that there is no significant ionization or recombination occurring over the time scale of interest. For a plasma of number density  $n$  and velocity  $\mathbf{u}$  the continuity equation is as follows:

$$\frac{\partial n}{\partial t} = -\nabla \cdot (n\mathbf{u}) . \quad (2.15)$$

The density can be written as  $n(t) = (n_0 + n_1(t))$  where  $n_0$  and  $n_1$  are the constant background and perturbed number densities respectively. Since  $n_0$  is constant, and  $n_1$  is small compared to  $n_0$ , the derivative of the continuity equation with respect to time can be written as:

$$\frac{\partial^2 n_1}{\partial t^2} = -n_0 \nabla \cdot \frac{\partial \mathbf{u}}{\partial t} . \quad (2.16)$$

From Newton's second law and the Lorentz force law, the acceleration of the fluid is given by:

$$\frac{\partial \mathbf{u}}{\partial t} = \frac{q}{m} (\mathbf{E} + \mathbf{u} \times \mathbf{B}) \quad (2.17)$$

where  $m$  and  $q$  are the mass and charge of the fluid particles respectively. The plasma is initially unperturbed, and the thermal motion of the plasma particles is negligible. If the plasma is excited by a highly relativistic charge moving through it the force due to the charge's electric field is transverse, and so is the plasma flow. The magnetic field of the moving charge is azimuthal and thus  $\mathbf{u} \times \mathbf{B} = 0$ . Substituting Equation 2.17 into Equation 2.16 gives:

$$\frac{\partial^2 n_1}{\partial t^2} = -\frac{n_0 q}{m_e} \nabla \cdot \mathbf{E} . \quad (2.18)$$

Gauss's law states  $\nabla \cdot \mathbf{E} = \rho/\varepsilon_0$  where  $\rho$  is the charge density. We can thus write:

$$\frac{\partial^2 n_1}{\partial t^2} = -\frac{n_0 q}{m_e \varepsilon_0} \rho . \quad (2.19)$$

Consider a highly relativistic point charge moving along the  $z$ -axis through the initially uniform plasma. In cylindrical polar coordinates the overall charge density is  $\rho = Q\delta(r)\delta(z - v_b t) - en_1$  where  $Q$  is the magnitude of the point charge,  $v_b$  is its velocity and the fluid charge carrier  $q$  becomes the electronic charge  $-e$ . Equation 2.19 becomes [66]:

$$\frac{\partial^2 n_1}{\partial t^2} = \frac{n_0 e^2}{\varepsilon_0 m_e} \left[ \frac{Q}{e} \delta(r)\delta(z - v_b t) - n_1 \right] . \quad (2.20)$$

Writing  $n_0 e^2 / \varepsilon_0 m_e$  as  $\omega_p^2$  and rearranging terms gives the following:

$$\frac{\partial^2 n_1}{\partial t^2} + \omega_p^2 n_1 = \frac{\omega_p^2 Q}{e} \delta(r)\delta(z - v_b t) . \quad (2.21)$$

This is the equation for an undamped harmonic oscillator, excited by an instantaneous kick at  $t = z/v_b$ . This can be solved by considering the behaviour of the system before and after the kick. For convenience, the  $\delta$ -function can be rewritten in terms of  $t$  rather than  $z$ , and dot notation is used for time derivatives to save space, so Equation 2.21 can be restated as:

$$\ddot{n}_1 + \omega_p^2 n_1 = \frac{\omega_p^2 Q}{ev_b} \delta(r) \delta(t - z/v_b) . \quad (2.22)$$

The perturbed plasma density,  $n_1$  must be zero for  $t < z/v_b$  as before this, since the moving charge is highly relativistic, it can have no effect on the plasma. For  $t > z/v_b$ , there is no driving force and the plasma will respond as a harmonic oscillator at the plasma frequency  $\omega_p$ :

$$n_1 = A \sin [\omega_p(t - z/v_b)] + B \cos [\omega_p(t - z/v_b)] \quad (2.23)$$

where  $A$  and  $B$  are the amplitudes of each term. It is necessary to glue the expressions for the plasma density before and after the kick together using junction conditions. To do this we integrate Equation 2.23 over a small interval containing the instant of the kick,  $z/v_b - \epsilon \leq t \leq z/v_b + \epsilon$ :

$$\int_{\frac{z}{v_b} - \epsilon}^{\frac{z}{v_b} + \epsilon} \ddot{n}_1 dt + \int_{\frac{z}{v_b} - \epsilon}^{\frac{z}{v_b} + \epsilon} \omega_p^2 n_1 dt = \int_{\frac{z}{v_b} - \epsilon}^{\frac{z}{v_b} + \epsilon} \frac{\omega_p^2 Q}{ev_b} \delta(r) \delta(t - z/v_b) . \quad (2.24)$$

The second term on the LHS is small because  $n_1$  is close to zero over the interval. This gives:

$$[\dot{n}_1]_{\frac{z}{v_b} - \epsilon}^{\frac{z}{v_b} + \epsilon} = \frac{\omega_p^2 Q}{ev_b} \delta(r) . \quad (2.25)$$

We now consider the behaviour of the system as  $t$  approaches 0 from both the positive and negative directions, denoted by + and – superscripts to the limits respectively. In the limit  $\epsilon \rightarrow 0$ :

$$\dot{n}_1|_{t \rightarrow \frac{z}{v_b}+} - \dot{n}_1|_{t \rightarrow \frac{z}{v_b}-} = \frac{\omega_p^2 Q}{ev_b} \delta(r) . \quad (2.26)$$

As  $t$  approaches  $z/v_b$  from the negative direction,  $n_1$  remains zero by causality. Hence

$$n_1|_{t \rightarrow \frac{z}{v_b}+} = \frac{\omega_p^2 Q}{ev_b} \delta(r) \quad (2.27)$$

Now we need to match this variation of  $n_1$  to the variation for  $t > z/v_b$ . Since  $n_1 = 0$  for  $t < z/v_b$ ,  $B$  in Equation 2.23 must be zero. We can now differentiate Equation 2.23 with respect to time to obtain an expression for  $\dot{n}_1$ , and substitute in the result from Equation 2.27:

$$\dot{n}_1 = \omega_p A \cos [\omega_p(t - z/v_b)] \quad (2.28)$$

$$\frac{\omega_p^2 Q}{ev_b} \delta(r) = \omega_p A \cos [\omega_p(t - z/v_b)] \quad (2.29)$$

Hence, at  $t = z/v_b$ :

$$A = \frac{\omega_p Q \delta(r)}{ev_b} \quad (2.30)$$

giving

$$n_1(t) = \frac{\omega_p Q \delta(r)}{ev_b} \sin [\omega_p(t - z/v_b)] H(t - z/v_b) \quad (2.31)$$

where  $H(x)$  is the Heaviside step function with a value of zero when its argument is negative and a value of 1 when its argument is positive. We now have an expression for the plasma density as a function of time. The

quantities of interest however, are the electric and magnetic fields, which can be obtained by considering the wave equation in the case of non-zero charge and current density:

$$\left( \frac{\partial^2}{\partial t^2} - c^2 \nabla^2 \right) \mathbf{E} = -\frac{1}{\epsilon_0} \frac{\partial \mathbf{j}}{\partial t} - c^2 \nabla (\nabla \cdot \mathbf{E}) . \quad (2.32)$$

The current density in a plasma is  $\mathbf{j} = -en_0\mathbf{u}$ . The acceleration can be obtained from the Lorentz force law (Equation 2.17):

$$\frac{\partial \mathbf{j}}{\partial t} = -\frac{e^2 n_0}{m_e} \mathbf{E} = \epsilon_0 \omega_p^2 \mathbf{E} \quad (2.33)$$

Considering  $t > z/v_b$ , the charge density excludes the driving point charge. The wave equation can then be written as:

$$\left( \frac{\partial^2}{\partial t^2} - c^2 \nabla^2 \right) \mathbf{E} = \omega_p^2 \mathbf{E} - c^2 \nabla \left[ \frac{\omega_p Q \delta(r)}{\epsilon_0 v_b} \sin [\omega_p(t - z/v_b)] H(t - z/v_b) \right] . \quad (2.34)$$

Rearranging terms and writing  $\nabla_\perp = \frac{\partial^2}{\partial x^2} + \frac{\partial^2}{\partial y^2}$  gives:

$$\begin{aligned} \left[ \frac{\partial^2}{\partial t^2} - \omega_p^2 - c^2 \left( \frac{\partial^2}{\partial z^2} + \nabla_\perp^2 \right) \right] \mathbf{E} = \\ - c^2 \nabla \left[ \frac{\omega_p Q \delta(r)}{\epsilon_0 v_b} \sin [\omega_p(t - z/v_b)] H(t - z/v_b) \right] . \end{aligned} \quad (2.35)$$

Since the point charge is assumed to be highly relativistic,  $v_b$  can be replaced by  $c$ . If the wakefield depends only on the combined coordinate

$z - ct$ , the  $z$  and  $t$  derivatives cancel. Also writing  $\omega_p/c = k_p$ :

$$(\nabla^2 - k_p^2) \mathbf{E} = -c^2 \nabla \left[ \frac{\omega_p Q \delta(r)}{\varepsilon_0 c} \sin [\omega_p(t - z/v_b)] H(t - z/v_b) \right] . \quad (2.36)$$

the gradient on the RHS can be calculated, and the  $z$ -component which is of interest can be taken:

$$(\nabla^2 - k_p^2) E_z = \frac{Q k_p^2 \delta(r)}{\varepsilon_0} \cos [k_p(z - ct)] H(t - z/c) . \quad (2.37)$$

A differential equation of the form  $\frac{\partial^2 w}{\partial x^2} + \frac{\partial^2 w}{\partial y^2} + \lambda w = -\phi(x, y)$  is an inhomogeneous Helmholtz equation. For  $\lambda < 0$ , the Green's function for this equation is a zero-order modified Bessel function of the second kind,  $K_0$ [68]:

$$E_z = -\frac{Q k_p^2}{2\pi\varepsilon_0} K_0(k_p r) \cos [k_p(z - ct)] H(t - z/c) . \quad (2.38)$$

As is expected for the response to a  $\delta$ -function,  $K_0(k_p r)$  is a maximum as its argument approaches zero, so the maximum electric field is on the  $z$ -axis. Figure 2.3 shows a 3-dimensional plot of the electric field as a function of  $z - ct$  and  $r$ .

Given the expression for the longitudinal component of the wakefield, in order to find the transverse wakefield the Panofsky-Wenzel theorem is applied [69, 70]. The Panofsky-Wenzel theorem can be derived by considering the an electromagnetic field acting on a charged particle moving with velocity  $v$  in the  $z$ -direction. The magnetic force is proportional to:

$$v \hat{\mathbf{z}} \times \mathbf{B} = v \hat{\mathbf{z}} \times (\nabla \times \mathbf{A}) . \quad (2.39)$$

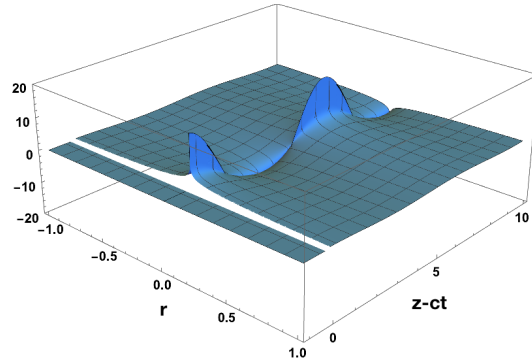


Figure 2.3: Plot of the longitudinal component of the electric field for the plasma response to a point charge.

The vector product for vector fields  $\mathbf{a}$  and  $\nabla \times \mathbf{b}$  can be written as:

$$\mathbf{a} \times (\nabla \times \mathbf{b}) = \nabla(\mathbf{a} \cdot \mathbf{b}) - (\mathbf{a} \cdot \nabla)\mathbf{b} - (\mathbf{b} \cdot \nabla)\mathbf{a} - \mathbf{b} \times (\nabla \times \mathbf{a}) \quad (2.40)$$

thus the magnetic force can be written as:

$$v\hat{\mathbf{z}} \times (\nabla \times \mathbf{A}) = \\ \nabla(\mathbf{A} \cdot v\hat{\mathbf{z}}) - \mathbf{A} \times (\nabla \times v\hat{\mathbf{z}}) - (\mathbf{A} \cdot \nabla)v\hat{\mathbf{z}} - (\hat{\mathbf{z}} \cdot \nabla)\mathbf{A} . \quad (2.41)$$

The curl of  $v\hat{\mathbf{z}}$  and the scalar product of  $\mathbf{A}$  and  $\hat{\mathbf{z}}$  are both zero, giving:

$$\hat{\mathbf{z}} \times (\nabla \times \mathbf{A}) = \hat{\mathbf{z}} \nabla A_z - v \frac{\partial \mathbf{A}}{\partial z} . \quad (2.42)$$

The partial derivative can be replaced with a full derivative since  $\mathbf{A}$  have an explicit time dependence. The force, including the electric scalar potential is:

$$\mathbf{F} = q \left( -\nabla\phi + v\nabla A_z - v \frac{d\mathbf{A}}{dz} \right) \quad (2.43)$$

and dividing by  $v$  and integrating over the whole region  $R$  that the fields are non-zero gives the change in momentum:

$$\Delta \mathbf{p} = q \int_R \left[ \frac{d\mathbf{A}}{dz} + \nabla \left( A_z - \frac{\phi}{v} \right) \right] dz . \quad (2.44)$$

The integrated value of  $\mathbf{A}$  is zero for an isolated system [70], thus the change in momentum can be written as a gradient:

$$\Delta \mathbf{p} = q \nabla \left[ \int_R \left( A_z - \frac{\phi}{v} \right) dz \right] \quad (2.45)$$

and so, as  $\nabla \times (\nabla \Omega) = 0$ , the change in momentum is irrotational. This can be written as:

$$\frac{\partial \Delta p_{||}}{\partial z} = - \frac{\partial \Delta p_{\perp}}{\partial r} \quad (2.46)$$

where  $p_{||}$  and  $p_{\perp}$  are the longitudinal and transverse momentum respectively. The change in momentum of the particle must be due to the fields acting on the particle. The momentum change can thus be replaced with the wake potential  $W = \int F dz$  and the same relation applies for the components of the wake potential:

$$W_{||,\perp} = \left( \mathbf{E} + \frac{\mathbf{v} \times \mathbf{B}}{c} \right)_{z,r} \quad (2.47)$$

and:

$$\frac{\partial W_{||}}{\partial r} = \frac{\partial W_{\perp}}{\partial z} . \quad (2.48)$$

Applying the Panofsky-Wenzel theorem to Equation 2.38 and integrating to find the transverse wake potential gives:

$$W_{\perp} = E_r - B_{\theta} = -\frac{Qk_p^2}{2\pi\varepsilon_0} K_1(k_p r) \sin [\omega_p(t - z/c)] H(t - z/c) . \quad (2.49)$$

Equations 2.38 and 2.49 give the longitudinal and transverse plasma wakefields for a relativistic point charge moving through a plasma, under the assumption that the plasma density perturbation is small compared to the background density. These can be considered to be the Green's functions for the response of a plasma to a charge. A real particle distribution is not point-like, but has finite size and density. In order to find the response to an arbitrary charge distribution, the product of the Green's function and the charge distribution must be integrated. For this we replace the charge  $Q$  with the charge density  $\rho$ . The charge density can often be separated into a longitudinal component  $\rho_{\parallel}(\zeta')$  and transverse component  $\rho_{\perp}(r', \theta)$  where  $\rho = \rho_{\parallel}\rho_{\perp}$ . The primed coordinates refer to the position relative to the bunch, over which we integrate to find the fields as a function of the unprimed coordinates. For a Gaussian charge density we have:

$$\rho_{\parallel}(\zeta') = \exp\left(-\frac{\zeta'^2}{\sigma_z^2}\right) \quad (2.50)$$

$$\rho_{\perp}(r', \theta) = \exp\left(-\frac{r'^2}{\sigma_r^2}\right) \quad (2.51)$$

where  $\zeta = z - ct$  is the longitudinal coordinate relative to the bunch. The longitudinal wakefield can now be written as the product of func-

tions  $Z'(\zeta)$  and  $R(r)$ , where  $Z'(\zeta)$  is the partial  $\zeta$  derivative of  $Z(\zeta)$  for convenience when applying the Panofsky-Wenzel theorem:

$$W_{\parallel} = Z'(\zeta)R(r) \quad (2.52)$$

where:

$$Z'(\zeta) = \int_{-\infty}^{\infty} \rho_{\parallel}(\zeta') \cos [k_p(\zeta - \zeta')] d\zeta' \quad (2.53)$$

$$R(r, \theta) = \frac{k_p^2}{2\pi\varepsilon_0} \int_0^{2\pi} d\theta \int_0^{\infty} \rho_{\perp}(r', \theta) K_0(k_p|r - r'|) r' dr' . \quad (2.54)$$

By the Panofsky-Wenzel theorem the transverse wakefield can similarly be written as

$$W_{\perp} = Z(\zeta)R'(r) . \quad (2.55)$$

The integral  $Z'(\zeta)$  can be solved to get:

$$Z'(\zeta) = \sqrt{2\pi}\sigma_z \exp\left(-\frac{k_p^2\sigma_z^2}{2}\right) \cos(k_p\zeta) \quad (2.56)$$

however the integral for  $R(r, \theta)$  is more difficult to evaluate, and simplifying assumptions are necessary. In the case of a wide beam, where the bunch density remains constant over a radius large compared to  $\lambda_p$ ,  $R(0)$  i.e. the value of the integral near the  $z$ -axis remains close to 1. Therefore the electric field on the axis, after some rearrangement of constants, is:

$$E_z = \frac{\sqrt{2\pi} m_e c^2}{e} \frac{q n_b}{e n_p} k_p^2 \sigma_z \exp\left(-\frac{k_p^2\sigma_z^2}{2}\right) \cos(k_p\zeta) . \quad (2.57)$$

In the case of a Gaussian beam,  $R(0)$  can be written in terms of the incomplete gamma function  $\Gamma(a, x) = \int_x^\infty t^{a-1} e^{-t} dt$  [67]:

$$R(0) = \left( \frac{k_p^2 \sigma_r^2}{2} \right) \exp \left( \frac{k_p^2 \sigma_r^2}{2} \right) \Gamma \left( 0, \frac{k_p^2 \sigma_r^2}{2} \right) \quad (2.58)$$

This gives an expression for the total electric field on the axis:

$$E_z = \frac{\sqrt{2\pi} m_e c \omega_p}{e} \frac{q n_b}{e n_p} k_p \sigma_z \exp \left[ \frac{k_p^2}{2} (\sigma_r^2 - \sigma_z^2) \right] \Gamma \left( 0, \frac{k_p^2 \sigma_r^2}{2} \right) \cos(k_p \zeta) \quad (2.59)$$

Considering just the amplitude of the wakefield, the cosine term can be set to 1. The constants can be simplified by writing them in terms of the bunch population  $N$ , and re-writing  $n_p$  in terms of  $\omega_p$ . For a Gaussian bunch  $N = (2\pi)^{3/2} \sigma_r^2 \sigma_z n_b$ :

$$E_z = \frac{qN}{4\pi\epsilon_0} k_p^2 \left\{ \exp \left[ \frac{k_p^2}{2} (\sigma_r^2 - \sigma_z^2) \right] \Gamma \left( 0, \frac{k_p^2 \sigma_r^2}{2} \right) \right\} . \quad (2.60)$$

The term inside the curly brackets is a function of  $k_p \sigma_r$  and  $k_p \sigma_z$ . The amplitude can be rewritten in terms of a function  $\Omega$ :

$$E_z = \frac{qN}{4\pi\epsilon_0 \sigma_r \sigma_z} \Omega(k_p \sigma_r, k_p \sigma_z) . \quad (2.61)$$

For fixed  $n, \sigma_r$  and  $\sigma_z$ ,  $\Omega$  is maximized for a plasma density corresponding to a plasma wavenumber  $k_1$ . At this optimum plasma density, the value of  $\Omega$  depends only on the aspect ratio of the bunch  $r_a = \sigma_r / \sigma_z$ . For small aspect ratios i.e. long, narrow bunches, it was found that the optimum wavenumber  $k_1 \sigma_z \approx \sqrt{2}$  [67]. A factor of  $r_a$  can be taken out to obtain a

new function  $\Pi(r_a)$  which is logarithmic in  $r_a$  for small aspect ratio:

$$E_z = \frac{qN}{4\pi\varepsilon_0\sigma_z^2} \Pi(r_a) . \quad (2.62)$$

An asymptotic expansion of this expression in the small aspect ratio limit gives a usable expression for the wakefield in terms of the bunch shape and plasma density [67]:

$$E_z = \frac{qN}{4\pi\varepsilon_0\sigma_z^2} \frac{2}{e} [-0.577 - 2 \log(r_a)] \quad (2.63)$$

where e here the exponential constant rather than the elementary charge. Using the optimum wavenumber  $k_p\sigma_z = \sqrt{2}$  gives  $r_a = k_p\sigma_r/\sqrt{2}$  and the electric field can be written as:

$$E_z = \frac{qN}{\pi e \varepsilon_0 \sigma_z^2} [0.058 - \log(k_p\sigma_r)] . \quad (2.64)$$

For  $k_p\sigma_r \ll 1$ , the log term is negative and larger than the constant, so the constant can be neglected. The formula for the electric field can be written as a convenient engineering formula:

$$E_z \approx 529 \text{ MVm}^{-1} \frac{q}{e} \frac{N}{10^{10}} \left( \frac{200 \text{ }\mu\text{m}}{\sigma_z} \right)^2 \log \left( \sqrt{\frac{10^{22}}{n_e} \frac{50 \text{ }\mu\text{m}}{\sigma_r}} \right) \quad (2.65)$$

where  $q/e$  is the charge of the incident species in units of the elementary charge, with the exponential constant and the magnitude of the elementary charge absorbed into the leading constant.

The wakefield amplitude in the case of a low aspect ratio bunch depends primarily on the bunch charge and length. There is a weaker logarithmic dependence on the plasma density and bunch radius, subject to the assumptions that lead to the linear theory remaining valid. As noted by Lu *et al.* [67], the linear theory is arrived at by considering the response of the plasma to a point charge, i.e. a charge distribution of infinite density and infinitesimal size, while the assumption of the linear theory is that the bunch density and hence the density perturbation is small compared to the plasma density. However, the wakefield obtained by integrating over this Green's function solution does conform to the assumptions of the linear theory and is hence valid.

### 2.3.1 Transformer ratio

The transformer ratio  $R$  is the ratio of the accelerating field to the decelerating field experienced by the drive bunch. It is important to achieving high efficiency in plasma wakefield accelerators. The transformer ratio can be calculated by considering a pair of infinitesimally short bunches of population  $N_1$  and  $N_2$ , energy per particle  $E_1$  and  $E_2$  at positions  $\zeta_1 = 0$  and  $\zeta_2$  respectively. The wakefield produced per unit charge as a function of position behind the bunch is  $W(\zeta)$ , and the wakefield is assumed to be linear. The energy loss of bunch 1 is [71]:

$$\frac{dN_1 E_1}{dz} = (-eN_1) N_1 e W(0) = -e^2 N_1^2 W(0) . \quad (2.66)$$

Bunch 2 sees the wakefield induced by bunch 1 and its own wakefield. Hence the energy loss for bunch 2 is:

$$\frac{dN_2 E_2}{dz} = (-eN_2)N_2 e W(0) - (-eN_2)N_1 e W(\zeta_2) \quad (2.67)$$

where the first term is due to the wakefield of bunch 2 and the second term is due to the wakefield of bunch 1 at position  $\zeta$ . By conservation of energy, the change in energy of the two bunches must be less than zero:

$$\frac{dN_1 E_1}{dz} + \frac{dN_2 E_2}{dz} = -e^2 [W(0) (N_1^2 + N_2^2) + W(\zeta_2)N_1 N_2] \leq 0 \quad (2.68)$$

or equivalently:

$$W(0) (N_1^2 + N_2^2) + W(\zeta_2)N_1 N_2 \geq 0 . \quad (2.69)$$

$N_1$  and  $N_2$  are arbitrary values, so for the inequality to hold for any  $N_1$  and  $N_2$ :

$$-W(\zeta_2) \leq 2W(0) . \quad (2.70)$$

Applying this inequality to Equation 2.67 gives a limit on the accelerating gradient  $G$  for the trailing bunch:

$$G = \frac{dE_2}{dz} \leq (2N_1 - N_2) e^2 W(0) . \quad (2.71)$$

The energy gain by the trailing bunch will be when it experiences the maximum possible gradient over the maximum possible length. The dis-

tance  $L$  over which the drive bunch loses all of its energy is [71]:

$$L = \frac{E_1}{e^2 N_1 W(0)} \quad (2.72)$$

hence the maximum energy gain for the trailing bunch is:

$$\Delta E_2 = GL = E_1 \left( 2 - \frac{N_2}{N_1} \right) . \quad (2.73)$$

The energy gain is maximized as  $N_2$  approaches zero, and the maximum energy gain for a particle in the trailing bunch is twice the per-particle energy of the drive bunch. The energy transfer efficiency  $\eta$  is the fraction of the drive bunch energy that is transferred to the witness bunch. This can be calculated as:

$$\eta = \frac{N_2 \Delta E_2}{N_1 E_1} = \frac{N_2}{N_1} \left( 2 - \frac{N_2}{N_1} \right) . \quad (2.74)$$

The efficiency is maximized for equal drive and witness bunch charges, however this limits the transformer ratio to 1, as is obvious from energy conservation. In practice it is not possible to achieve all of the limits for the quantities discussed, so the best transformer ratio and efficiency achieved will be lower than the maximum possible values. Although the above derivation uses the assumption of infinitesimally short bunches it can be shown that the same limits apply to real particle bunches if they are longitudinally symmetric about their midpoint, and propagating in a single mode structure.

## 2.4 Ponderomotive force

In a beam-driven plasma accelerator, the force that excites the plasma wave is due to the electric field of the drive bunch. In a laser-driven accelerator the excitation of the plasma occurs due to a less obvious mechanism - the ponderomotive force. This is the force which acts on charged particles that are subject to a non-uniform, oscillating electromagnetic field, such as that of a laser pulse. The motion of particles in the field is a superposition of a rapid oscillation at the frequency of the field and a slow drift of the oscillation centre. It can be shown that the ponderomotive force  $f_p$  that results is the gradient of a ponderomotive potential  $\phi_p$  where [72]:

$$f_p = -\nabla\phi_p ; \phi_p = -\frac{e^2}{2m\omega^2}\langle\mathbf{E}^2\rangle \quad (2.75)$$

where  $\mathbf{E}$  is the electric field of the laser and  $\omega$  is its angular frequency. The ponderomotive force acts to push charged particles in the direction of lower electromagnetic field intensity, and the direction is independent of the charge of the particle. However, the force is inversely proportional to the mass of the particle, and thus the acceleration is inversely proportional to the square of the mass. Due to the much larger ion mass the acceleration due to the ponderomotive force can be considered negligible for ions compared to electrons. This expression for the ponderomotive force is applicable as long as the laser pulse consists of many cycles, and

the plasma electron motion remains non-relativistic, which may not be the case in experiments.

## 2.5 Nonlinear regime

The linear theory of PWFA breaks down as bunch densities become larger than the background plasma density. When the peak bunch density  $n_b$  is larger than the background plasma density  $n_p$ , the bunch is able to expel all plasma electrons from the axis, generating a region of zero plasma electron density, referred to as a blowout region or bubble. A linear treatment of the plasma density is no longer appropriate as no further plasma electron can be expelled, and thus superposition of wakefields is no longer possible. The limits of linear fluid theory were studied by Lu *et al.* [67]. For a negatively-charged driver, reducing the radius of the drive bunch leads to an increase in the accelerating field only up to the point that  $n_b > 10n_p$ . Beyond this density the accelerating field remains constant as bunch radius is reduced. Once the blowout radius is much larger than the bunch radius, the wakefield only depends on the charge of the drive bunch and not its density. It was also found that the predictions of the useful accelerating gradient from applying the linear theory agree with simulation results up to this limit. For a positron drive beam however, it was found that the limit of the linear theory is approximately  $n_b = n_p$ .

An important element of a nonlinear plasma wakefield is the shape of the blowout region. By considering the trajectory of plasma electrons

in the edge of the blowout region - the electron sheath - Lu *et al.* [62] were able to obtain an expression that predicts the blowout radius  $r_b$  as a function of  $\zeta$ , and this prediction was found to be in good agreement with results from particle-in-cell simulation. In the ultrarelativistic blowout regime, where the maximum plasma electron energy is much greater than the electron mass energy, and the maximum blowout radius  $r_m \gg c/\omega_p$ , the formula for  $r_b$  can be written as:

$$r_b \frac{d^2 r_b}{d\zeta^2} + 2 \left( \frac{dr_b}{d\zeta} \right)^2 + 1 = \frac{4\lambda(\zeta)}{r_b^2} \quad (2.76)$$

where  $\lambda(\zeta)$  is the radial line charge of the driving bunch. If the driving bunch is short compared to the plasma wavelength this can be set to zero over the majority of the blowout region. With  $\lambda(\zeta)$  set to zero, the equation for the blowout radius is close to the equation of a circle. As such, the blowout region behind the driver is nearly spherical, while the region near to the driver deviates from this. The ultrarelativistic regime is commonly reached in laser-driven wakefields but not in beam driven cases, as particle beams tend to be much narrower than the plasma wavelength [62, 63]. Hence the blowout region in an LWFA is often approximately spherical and this is referred to as the bubble regime, while in PWFA the nonlinear regime continues to be referred to as blowout.

## 2.6 Summary

The linear theory of plasma wakefield acceleration provides a basis for estimating the important characteristics of the wakefield that is driven by a charged particle bunch. The predictions of the linear theory are accurate under its assumptions of low-aspect ratio bunches and small plasma density perturbations. Even when the parameters of the bunch and plasma are beyond the assumptions of the linear theory it has still been found that the linear theory predictions can be close to the true values. In the extreme nonlinear regime the predictions of the linear theory become less useful.

# Chapter 3

## Particle-in-cell simulation of plasma wakefield acceleration

### 3.1 Why carry out simulations?

There are two major reasons to study plasma wakefield acceleration by simulation prior to constructing experiments. The first is the reduced resource usage of simulations: although the computer time and energy usage of simulations can be significant, high performance computers (HPC) are much more available than particle accelerators with the required beam parameters. The second benefit of simulations is greatly increased flexibility compared to experiment. A simulation's parameters can be changed as required to almost any value, subject to the limitations of computer performance, whereas a conventional accelerator or laser typically has parameters that can vary only over a relatively small range. Despite the advantages of simulations, experiments remain necessary. It

is difficult for a simulation to fully take into account real-world factors such as variations and imperfections in starting parameters and external interference. A simulation must also make assumptions about the length and time scales of the phenomena being studied and choose parameters such as time-step and spatial resolution in order for these to be resolved. An experiment may reveal behaviour that was not expected either due to the simulation failing to resolve the effect or not including the relevant physics. Thus simulations and experiments are both useful and necessary tools for developing new techniques in particle accelerators: simulations provide a convenient way to develop new concepts at low cost in money and time while experiments are necessary to verify simulation results in the real world.

## 3.2 Particle-in-cell simulation

A plasma consists of an ensemble of charged particles - electrons and ions - moving in an electromagnetic field. The fields are determined by the distribution and velocity of charged particles, while the motion of the particles is dictated by the fields as well as the initial conditions. A plasma of interest in plasma wakefield acceleration has typical dimensions of centimetres and density of  $10^{20} \text{ m}^{-3}$ . For a plasma of volume  $1 \text{ cm}^3 = 10 \times 10^{-6} \text{ m}^3$  at this density the total particle number is  $\sim 10^{14}$ . Each particle in a simulation must have a number of position and velocity components associated with it, each typically represented by a 32-bit double precision floating point number, giving a memory requirement

of several hundred bits per particle. The total memory requirement to model every real particle would thus be at least  $\sim 10^{15}$  bytes. Given computer memory capacity is measured in gigabytes i.e. approximately  $10^9$  bytes, modelling such a large number of particles is far beyond the capabilities of current computers, or any that are likely to be available in the foreseeable future. Even if such computers are available, a more efficient method of carrying out these simulations would still be highly desirable. The particles can instead be modelled either as a fluid or as macroparticles, or superparticles, in which a large number of real particles are represented by a single macroparticle carrying the combined charge and mass of the particles it represents [73]. A fluid model is limited compared to a particle model as it does not allow for collisions or a distribution of particle velocities to exist in a single region [74]. In a particle-in-cell simulation particle position and velocity (phase space coordinates) are continuous values, while fields are calculated on a simulation grid. Maxwell's equations and the equations of motion for the particles are then solved using a finite-difference method and thus the simulation is discretized in space and time. The discretization is necessary for the plasma to be modelled on a computer with finite memory. As the resolution of the fields is limited by the grid spacing, the macroparticle model can be valid as real particles represented by the same macroparticle will see similar fields and thus move together.

In the finite difference method, the solution to a differential equation is approximated by replacing the derivative with a finite difference. If the derivative is with respect to time the finite difference is a time-step. A

finite-difference time-domain algorithm for solving Maxwell's equations in isotropic media was developed by Yee [75]. In a simulation with particles present, as opposed to a pure electromagnetic simulation, once the electric and magnetic fields have been calculated, a particle push occurs. The push updates particle positions according to the forces acting on them and the new particle positions are used to calculate charge density and current density which are then used to calculate the fields once more. An illustration of the algorithm is shown in Figure 3.1. The particle push in a PIC simulation typically uses a leap-frog method, in which particle position and velocity are calculated at alternating half-time-steps and are thus not evaluated simultaneously [61].

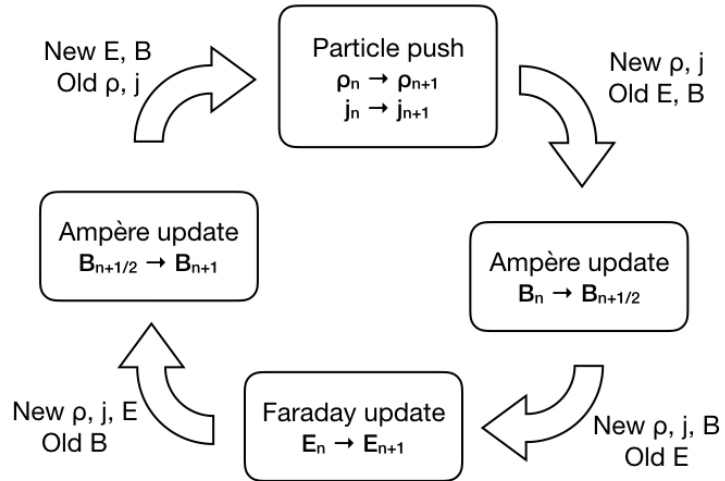


Figure 3.1: Flowchart showing simplified cycle of particle-in-cell simulation scheme.

### 3.2.1 Dimensionality

Despite the reduction in memory and computing power requirements that can be achieved using macroparticles and limited grid resolution, a three-dimensional simulation of a plasma may still be extremely demanding. However, exploiting symmetries in a system to be studied can allow for useful simulations to be run in fewer dimensions. The memory requirements for a simulation can be estimated by considering the number of cells, particles and field components that need to be represented. Consider a  $D$ -dimensional simulation with  $n$  cells in each dimension and  $p$  particles per cell. For each cell there are  $2pD$  variables associated with the particles (position and velocity components for each dimension) and  $3D + 1$  field components (scalar charge density and vector components for each dimension for electric and magnetic fields and current density). There are  $n^D$  cells in total giving a total number of variables of  $n^D [1 + D (3 + 2p)]$ . Assuming ten particles per cell, and each variable requiring 32 bits of memory, this gives memory requirements of 280 GB, 188 MB and 96 kB in three, two, and one dimension respectively. Three-dimensional simulations are thus more likely to be limited by memory requirements, and are too demanding to be realistically carried out on a microcomputer of current capabilities, while one- and two-dimensional simulations may be viable on most computers from a memory perspective, processing power and thus the time required for a simulation may put limits on what is practical. Compared to laser wakefield acceleration simulations, which need to resolve the laser wavelength of less than one

micrometer, PWFA simulations only need to resolve the bunch dimensions which are typically orders of magnitude larger. Hence depending on the exact parameters, a two-dimensional simulation of PWFA may be practical on a desktop computer.

Two-dimensional simulations presented in this thesis use a Cartesian coordinate system. In a two-dimensional Cartesian simulation, the simulation represents a slice of the system being modelled. In VSim the remaining dimension is assigned unit extent, and it is thus necessary to take this into account when measuring quantities that depend on dimensionality such as charge density. Two-dimensional simulations also have some limitation in the accuracy of the transverse variation of fields. Gauss's law in three dimensions gives rise to the inverse-square relationship for field strength, as the area of a Gaussian surface increases with the square of radius. In two dimensions the field strength falls as  $1/r$ , as a Gaussian surface is replaced with a Gaussian loop. Simulations are thus set up in such a way that the field strength in the two-dimensional simulations corresponds to the actual field strength in three dimensions on the simulation axis. Two dimensional simulations are able to provide an indication of the plasma response suitable for validating concepts. Three dimensional simulations are necessary if exact results are required. The Debye radius, which determines the length scale over which plasma screening occurs and is independent of dimensionality, is typically small. For a plasma of density  $1 \times 10^{20} \text{ m}^{-3}$  and temperature 1000 K the Debye length is approximately  $0.2 \mu\text{m}$  whereas the variation in the transverse

fields of the bunch are over length scales comparable to the size of the bunch i.e. tens of  $\mu\text{m}$ .

### 3.2.2 Instabilities

Any simulation can only approximate a physical system, so there is a risk that as a simulation proceeds over a large number of time-steps the inaccuracies of the simulation build up in a runaway fashion and lead to results that do not correspond to the real world. One important condition for stability is the Courant-Friedrichs-Lowy (CFL, or Courant) condition [76], which limits the size of the time-step that can be taken when using a finite-difference method. The CFL condition requires that finite difference calculations must take into account all relevant information [77]. Since a calculation is based on the fields  $(E, B, j, \rho)$  at the cell boundaries, taking into account properties of a cell and adjacent cells only, if the time step is longer than the light travel time across a cell, non-adjacent cells may influence one another and thus not all information is taken into account. Mathematically, in three dimensions the CFL condition requires [75]:

$$\Delta t < \frac{1}{c} \sqrt{(\Delta x^2) + (\Delta y^2) + (\Delta z^2)} \quad (3.1)$$

The CFL condition is necessary for stability but it does not guarantee that a simulation will be accurate. It is also necessary to ensure that the time-step is short enough to resolve the shortest time-scale effects of interest; in a plasma accelerator simulation this may be the plasma fre-

quency or laser frequency if a laser is present. Since the spatial grid must also resolve the wavelength of the plasma or laser oscillations, the CFL condition and requirement to resolve are likely to give similar restrictions.

Another instability that can lead to unphysical results is the numerical Cherenkov instability. This occurs when relativistic particles in a simulation are able to exceed the phase velocity of short-wavelength fields [61]. Since the instability results from a particle travelling faster than the speed as light in that medium, where the medium in question is the simulation grid, the numerical Cherenkov instability is comparable to real-world Cherenkov radiation, hence the name. The instability cannot be completely eliminated, but it can be kept under control by current smoothing [78].

### 3.3 PIC simulations using VSim

There are a wide variety of PIC codes available which offer different features and are thus suitable for different purposes. The simulations that provided the results presented in this thesis were carried out using VSim [74, 79]. VSim is an arbitrary-dimensional, explicit PIC code and importantly provides a Poisson solver routine, which allows the simulation to be initialized with a beam present with correct electric and magnetic fields. In simulations of drive and witness bunches it is desirable to separate the bunches into different species in order simplify analysis. The included Poisson solver in VSim was not able to initialize fields for multiple beam species, as the second species would overwrite the fields of the

first. It was necessary for the field initialization macro to be modified in order to avoid this conflict.

The numerical Cherenkov instability was also found to be a significant problem in simulations over several thousand time-steps. The instability appeared as an alternating field with spatial frequency similar to the grid spacing. It was initially seen to grow in the longitudinal component of the electric field of the beam, which is very small for a highly relativistic bunch, making the initially small instability more noticeable. Over the course of several thousand time-steps however, the amplitude of the spurious fields grew until it was comparable to that of the plasma fields, and thus could be assumed to significantly impact the reliability of the simulation results. It was necessary to ensure that the effect of the numerical Cherenkov instability could be kept small enough that the simulation results would remain reliable. Current smoothing, using four passes of a 1-2-1 filter before applying the Ampère update step, was applied using a macro provided by J. Smith. This was found to keep the numerical Cherenkov instability under control to a sufficient degree for the simulation lengths required.

A VSim simulation is defined by a preprocessor file, which is processed to produce a less-human-readable input file, which is in turn read by the simulation engine [80]. The preprocessor file for the simulations presented here was parameterized in terms of resolution, in cells per beam RMS length/width, and extent, in multiples of beam rms. The resolution was chosen in order to resolve the plasma wavelength and the bunch width and length. In most simulations the plasma wavelength was sig-

nificantly longer than the bunch length, and the bunch length greater than the width, making the bunch width the smallest size that needed to be resolved. A resolution of approximately 10 cells per RMS width was found to be sufficient to resolve a Gaussian bunch. However, a particle bunch is focused by a plasma, and will thus decrease in transverse size, and reach a minimum size that depends on its transverse emittance. Hence a resolution higher than that needed to resolve the initial bunch may be required. In a simulation where the emittance is initially zero, the minimum bunch size may be very small (though emittance will not remain zero due to non-linear focusing and space charge effects). However, this may not invalidate the simulation results as the total beam charge is preserved and the fields at a large radius from the bunch will remain similar.

In the direction transverse to that of bunch propagation, a Matched Absorbing Layer (MAL) boundary condition was used. This boundary condition provided by VSim is similar to the more commonly used Perfectly Matched Layer (PML), in that it damps incoming waves in a specified region at the simulation boundaries, however it is more stable in the presence of particles than the PML [80]. The boundary condition for particles was an absorbing box: particles which reach the simulation boundaries are removed. Results were monitored to ensure that no significant portion of particles escaped the simulation transversely. In the case of particles escaping the simulation window or other parameters were modified such the fraction of escaping particles was kept small.

Although two-dimensional simulations typically require relatively little memory, and can in principle be run on a desktop computer, simulations of the resolution and propagation length required were too demanding on processing power to be realistically run on a desktop. Increasing the resolution not only increases the number of cells present and thus the number of calculations that need to be performed each time-step, but also reduces the CFL limit on the time-step, requiring a greater number of time-steps to be taken for a given overall simulation length. A single simulation may take several hours to complete, which would make detailed parameter scans impractical due to the time required. The supercomputers JUROPA and its successor JURECA at Forschungszentrum Jülich were used for these simulations under projects HHH20 and HHH36. These machines also have sufficient memory to carry out three-dimensional simulations which are impractical on a desktop computer.

## 3.4 Summary

Particle-in-cell simulation is a useful tool for studying and developing plasma accelerator techniques prior to testing these in experiments with associated demands on finances, facilities, space and expertise. However, the limitations of simulations must also be recognized. In order to reduce the computing requirements on simulations, reduced dimensionality, resolution and particle number may be used. The limited accuracy and reliability of simulations makes experiments necessary to verify results in the real world, but the foundation laid by simulations ensures that

experimental tests can make the most efficient use possible of limited resources.

# Chapter 4

## Beam-driven plasma wakefield acceleration

### 4.1 The CLARA accelerator

CLARA (Compact Linear Accelerator for Research and Applications) is a proposed electron linear accelerator at Daresbury Laboratory [81]. Its main purpose is to serve as a test facility for free electron laser (FEL) techniques, providing a dedicated machine that is not restricted by customer use, unlike many existing light sources. It has been proposed to add a Plasma Accelerator Research Station (PARS) to CLARA on a separate beam-line parallel to the main CLARA beam-line, with the CLARA electron beam transported to PARS using a dogleg prior to the FEL undulators [82]. This would enable PARS to operate in parallel with CLARA without interfering with FEL experiments, as a PWFA experiment would typically only require electron bunches at a low repe-

tition rate, at least for initial experiments. A diagram of the proposed PARS layout is shown in Figure 4.1. The PARS beam-line is proposed to run parallel to the CLARA beam-line with an offset of 1.5 m giving sufficient room for a final focus, plasma cell, diagnostics and beam dump while being contained within the shielding provided for the main CLARA machine.

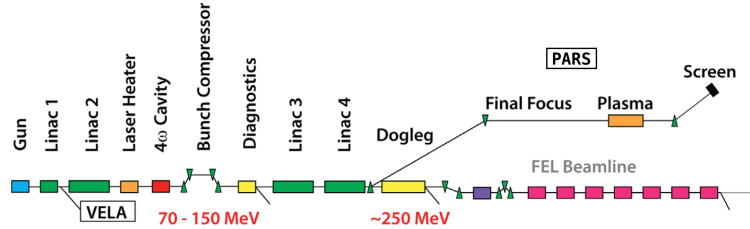


Figure 4.1: Diagram showing the proposed layout of PARS in relation to CLARA. Credit G. Xia. Not to scale.

CLARA is designed to be capable of operating in a number of modes in order to produce different beam profiles for applications with different FEL schemes. The ultra-short pulse mode and Self-Amplified Spontaneous Emission (SASE) mode are of particular interest when considering the application of CLARA to plasma wakefield acceleration experiments. Beam parameters for the relevant operating modes are shown in Table 4.1.

When considering the application of CLARA to PWFA, among the most important parameters are bunch density and peak current, and the bunch length. The SASE and ultra-short modes appear to be the most attractive as they offer high currents and short bunches. The most suitable bunch parameters depend on the plasma source that would be used in an experiment. The available plasma density determines the

Table 4.1: Relevant CLARA beam parameters from conceptual design report [81].

Parameter	Unit	Seeding	SASE	Ultra-short
Max energy	MeV	250	250	250
Bunch charge	pC	250	250	20-100
Repetition rate	Hz	1-100	1-100	1-100
RMS bunch length	μm	255-75	75	7.5
RMS bunch radius	μm	20	20	20
Aspect ratio	-	0.08-0.27	0.27	2.67
Norm. emittance $x/y$	mm mrad	$\leq 1$	$\leq 1$	$\leq 1$
Peak bunch density	$10^{21} \text{ m}^{-3}$	1.0-3.3	3.3	2.6-13
Peak current	A	125-400	400	$\sim 1000$

accelerating gradient that can be produced for a given bunch, and the plasma length may limit the energy gain that can be achieved. If the plasma length is relatively long, too high an accelerating gradient would cause the bunch energy to be depleted before the end of the plasma, while if the plasma length is short, the energy gain will be limited if the accelerating gradient is not large. Applying the linear theory of PWFA to the CLARA bunches listed gives an estimate of the accelerating gradients that can be achieved as a function of plasma density. For convenience, the engineering formula for the gradient predicted by the linear theory is repeated here:

$$E_z \approx 529 \text{ MV m}^{-1} \frac{q}{e} \frac{N}{10^{10}} \left( \frac{200 \text{ μm}}{\sigma_z} \right)^2 \log \left( \sqrt{\frac{10^{22}}{n_e}} \frac{50 \text{ μm}}{\sigma_r} \right). \quad (4.1)$$

For the SASE mode bunch for a plasma density equal to the peak bunch density, the linear theory gives an amplitude of  $864 \text{ MV m}^{-1}$ , while for the ultra-short mode with the maximum charge of  $100 \text{ pC}$ , the formula

gives an amplitude of  $18.5 \text{ GV m}^{-1}$ . However, for the case of the ultra-short mode, the linear theory prediction is not accurate as it is based on the assumption of a low-aspect ratio bunch, and the aspect ratio for the ultra-short mode is greater than one. The actual gradient that should be expected for the ultra-short mode would be significantly lower than predicted by the above formula.

## 4.2 Plasma sources

The plasma sources considered for experiments using CLARA include the alkali metal vapour oven source, gas jet and pre-ionized discharge sources. The choice of plasma source for experiments is determined by the requirements on plasma density, length and duration, and the complexity and cost of the necessary equipment. The main plasma sources used in plasma wakefield experiments and briefly discussed and their strengths and weaknesses compared.

### 4.2.1 Alkali metal vapour source

The alkali metal vapour oven consists of a tube connected to one or more chambers containing an alkali metal - typically lithium or rubidium. Under vacuum, the metal is heated by an electrical heating element, which causes the metal to sublime. This generates a low-pressure neutral vapour within the tube. The vapour can then be ionized to generate a plasma. It can also be built to an arbitrary length by providing a sufficient number of vapour source chambers for the length of plasma

required, subject to the method of ionization being capable of acting over the length in question. Two suitable methods for ionizing a long column of alkali metal vapour in a beam-driven PWFA are laser-ionization and field ionization. Field ionization by the particle bunch is possible if the transverse electric field of the bunch is sufficiently large. The rate of ionization by an electrostatic field can be calculated using the Ammosov-Delone-Krainov (ADK) formula [83]. The time resolved ADK formula is as follows [80]:

$$R_i = 4.13 \times 10^{16} \frac{Z^2}{2n_{\text{eff}}^2} \left( \frac{2e}{n_{\text{eff}}} \right)^{2n_{\text{eff}}} \frac{1}{2\pi n_{\text{eff}}} \left( 2 \frac{E_h}{E_L} \frac{Z^3}{n_{\text{eff}}^3} \right)^{2n_{\text{eff}}-1} \exp \left( -\frac{2}{3} \frac{E_h}{E_L} \frac{Z^3}{n_{\text{eff}}^3} \right) \quad (4.2)$$

where  $R_i$  is the rate of ionization,  $Z$  is the charge state of the ionized particle,  $n_{\text{eff}} = Z/\sqrt{U/13.6 \text{ eV}}$ ,  $U$  is the ionization energy of the atom in eV,  $E_L$  is the ionizing electric field strength and  $E_h = m_e^2 q_e^5 / 4\pi \epsilon_0 \hbar^4 = 5.13 \times 10^{11} \text{ V m}^{-1}$ . To obtain an order-of-magnitude estimate of the rate of ionization required to field-ionize a plasma in PWFA, one can consider that ionization must take place at a rate sufficient that the vapour is substantially or completely ionized over the duration of the bunch as it passes through. For a bunch length of  $7.5 \mu\text{m}$ , the temporal bunch length is  $25 \text{ fs}$  so the rate of ionization must be much greater than  $4 \times 10^{13} \text{ s}^{-1}$ . Figure 4.2 shows ionization rate as a function of electric field for lithium and rubidium. In order to achieve the required rate of ionization, an electric field of approximately  $10 \text{ GV m}^{-1}$  would be required. The large electric fields necessary to ionize the vapour by field ionization requires the use of alkali metal vapour due to these elements having the lowest first

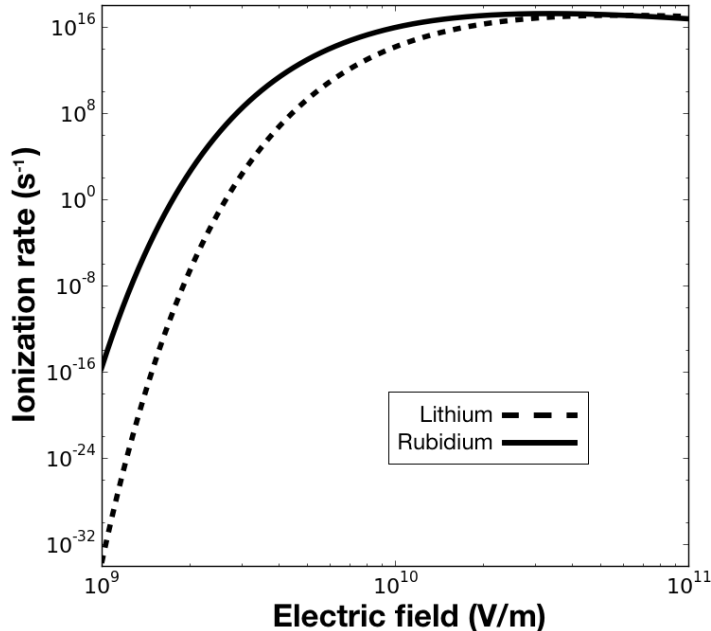


Figure 4.2: Tunnelling ionization rate as a function of electric field for lithium and rubidium.

ionization energies: 5.39 eV for Li and 4.18 eV for Rb [84]. The first ionization energies of sodium and potassium lie between these values. The reactivity of these elements makes them difficult to handle, potentially complicating the operation of a plasma source that uses them.

The electric field of the CLARA bunches can be estimated using Gauss's law, assuming a uniform cylindrical distribution. This gives an electric field at 100  $\mu\text{m}$  of  $1.2 \text{ GV m}^{-1}$  for the ultra-short pulse mode, indicating that the CLARA beam does not have a sufficiently large field to ionize an alkali metal vapour effectively, by a factor of approximately 10. Monte Carlo ionization simulations carried out using VSIM confirmed that in order to achieve field ionization using the CLARA beam the

bunch radius would have to be dramatically decreased. If an alkali metal vapour plasma source were to be used with CLARA, it would require laser-ionization, or another form of external ionization, to generate a plasma. Experiments using field ionization were carried out at FACET, and it was found that the increased response time of the plasma that results led to an effect referred to as bunch head erosion [40]. Due to the lack of plasma focusing the head of the bunch was scattered by the neutral vapour and a density decrease of the bunch head resulted. This is a concern in PWFA as one of the main attractions of the beam-driven accelerator is that it can achieve stable acceleration over extended distances. As a combined result of the large fields required and bunch head erosion, field ionization of alkali metal vapour is not considered to be a viable plasma source for wakefield acceleration.

#### 4.2.2 Gas jet source

A gas jet source consists of a nozzle emitting a jet of gas perpendicular to the axis of the beam. This gas jet can be ionized by a laser to form a plasma. The mechanism by which the gas is ionized by the laser is multiphoton ionization, in which an atom absorbs several laser photons of energy below the threshold for ionization almost simultaneously, providing sufficient energy for ionization to occur [85]. Gas jet sources are commonly used in laser wakefield acceleration where the short plasma length is not a major limitation, as the accelerating length is limited by intrinsic factors. Since a major advantage of PWFA over LWFA is the

longer lengths over which acceleration is possible, gas jet plasma sources are not generally well suited to PWFA experiments.

### 4.2.3 Discharge source

Another means of generating a plasma is a discharge source, in which an electrical discharge ionizes a neutral gas. A discharge source avoids relying on the availability of a high-intensity laser or particle bunch, needing only a relatively cheap high-voltage power source. A discharge source may be constructed from a glass capillary into which a low-pressure gas is introduced. Electrodes at each end of the capillary put a high voltage across the gas. As the ionization takes place via breakdown rather than by tunnelling as in field ionization, the voltage required is much lower. The breakdown voltage is given by Paschen's law, and depends on the intrinsic properties of the gas expressed via constants  $A$ ,  $B$  and  $\gamma$ , its density  $\rho$  and the gap between electrodes  $d$  as follows [86]:

$$V_B = \frac{Bpd}{\ln(Apd) - \ln[\ln(1 + 1/\gamma_s e)]} . \quad (4.3)$$

The lower field requirement for the discharge source allows a gas with higher ionization energy to be used compared to an alkali metal vapour, simplifying the system. Cheap, commercially available substances which are gaseous at room temperature and pressure, such as nitrogen, argon or hydrogen may be used [87]. A discharge source may have some safety concerns that need to be considered. Hydrogen may be attractive due to its low first ionization energy compared to more inert gases, but

there may be a risk of fire or explosion. Nitrogen and argon are inert and cheap, but have larger ionization energy than hydrogen. While the required voltages for discharge in these gases can be routinely achieved the requirement will lead to higher equipment costs. Heavier gases may also be multiply ionized making control of the plasma density more difficult whereas hydrogen, having a single electron, can only be singly ionized. Another consideration in choice of plasma source is the mass of the ions: it is usually assumed that the ions are much heavier than the electrons and thus do not move over the timescales considered in plasma wakefield acceleration. If the fields are very large and the ions relatively light however, this assumption may not be valid. It may thus be desirable to use a higher mass species for a plasma source to minimize ion motion.

### 4.3 PWFA with a single bunch

In order to investigate the viability of PWFA experiments at PARS, the experiment was modelled using particle-in-cell simulation. The CLARA SASE mode was chosen initially, as it was considered more important to demonstrate acceleration over an extended distance than to achieve the highest possible accelerating gradient. The simplest experiments that could be conducted using PARS involve driving a plasma wakefield with a single bunch. The properties of the wakefield can be determined by its effect on the bunch. If the bunch is sufficiently long compared to the plasma wavelength, the tail of the bunch can be accelerated, allowing direct measurement of the accelerating field. If the bunch is short compared

to the plasma wavelength, and no portion of the bunch is in an accelerating region, the decelerating field on the bunch can still be used to infer the amplitude of the wakefield. Measurements of the bunch after it has left the plasma are limited to determining the time-integrated wakefield at the bunch location. Simulations, however, allow for the electric field to be monitored directly everywhere. The longitudinal electric field after 3 mm propagation for a plasma density of  $3 \times 10^{21} \text{ m}^{-3}$  is shown in Figure 4.3a. The accelerating electric field of approximately  $1800 \text{ MV m}^{-1}$  is significantly larger than is predicted by the linear theory. As a result of the plasma density being initially comparable to the peak bunch density, the assumption of the linear theory that the density perturbation is small compared to the background density is not valid. After the drive bunch is focused by the plasma its density increases substantially and the linear theory assumption is even less valid. Nonetheless the linear theory prediction is within a factor of two of the simulated gradient. This is in line with expectations that for an electron drive bunch the applicability of the linear theory holds for a beam density up to ten times the plasma density. A pseudocolour plot of the plasma electron density is shown in Figure 4.3b where the blowout region is visible with a maximum blowout radius of approximately  $30 \mu\text{m}$ . This can be compared to the plasma wavelength of  $612 \mu\text{m}$  showing that the ultrarelativistic blowout regime (see Section 2.5) is not reached as evidenced by the non-spherical blowout region.

Previous simulations with the CLARA bunch have shown that the prediction of the linear theory is closely matched for an initial plasma

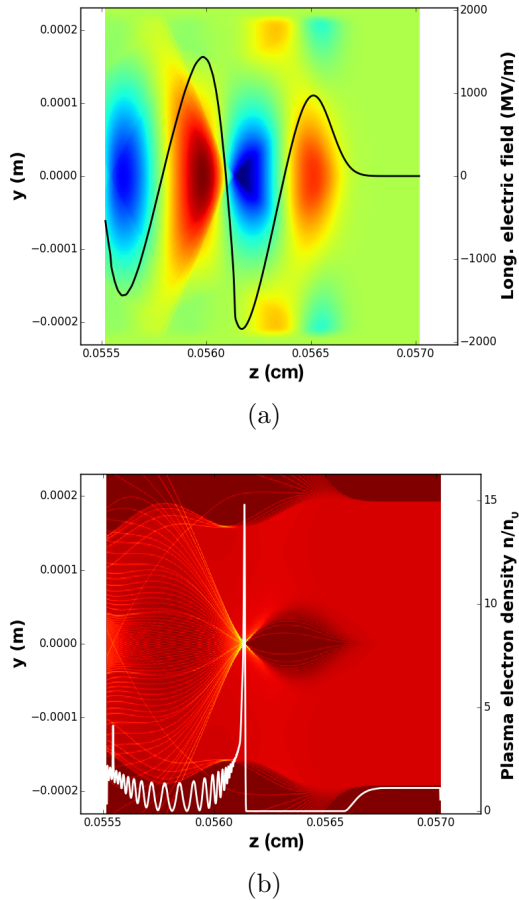


Figure 4.3: Pseudocolour plot and lineout along the  $z$ -axis of (a) the longitudinal component of the electric field and (b) plasma electron density for the 250 MeV CLARA bunch after 5 cm propagation.

density ten times higher than the peak bunch density [82], while for a density an order of magnitude lower than the bunch, the accelerating field is considerably lower.

### 4.3.1 CLARA Front End

In order to support potential preliminary experiments, simulations were carried out using bunch parameters for CLARA Front End. This in-

cluded both Gaussian bunches using baseline parameters and particle distributions from particle tracking for the full accelerator. Baseline parameters are given in Table 5.1. This gave an opportunity to compare results from these two significantly different representations of the output of the same experiment and determine how accurately a Gaussian bunch could approximate a realistic distribution for the purposes of plasma wakefield acceleration. Two- and three-dimensional simulations were also compared for the realistic distribution. The plasma was modelled as a cosine-flat-top profile: a cosine function ramp at the start and end of the plasma joined by a constant density region between. A plasma density of  $10^{21} \text{ m}^{-3}$  was chosen giving a plasma wavelength of 1.06 mm.

Since the energy of the CLARA-FE bunch with other parameters in the required range that could be provided to the experimental area was initially uncertain, simulations were carried out to determine the dependence on initial energy of the final properties of the bunch after passage through the plasma. Theory shows that the wakefield that can be driven by a bunch does not depend directly on the bunch's energy, but that the distance over which the wakefield can be driven before the bunch's energy is depleted does. In the case of a single bunch driven plasma wakefield where the tail of the bunch samples the field driven by the bunch head, after some distance the middle portion of the bunch which experiences the largest decelerating gradient becomes non-relativistic. The non-relativistic portion of the bunch then slips relative to the wakefield and moves out of the decelerating phase. The resultant reduction in the amount of the bunch that is available to drive the wakefield leads to a

decrease in the wakefield amplitude and hence the accelerating gradient that acts on the tail of the bunch.

The longitudinal phase space for the CLARA-FE bunch with initial energy of 10 MeV and 45 MeV are shown in Figure 4.4. In both cases some energy gain in the part of the bunch that initially forms the tail can be observed, but in the 10 MeV case the energy gain is substantially less despite the amplitude of the wakefield that is initially driven by the bunch being the same in both cases. The rearmost portion of the bunch in the 10 MeV phase space is the part of the bunch that was initially located in the region of maximum decelerating gradient and subsequently slips backwards as a result of energy loss. The change in average accelerating

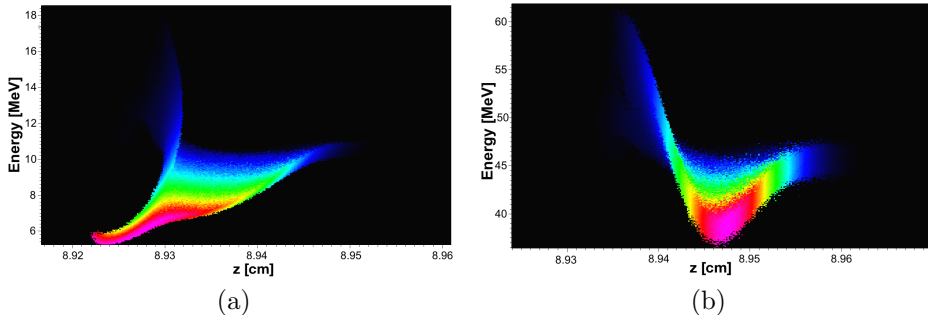


Figure 4.4: Longitudinal phase space for (a) 10 MeV and (b) 45 MeV initial energy for the CLARA-FE bunch after 9 cm propagation through the plasma.

gradient for particles in the tail of the bunch as a result of changing the initial energy of the bunch is shown in Figure 4.5. Above 20 MeV initial energy, the energy loss over the 10 cm plasma is insufficient to cause any portion of the bunch to become non-relativistic and beyond this energy

the initial energy of the bunch has no effect on the energy gain of the tail.

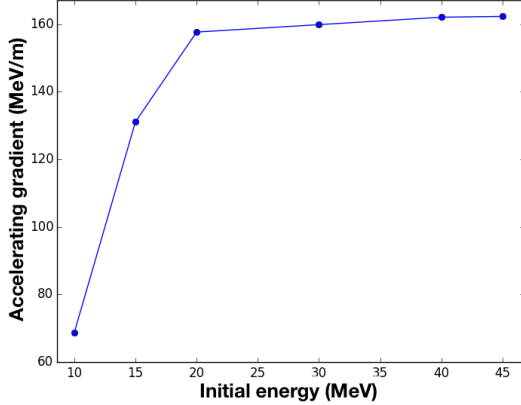


Figure 4.5: Plot of accelerating gradient experienced by particles in the tail of the CLARA-FE bunch against the initial energy of the bunch.

The realistic CLARA-FE particle distribution was generated using the particle tracking code ASTRA [88, 89]. This produced a three-dimensional particle distribution which was then compressed into two dimensions for use in two-dimensional particle-in-cell simulation. The weight on the macroparticles was scaled by a factor of  $\sqrt{2\pi}\sigma_r$  so that the peak density of the bunch was the same in both cases. Compared to the Gaussian particle distributions that were previously simulated, the realistic distribution has some important differences. The bunch has a correlated energy spread while the Gaussian bunches were assumed to have no correlated energy spread. This does not have a significant impact on the results of plasma wakefield acceleration as the final energy spread of the bunch after being accelerated by a large gradient over a large distance is an imprint of the variation of the accelerating gradient and the energy spread of the original bunch is insignificant. A more important

difference in the realistic bunch is the longitudinal charge distribution. Instead of a Gaussian this is a short, high density head followed by a longer low density tail. This is a convenient distribution for single-bunch plasma wakefield experiments, as it allows the wakefield to be driven primarily by the head with the tail sampling the wakefield. Figure 4.6 shows the initial and final longitudinal phase space for the realistic CLARA-FE bunch for a plasma of density  $1 \times 10^{22} \text{ m}^{-3}$  and of length 10 cm. The maximum energy of particles in the tail of the bunch is approximately 60 MeV giving an energy gain of 12 MeV corresponding to an average accelerating gradient of  $120 \text{ MeV m}^{-1}$ .

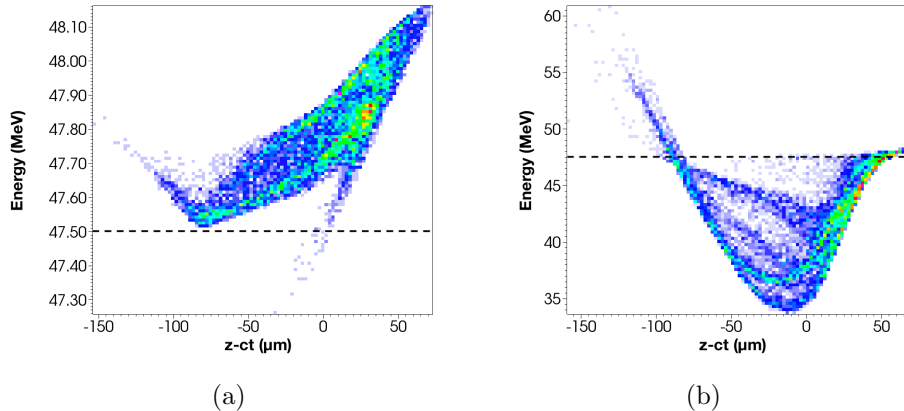


Figure 4.6: Longitudinal phase space for realistic CLARA-FE bunch, before (a) and after (b) propagation through a 10 cm plasma. Note the difference in  $y$ -axis scale between the two plots. The dotted line indicates 47.5 MeV.

The flattening of the particle distribution for two-dimensional simulation compromises the reliability of the results. Hence three-dimensional simulations were also carried out using the original distribution. The main difference between the original distribution and the flattened ver-

sion is that the long tail of the bunch is offset from the main bunch in  $z$ . This means that the tail does not experience the same accelerating field in both cases. However, the wakefield amplitude in the 3D case was larger and the maximum energy gain was slightly larger than the 2D case, at  $147 \text{ MeV m}^{-1}$ . An isosurface plot of the longitudinal electric field for the 3D case is shown in Figure 4.7. This can be compared with a pseudocolour plot showing the equivalent data in the 2D case, Figure 4.8. The two cases show both qualitatively similar results, with the shape of the wakefield mirroring the transverse distribution of the drive bunch. In the 2D case differing electric field at  $|y| > 1 \text{ mm}$  is in the region outside of the plasma column. The similar field in the 3D case is not shown as it would block the detailed wakefield of interest.

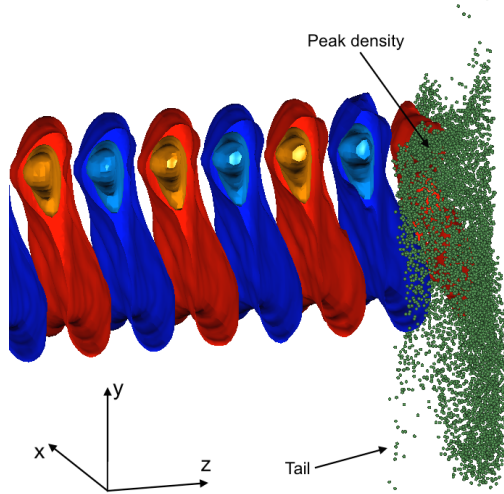


Figure 4.7: Isosurface plot of longitudinal electric field, and scatter plot of drive bunch particles for 3D simulation of CLARA-FE with a realistic particle distribution. The isosurface plot is sliced along the plane  $z = 0$ . Simulation macroparticles are represented by green spheres.

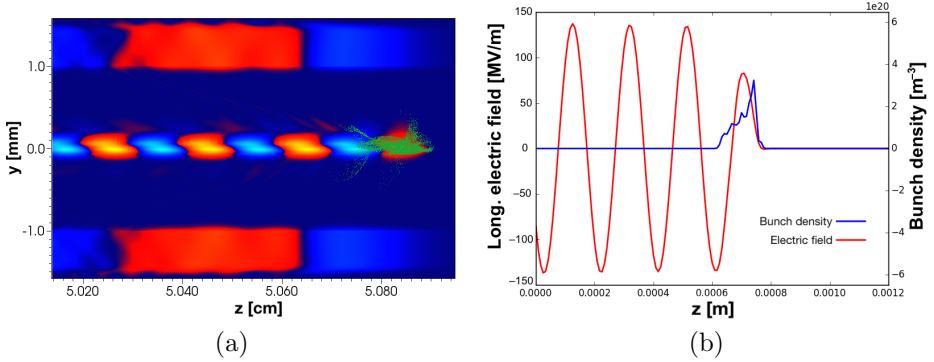


Figure 4.8: Plots showing electric field and bunch for a realistic CLARA-FE bunch projected into 2D, after a propagation distance of 5.08 cm. Macroparticles are green points. The lineout shows the longitudinal electric field and bunch density along the  $z$ -axis. The direction of propagation is to the right for both sub-figures.

## 4.4 PWFA with two Gaussian bunches

A two-bunch distribution is desirable to study beam loading effects and to produce a quasi-monoenergetic accelerated bunch. Generating a two-bunch distribution and delivering it to PARS however, is challenging. A two-bunch distribution has been successfully used in PWFA at FACET. This was achieved by dispersing a chirped bunch using a chicane beamline, and using a mask to scatter the central region of the bunch before reversing the dispersion. This generated two closely space bunch remainders. This method leads to a loss of a substantial portion of the bunch, which is less of a concern when using the high charge SLAC bunch compared to the relatively low charge CLARA bunch.

The practicalities of producing a two-bunch distribution with CLARA are not investigated here; instead the potential applications of such a

structure are considered. The aim is to establish whether pursuing a capability to generate two bunch structures would be worthwhile. To this end simulations were carried out using both symmetrical bunches and shaped bunch profiles. These studies may also provide information on the applicability of other similar accelerators to plasma wakefield acceleration.

The influence of the witness bunch of the wakefield is important in determining the resultant properties of the accelerated bunch. As discussed in Section 2.3.1, a compromise must be reached between efficiency and accelerating gradient. If the witness bunch charge is large, efficiency is high but average gradient will be low. In addition, as the front of the witness bunch will experience the unloaded wakefield while the rear of the bunch experiences a field from which a portion of the energy has been absorbed by the witness, in the case of a longitudinally symmetric witness bunch beam loading will also lead to an increase in energy spread of the witness bunch.

The plasma density used was  $5 \times 10^{21} \text{ m}^{-3}$ , somewhat higher than the peak bunch density. The witness bunch had RMS length of 10  $\mu\text{m}$  and radius 25  $\mu\text{m}$ . The drive bunch charge was 250 pC and its length was 75  $\mu\text{m}$ . The effect of witness bunch charge on the resultant energy of the witness bunch, and its energy spread, are shown in Figure 4.9. For large witness bunch charges, overall energy is lost from the witness bunch. This is a result of the witness bunch charge being sufficient to reverse the sign of the wakefield. The energy spread is minimized for intermediate bunch charge, where the wakefield is partially flattened. This is illustrated in

Figure 4.10, which shows the longitudinal electric field on the axis for different bunch charges. The wakefield profile in two dimensions for the case of Gaussian drive and witness bunches is shown in Figure 4.11. These results indicate that a witness bunch charge of approximately 20% of the drive bunch charge provides a good compromise between efficiency and beam quality.

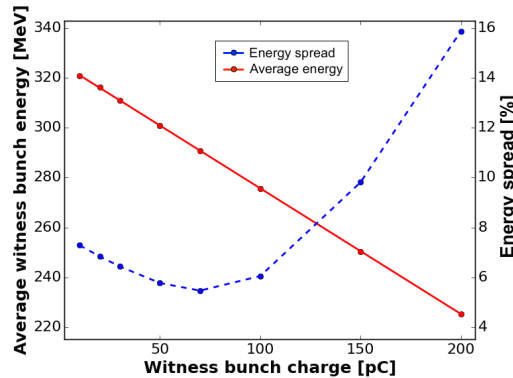


Figure 4.9: Energy spread and average witness bunch energy after 10 cm propagation through a plasma for variation of witness bunch charge, for constant witness bunch dimensions and drive bunch and plasma parameters.

Although choosing appropriate parameters for a Gaussian bunch can improve the resultant beam quality, the symmetrical bunch profile limits the degree of improvement possible. Specially shaped bunch profiles can however exceed the capability of Gaussian bunches in modifying the wakefield to achieve the highest possible beam quality.

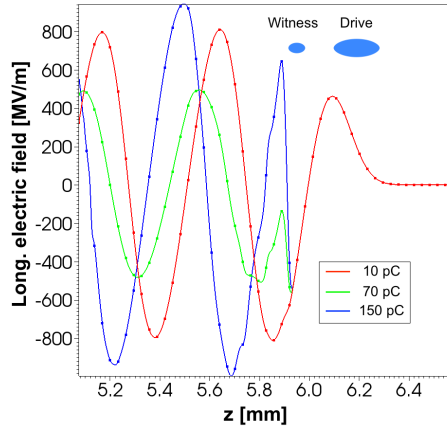


Figure 4.10: Longitudinal electric field on the axis for witness bunch charges of 10, 50 and 150 pC. Both drive and witness bunches were Gaussian in profile, and the witness bunch dimensions were the same for all charges.

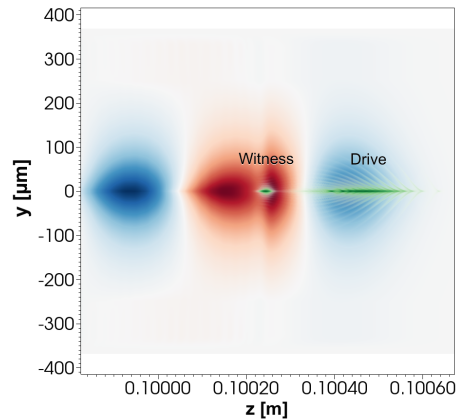


Figure 4.11: Longitudinal electric field (red/blue) and bunch charge distribution (green) for Gaussian drive and witness bunches. The direction of propagation is to the right.

## 4.5 Shaped bunches

The accelerating and decelerating fields within a bunch are the primary concern in any accelerator as this is what determines the energy loss of the drive bunch, and the energy gain and quality of the witness bunch.

One way to modify the fields within a bunch is to use a bunch with a particular current profile which modifies the wakefield to have the desired properties. In this section, the effect of certain current profiles for the drive and witness bunches are considered.

#### 4.5.1 Longitudinally shaped drive bunch

The maximum transformer ratio that can be achieved using a longitudinally symmetric drive bunch, in a single mode structure, is 2 [90]. It is possible to achieve higher transformer ratios using multiple modes that superimpose in such a way as to increase the accelerating field [91]. However, this is not relevant to a plasma wakefield accelerator where only a single mode with frequency  $\omega_p$  is supported. A tailored bunch profile however, can achieve an increased transformer ratio in a single-mode structure. For a triangular bunch profile, in which the current ramps up linearly over the length of the bunch (see Figure 4.12), the decelerating field can be calculated by integrating the wake potential over time, where the wake potential is given by  $A \cos(\omega t)$  [91] where  $A$  is an amplitude and the frequency  $\omega$  is the frequency of the mode being considered. Assuming a sinusoidal wakefield (i.e. the linear regime) this is equally valid for a wakefield in an RF cavity or a plasma wakefield, in which case the frequency is the plasma frequency  $\omega_p$  and the structure is single-mode. The bunch current is given by  $I(t) = I\omega_p t$  for  $0 < t < T$  and zero otherwise, with  $T = 2N\pi/\omega_p$  where  $N$  is an integer. Inside the bunch the limit on

the integral is a point  $t$  within the bunch:

$$V^-(t) = I\omega_p \int_0^t At' \cos [\omega_p(t-t')] dt' = \frac{AI}{\omega_p} (1 - \cos \omega_p t) \quad (4.4)$$

and behind the bunch the potential is given by integrating over the whole bunch:

$$V^+(t) = I\omega_p \int_0^T At' \cos [\omega_p(t-t')] dt' = \frac{2N\pi AI}{\omega_p} \sin (\omega_p t) . \quad (4.5)$$

$V^-$  and  $V^+$  are the decelerating potential within the bunch, and the partially accelerating potential behind the bunch, respectively. Inside the bunch, the factor  $1 - \cos(\omega_p t)$  means the field is always decelerating, and the amplitude is  $AI/2\omega_p$ . Behind the bunch the field is sinusoidal with amplitude  $2N\pi AI/\omega_p$ . The transformer ratio is the ratio of the amplitudes of these fields  $R = \pi N$ . Hence transformer ratios greater than two can be achieved using a triangular bunch which rises over an integer number of plasma wavelengths.

The requirement that the bunch be a multiple of the wavelength of the mode in question creates a challenge in a plasma accelerator as bunch density is an important consideration in achieving high accelerating gradients. If the bunch charge is limited, extending the bunch length or increasing the plasma density to reduce the plasma wavelength may lead to the plasma density becoming very large compared to the bunch density, which limits the wakefield amplitude.

Shaped bunch profiles have been successfully demonstrated experimentally. One method is to manipulate the phase space of an initially chirped bunch using sextupole magnets within a dogleg beam-line [92]. A ramped current profile has also been produced using a superconducting linac operating at two frequencies [93]. This scheme was demonstrated using the FLASH accelerator at DESY. The ramped bunch scheme is intended to be used in experiments on dielectric wakefield acceleration and with the FLASHForward plasma wakefield experiment. A ramped drive bunch scheme in the blowout regime has been developed and demonstrated in simulations [94]. It was found that a similar triangular bunch profile is effective in the non-linear regime. The use of a train of bunches with increasing charge per bunch to achieve a similar transformer ratio increase to the ramped bunch scheme was studied in one-dimensional particle-in-cell simulation by Katsouleas *et al.*[66]. The purpose of the simulations presented here is to show that a shaped bunch with parameters similar to the CLARA beam is capable of achieving an increased transformer ratio in the linear regime.

For the purposes of simulations, it was assumed that CLARA would be capable of generating a ramped bunch profile with parameters otherwise comparable to those available in the SASE mode. Using plasma density of  $5 \times 10^{21} \text{ m}^{-3}$ , the plasma wavelength is  $472 \mu\text{m}$ . Bunch lengths equal to the plasma wavelength and twice the plasma wavelength were tested. The bunch charge was chosen to match the peak density of the ramped bunch to that of the SASE mode bunch. This gives a total charge of  $160 \text{ pC}$  for the one wavelength bunch and  $320 \text{ pC}$  for the

two wavelength bunch. The transverse density profile of the bunches remained Gaussian.

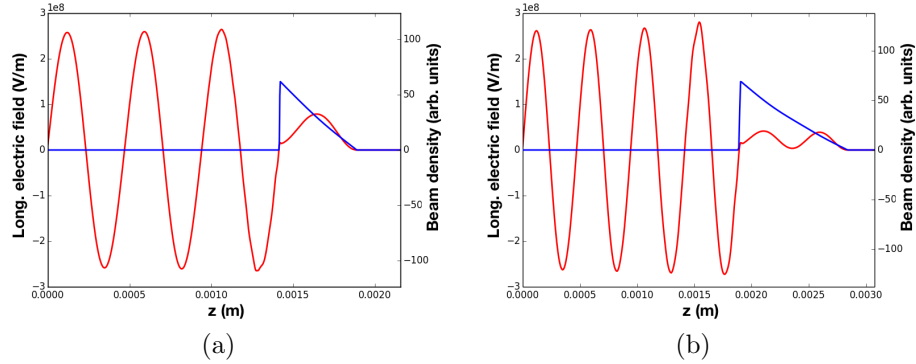


Figure 4.12: Plot of longitudinal electric field (red) and drive bunch density (blue) for a ramped drive bunch length of a) one plasma wavelength and b) two plasma wavelengths.

In the case of the one plasma wavelength bunch, the accelerating field is  $265 \text{ MV m}^{-1}$  while the peak decelerating field is  $79 \text{ MV m}^{-1}$  giving a transformer ratio of 3.35 or  $1.07\pi$ . For a bunch length of two plasma wavelengths the corresponding fields are  $273 \text{ MV m}^{-1}$  and  $41 \text{ MV m}^{-1}$  giving a transformer ratio of 6.66 or  $2.12\pi$ . These transformer ratio figures are in good agreement with the theoretical prediction of  $N\pi$  for  $N$  of one and two respectively.

The two plasma wavelength bunch was tested with a Gaussian witness bunch of 20 pC charge over a plasma length of 20 cm. Figure 4.13 shows the longitudinal phase space for the drive and witness bunches in this case. The average energy gain of the witness bunch over 20 cm was 55 MeV, giving an average gradient of  $275 \text{ MeV m}^{-1}$ , while the maximum energy loss of the drive bunch was 10 MeV. Since the wakefield depends

on the drive bunch structure, it can be estimated that acceleration of the witness bunch will end when the drive bunch structure changes as a result of energy loss. This will occur when the part of the bunch which experiences maximum energy loss becomes non-relativistic. Assuming this occurs when the minimum energy of the drive bunch falls below 10 MeV, this would allow the witness to be accelerated over 4.8 m and the final witness bunch energy could be as high as 1.3 GeV. Although this only gives a moderate accelerating gradient, it is significantly higher than the  $< 100 \text{ MV m}^{-1}$  that is typical in conventional RF accelerators. The long distance over which the gradient can be achieved illustrates a key advantage of the beam driven plasma wakefield accelerator compared to the laser driven case.

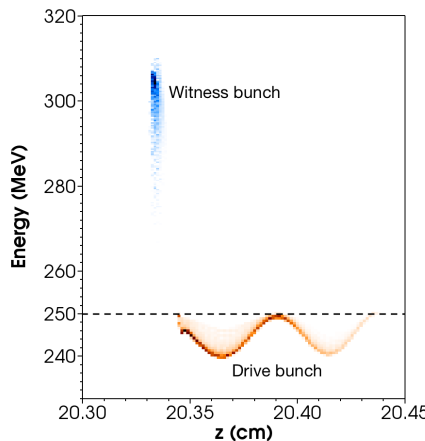


Figure 4.13: Longitudinal phase space after 20 cm propagation in plasma for drive and witness bunches for a drive bunch ramped over two plasma wavelengths. As some witness were lost transversely from the accelerating region, the witness phase space excludes particles greater than 50  $\mu\text{m}$  from the axis.

In the linear regime, simulations show that the theoretical predictions for the transformer ratio with a ramped drive bunch are accurate for parameters comparable with the CLARA bunch. An experimental test of the behaviour of a ramped bunch in the non-linear regime would be difficult due to the limited charge of the CLARA bunch. Simulations were carried out to test the effect of a ramped drive bunch in the non-linear regime, however the bunch parameters are some way away from what is likely to be achievable with CLARA. Using a bunch of peak density  $4.2 \times 10^{20} \text{ m}^{-3}$  and a plasma of density  $5 \times 10^{20} \text{ m}^{-3}$ , a transformer ratio of 5.6 was achieved. The bunch charge was 1.58 nC, several times higher than available from CLARA. As the bunch was focused as it entered the plasma, the peak density increased significantly and the plasma electron density in a substantial region around the bunch reached zero, despite the initial bunch density being only slightly higher than the plasma density. The transformer ratio is somewhat lower than that predicted for a two- $\lambda_p$  bunch, but is still significantly greater than two.

#### 4.5.2 Longitudinally shaped witness bunch

Using a shaped witness bunch can also have a beneficial effect on beam quality. In a Gaussian witness bunch profile, the front of the witness bunch experiences the unloaded wakefield of the drive bunch, while the rear of the witness bunch experiences a superposition of the drive and witness bunch fields. An asymmetric witness bunch profile, however, can be chosen such that the variation in the unloaded wakefield is cancelled

out by the witness bunch, and the whole witness bunch experiences a constant accelerating field. It can be shown that a flat accelerating region can be generated by a witness bunch with a down-ramp profile i.e. a charge density that rises sharply and then decreases linearly with longitudinal position [66, 95]. The wakefield is flattened behind the front of the bunch, so the positioning of the bunch in relation to the peak of the unloaded wakefield  $E_0$  determines the constant accelerating field and hence efficiency, maximum bunch length  $l_{\max}$ , and the amount of charge that can be accelerated. For a bunch of peak density  $\rho_b$ , with a head at  $\zeta = \zeta_0$ , where  $\zeta = z - ct$ , and for a plasma with plasma wavenumber  $k_p$  and perturbed density  $n_1$ ; the maximum density of the bunch, maximum length and accelerating field  $E_a$  are given by [66]:

$$\rho_b(\zeta_0) = -en_1 \sin(k_p \zeta_0) \quad (4.6a)$$

$$l_{\max} = k_p^{-1} \tan(k_p \zeta_0) \quad (4.6b)$$

$$E_a = E_0 \cos(k_p \zeta_0). \quad (4.6c)$$

The amount of charge that can be accelerated depends on the bunch density and the bunch length. These parameters are maximized for  $k_p \zeta_0 = \pi/2$ , giving  $\zeta_0 = \lambda_p/4$  i.e. the bunch head is one quarter of a plasma wavelength ahead of the peak. This corresponds to a witness bunch which sits at the zero point of the wakefield and is neither accelerated nor decelerated. As  $k_p \zeta_0$  approaches  $\pi/2$ ,  $l_{\max}$  approaches infinity. The case of zero accelerating field is not relevant to a real accelerator

however, and an infinitely long bunch with infinite charge, or a bunch approaching this limit, would create a non-linear wakefield, invalidating the equations above. Conversely, the accelerating field is maximized for a bunch at the peak of the unloaded wakefield ( $\zeta_0 = 0$ ), but under the requirement of a flat accelerating region this gives a bunch of zero length and charge. Neither of the extremes are useful in a practical accelerator. An appropriate compromise between witness bunch charge and accelerating field is needed to achieve good performance and efficiency. For an ultrarelativistic bunch the field at a given point is independent of the bunch behind that point. Hence the bunch can be truncated as desired in order to select its charge or length without influencing the properties of the wakefield at any point within the bunch. Compared with the triangular profile of the maximum length bunch, the truncated bunch gives a trapezium profile.

The shaped witness bunch was simulated in the wakefield of a Gaussian bunch representative of the CLARA SASE mode. A value of  $k_p \zeta_0$  of 0.1 was used, placing the witness bunch 0.1 plasma wavelengths in front of the peak of the unloaded wakefield. This gave a witness bunch length of 173  $\mu\text{m}$  and a charge of 67 pC. The energy spread of the witness bunch after 8 cm acceleration length was approximately 5%. The average energy gain for the witness bunch was 20 MeV giving an accelerating gradient of  $250 \text{ MeV m}^{-1}$ . The bunch-to-bunch efficiency, i.e. the ratio of the energy gained by the witness bunch to the energy lost by the drive bunch, was 26%. Figure 4.14 shows the location of the drive and witness bunches in the wakefield and the degree of flattening of the wakefield

due to the shaped witness bunch. The imperfect flattening may be a result of the limited resolution of the simulation: the theory requires an instantaneous rise in the witness bunch current whereas in simulations the bunch current may only rise over a minimum of a single cell.

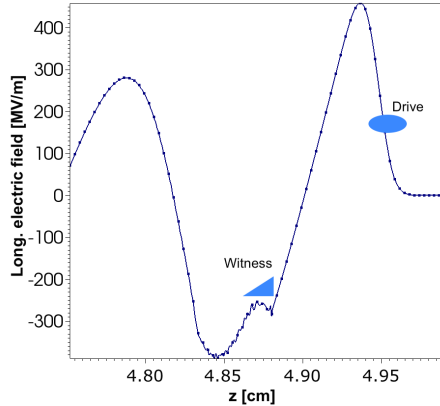


Figure 4.14: Plot of the wakefield of a Gaussian bunch loaded with a triangular down-ramped current profile witness bunch. The locations of the drive and witness bunches are illustrated.

## 4.6 Summary

Particle-in-cell simulations show that demonstration of plasma wakefield acceleration using the CLARA beam is viable for acceleration of the bunch tail with little modification to expected parameters. It has also been shown that the CLARA-FE bunch, including for a realistic distribution produced by particle tracking, is suited to demonstrating tail acceleration. Modifications of the CLARA bunch were also studied to determine the bunch parameters that would be required to demonstrate higher performance plasma wakefield acceleration in terms of witness bunch energy

spread and transformer ratio. Ramped drive bunches show an increase in transformer ratio in line with theory, while requiring a modest increase in the CLARA-FE bunch charge. A 250 MeV drive bunch ramped over two plasma wavelengths was shown to be potentially capable of accelerating a witness bunch to 1.3 GeV. Simulations of ramped witness bunch profiles have also shown some success in flattening the wakefield and achieving reduced energy spread. Experiments using ramped bunch profiles would require a means of generating a such a profile and delivering it to the experimental area.

# Chapter 5

## Study of plasma lens effect

### 5.1 Focusing in particle accelerators

A particle beam propagating freely in a particle accelerator will inevitably diverge over time due to its non-zero emittance, energy spread, and space charge forces. In order to keep the beam confined it must undergo periodic focusing. It is also frequently necessary to manipulate the properties of the beam in order to provide required parameters for the accelerator components, or final parameters for the delivered beam. Most accelerators focus the beam by means of either dedicated quadrupole magnets or combined function magnets, which have substantial quadrupole and dipole field components. A quadrupole acts to defocus the beam in one plane and focus it in the other. A periodic lattice of quadrupoles and intervening drift spaces is able to keep a beam focused over an indefinite length. One limitation of conventional magnetic quadrupoles is the focusing strength that can be achieved. Superconducting quadrupoles

such as those used in the Large Hadron Collider (LHC) or proposed for the International Linear Collider (ILC) are limited in the field strengths that can be achieved. A superconducting design for the ILC QD0 final focus quadrupole is planned to have a field gradient of  $144 \text{ T m}^{-1}$  [96]. The ILC final focus is intended to produce a flat bunch profile at the interaction region, in which the transverse bunch size is much smaller in the  $y$  dimension ( $\sim 5 \text{ nm}$ ) than in  $x$  ( $\sim 500 \text{ nm}$ ) [9]. The exact dimensions are dependent on the energy and projected upgrades. The final focus quadrupoles in the Large Electron Positron Collider (LEP) had a gradient of  $55 \text{ T m}^{-1}$  in comparison, with other quadrupoles in the same machine using lower gradients [97].

The strength of a focusing element can be characterized by the parameter  $K = 1/fl$ , where  $f$  is the focal length and  $l$  is the length of the lens. In order to focus a beam the lens must give a transverse kick to each particle in the bunch such that the resulting trajectories of the particles converge on the axis at a focal length. To achieve this the kick should be proportional to each particle's displacement from the axis and in the opposite direction. For a particle at initial transverse displacement  $x$  and longitudinal momentum  $p_z$ , which receives a transverse kick such that its new trajectory intersects the axis at  $f$ , the required magnetic field gradient can be calculated. The transverse momentum that the particle must gain can be determined from geometry in Figure 5.1:

$$p_x/p_z = \tan(\theta) = -x_0/f . \quad (5.1)$$

The force  $F$  that the lens must exert on the particle is thus:

$$F = \frac{\partial p_x}{\partial t} = \frac{p_x v_x}{l} \quad (5.2)$$

assuming that the lens is sufficiently thin that the particle's transverse position does not change significantly as it passes through the lens. If the force is exerted by a magnetic field  $B(x)$  the change in momentum can be written as:

$$p_x = q l B(x) . \quad (5.3)$$

Substituting into the Equation 5.1 and rearranging to obtain an expression for the magnetic field gradient  $G = B(x)/x$ , while writing  $K = 1/f l$  gives:

$$G = \frac{p_z K}{q} . \quad (5.4)$$

Momentum can more usefully be written in terms of relativistic  $\gamma$  and the particle's mass  $m$ :

$$K = \frac{q G}{m c \sqrt{\gamma^2 - 1}} \quad (5.5)$$

showing that the focusing strength of a lens depends on the velocity of the incoming particle, its charge to mass ratio and the magnetic field gradient. A focusing element will be typically be designed to focus a beam of a particular species with pre-determined energy and thus the only variable that can be adjusted is the magnetic field gradient. The expression for the magnetic field gradient for a quadrupole lens can be compared with the equivalent quantity for a plasma lens.

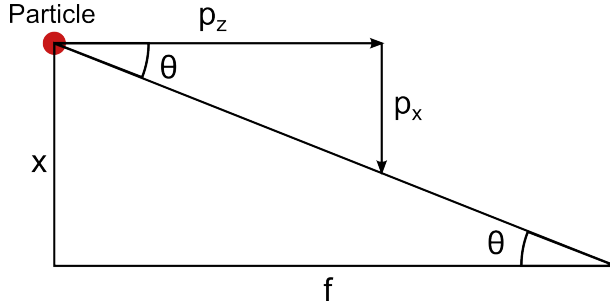


Figure 5.1: Diagram showing geometry of focusing of a particle to a focal length.

Solenoids may also be used as focusing elements in accelerators [98].

In an infinitely long solenoid the magnetic field is purely in the  $z$ -direction and the solenoid cannot focus a particle which initially propagates parallel to the magnetic field lines. However, a real solenoid has fringe regions at the start and end in which the magnetic field has radial and azimuthal components. The trajectory of particles passing through the solenoid is helical with net focusing proportional to displacement from the axis as is required for the component to act as a lens. The focal length of a solenoid lens is given by [98, 99]:

$$\frac{1}{f} = \left( \frac{q}{2\gamma mv} \right)^2 \int B^2(z) dz. \quad (5.6)$$

The focal length is proportional to square of the momentum  $\gamma mv$  of the beam and hence the focusing strength is inversely proportional to the square of momentum. As such, solenoids are not used for high energy beams: the focusing power of the lens compares unfavourably with the quadrupole lens where focusing strength is inversely proportional to the first power of momentum. Solenoids are however used for focusing low

energy beams in particle accelerators and other applications such as electron microscopes [98] where radially symmetric focusing is desirable.

## 5.2 Plasma focusing

Plasma wakefield acceleration exploits the large electric fields that can be supported by a plasma in the longitudinal direction, while the transverse fields of the plasma are not typically a desirable feature. These transverse fields can be exploited to focus a beam, combining a large focusing gradient, up to orders of magnitude larger than can be achieved with a quadrupole magnet, with the radially symmetric focusing of a solenoid. However these benefits come with the drawback of emittance growth due to aberrations.

### 5.2.1 Active and passive plasma lens

A plasma lens may be active or passive. In an active plasma lens, the focusing action is a result of an external energy source separate from the beam that is to be focused. One form of active plasma lens makes use of a laser pulse to excite the plasma with the resultant laser wakefield acting to focus a witness particle bunch. An experiment in which this form of plasma lensing was demonstrated used a second lensing gas jet after a laser wakefield acceleration stage to focus the resultant electron beam using the same laser pulse that was used to generate it [100]. It is proposed that such a lens would be useful in improving the transfer of the electron bunch from the plasma section into a conventional beam

transfer line. Another active plasma lens scheme uses a  $z$ -pinch to provide the focusing field. This has been demonstrated in experiments on ion beams[101, 102]. A  $z$ -pinch is a device in which a large voltage is applied across a plasma, generating a direct current due to the motion of the free charge carriers in the plasma. This current is in the  $z$ -direction, which in the case of a plasma lens is parallel to the bunch current. The plasma current produces an azimuthal magnetic field which acts to focus the bunch. Such active plasma lenses have been used to focus gold and argon ion beams with a gradient of  $120\text{ T m}^{-1}$ , comparable to gradients that can be achieved using magnetic quadrupoles, though focusing in both transverse directions simultaneously. This gradient was achieved with a maximum plasma current of  $400\text{ kA}$ .

A passive plasma lens in contrast uses the beam's wakefield in the plasma to achieve focusing, with the plasma in to which the beam is incident initially uniform and unexcited. A passive plasma lens is simple and capable of generating very large focusing gradients depending on the bunch properties. However, the focusing properties of the lens depend on the properties of the beam, making the passive lens less flexible than active focusing elements. Due to the finite response time of the plasma the head of the bunch exists in an unperturbed neutral plasma region and experiences no focusing force. This variation in focusing over the bunch leads to emittance growth.

A means of focusing particle beams using a passive plasma lens was proposed by P. Chen in 1985 [32], potentially generating focusing gradients orders of magnitude higher than quadrupole magnets can achieve.

Plasma focusing also focuses the beam in both transverse directions simultaneously, in contrast to a quadrupole which requires combinations of magnets to achieve net focusing in both directions. It was proposed to tailored bunch profile consisting of a thin disk followed by a cylindrical bunch. The thin disk precursor bunch allows the focusing force on the main bunch to be independent of  $\zeta$  [32]. It is not however clear how such a bunch structure, or an approximation of it, could be generated in practice. Another proposed plasma focusing scheme is the adiabatic plasma lens, which is intended to achieve focusing with negligible gain in emittance. This would consist of a plasma column of increasing density. For focusing of high density beams this would require a very high density plasma (approaching the density of a solid material) at the end of the column, which would be challenging to realize [103]. The effects of the interaction of an electron beam with a plasma lens on the background in a collider detector was studied by Weidemann, Chen and Ng [104]. It was found that the additional background due to the plasma lens may be significant, and that the luminosity enhancement from a plasma lens would have to be weighed against the increased background. The use of a plasma lens final focus or a conventional quadrupole-based setup would depend on the experiment being carried out and the ease with which the additional background could be separated from the useful data.

An early experiment on passive plasma lenses was conducted at the University of Tokyo in 1990-91 [105]. Focusing of an 18 MeV electron beam was demonstrated in the overdense regime, in which the plasma density is much greater than the beam density. The experiment used

a discharge plasma source with emittance measured using a series of phosphor screens downstream of the plasma. This experiment observed a decrease in the measured emittance which could not be conclusively explained, and is contrary to expectations [106]. It was suggested that the transverse emittance decrease could be caused by coupling of the transverse and longitudinal emittance by an unknown mechanism. However, the emittance decrease has not been observed in other plasma lens experiments. Plasma focusing was also studied using the Advanced Accelerator Test Facility (AATF) at Argonne National Laboratory [107]. Another overdense plasma lens experiment was carried out at the University of California Los Angeles, and showed a factor of four reduction in spot size with a focal length of 21 cm for an electron beam of 3.5 MeV [108]. Experiments using the Beam Test Facility at Lawrence Berkeley National Laboratory studied focusing in both the underdense and overdense regimes [109]. Plasma focusing in the underdense regime and threshold regime, where beam density and plasma density are comparable, was reported by M. C. Thompson et al. [110]. Recently plasma focusing of an electron bunch in a plasma wakefield driven by a laser pulse has been demonstrated [100]. Passive plasma focusing of a laser-wakefield accelerated bunch in a laser-ionized gas jet has shown a decrease in the solid angle subtended by an electron beam of a factor of two [111], in the overdense regime. Compared to bunches from conventional accelerators, LWFA-generated bunches may have large energy spread which introduces an additional source of variance in the effective focusing strength of the plasma lens. It was reported that the effect of the plasma lens on portions

of the bunch with different energy was dependent on the gap between the LWFA stage and the plasma lens [111].

### 5.2.2 Mechanism of passive plasma focusing

In the laboratory frame, a relativistic charged particle bunch propagating in a vacuum experiences electric and magnetic fields. The fields can be calculated using Gauss's and Ampère's laws. At a radius  $r$  within the bunch of uniform charge density  $\rho$ , the radial electric field is given by

$$E_r = \frac{\rho r}{2\varepsilon_0} \quad (5.7)$$

and the azimuthal magnetic field by

$$B_\theta = \frac{\mu_0 \rho v_b r}{2} \quad (5.8)$$

where  $v_b$  is the velocity of the beam. The magnetic and electric fields oppose each other and the difference in the force exerted on a particle in the beam can be calculated:

$$F_E - F_B = \frac{q\rho r}{2} (1 - \varepsilon_0 \mu_0 v_b^2) = \frac{q\rho r}{2} \frac{1}{\gamma^2}. \quad (5.9)$$

The electric and magnetic fields cancel to a factor of  $1/\gamma^2$ , so a highly relativistic bunch propagating in a vacuum will experience negligible focusing or defocusing forces. However, when a bunch propagates in a plasma, the plasma electrons are partially or fully expelled by the space

charge force of the bunch. The plasma ions respond much more slowly and can be considered to remain stationary in most cases. Behind the head of the bunch, the plasma ions cancel the bunch's space charge and hence the defocusing electric field. A plasma return current is also induced, however as the plasma electrons have been expelled from the beam axis this does not lead to cancellation of the bunch current. Thus the bunch experiences a strong focusing magnetic field, and a greatly reduced defocusing electric field leading to the high focusing gradients that are possible in a plasma.

The above calculation applies to a cylindrical bunch of uniform charge density. To obtain a more precise value for the magnetic field gradient, a realistic Gaussian bunch may be considered where the bunch charge varies as a function of  $r$  and  $\zeta = z - ct$ . For a cylindrically symmetric bunch of transverse and longitudinal RMS sizes  $\sigma_r$  and  $\sigma_z$  respectively and peak current density  $j_0$ , the bunch current density is:

$$j(r, \zeta) = j_0 \left[ \exp\left(-\frac{r^2}{2\sigma_r^2}\right) \exp\left(-\frac{\zeta^2}{2\sigma_z^2}\right) \right]. \quad (5.10)$$

Again applying Ampère's law, the azimuthal magnetic field  $B_\theta$  at a radius  $r$  can be calculated [112]:

$$B_\theta(r, \zeta) = \frac{1}{r} \exp\left(-\frac{\zeta^2}{2\sigma_z^2}\right) \left[ 1 - \exp\left(-\frac{r^2}{2\sigma_r^2}\right) \right] j_0 \mu_0 \sigma_r^2. \quad (5.11)$$

A plot of focusing magnetic field as a function of  $r/\sigma_r$  is shown in figure 5.2. Taking the derivative of the azimuthal magnetic field with

respect to  $r$ , neglecting the  $\zeta$  variation, as it simply scales the focusing strength with current density along the bunch, gives the focusing gradient [113]:

$$G = \frac{\partial B_\theta}{\partial r} = \mu_0 j_0 \left\{ \exp\left(-\frac{r^2}{2\sigma_r^2}\right) - \frac{\sigma_r^2}{r^2} \left[ 1 - \exp\left(-\frac{r^2}{2\sigma_r^2}\right) \right] \right\}. \quad (5.12)$$

Applying the limit  $r \ll \sigma_r$  to (5.12), using L'Hôpital's rule to evaluate the second term under this limit and integrating gives a similar result to (5.8), but with the peak current for the Gaussian beam  $j_0$  replacing the uniform current density  $j$ :

$$B_\theta = \frac{\mu_0 j_0}{2} r. \quad (5.13)$$

The magnetic field is linear in  $r$  for  $r \ll \sigma_r$ . Similarly applying the limit  $r \gg \sigma_r$  shows that the magnetic field falls as  $1/r$  at large distances from the beam. The form of the magnetic field is qualitatively the same for a Gaussian bunch as for a cylindrical bunch in both the limits of large and small  $r$  [113].

In the case of an overdense plasma lens, plasma electrons are not completely expelled by the beam and the plasma is only perturbed sufficiently to cancel the bunch charge. As long as the plasma density is high enough therefore, the focusing strength of the plasma lens is only dependent on the density of the bunch. In contrast, for the underdense plasma lens the degree to which the beam's space charge is cancelled depends

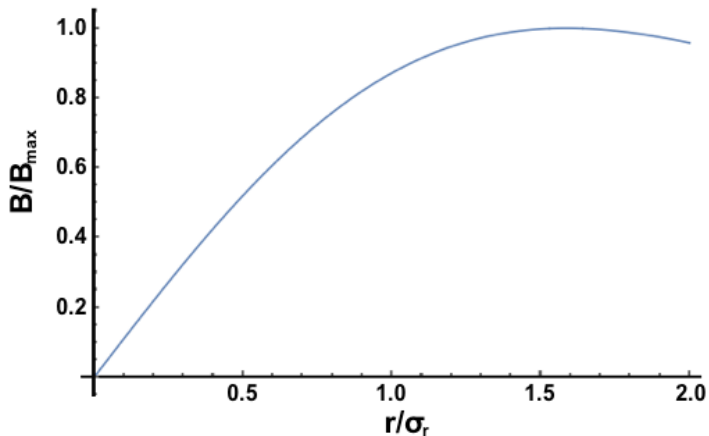


Figure 5.2: Azimuthal magnetic field, normalized to its maximum value  $B_{\max}$  vs. radial distance for a Gaussian beam.

on the density of the plasma and this is the factor which determines the focusing strength of the lens.

### 5.3 Aberrations

Ideally, a focusing element is capable of achieving focusing while maintaining beam quality, especially emittance. This requires that the focusing force be constant along the bunch's longitudinal coordinate, and be linear in  $r$ , such that particles not on the axis experience a focusing force proportional to their displacement. If these requirements are not achieved, the emittance will grow during focusing, and these are referred to as longitudinal and spherical aberrations respectively. A quadrupole magnet can be designed such that the spherical aberration is minimized, and since it provides a constant field, the longitudinal aberration is avoided. In contrast, these aberrations are a major challenge

in plasma lenses and are much more difficult to avoid. Figure 5.2 shows that in the limit of small  $r$  the focusing force for a Gaussian bunch is linear in  $r$ . Thus the majority of the bunch experiences a linear focusing force. Particles at  $r > \sigma_r$  experience a significantly non-linear focusing force due to the spherical aberration and these particles are responsible for the emittance increase.

If a Gaussian bunch of initial Twiss parameter  $\beta_0$  and emittance  $\epsilon_0$  is focused by a plasma lens of length  $l$  and focal length of  $f$ , with a deviation from the ideal focusing strength  $K = 1/fl$  of  $\Delta K$ , the error in angular deflection  $\delta\theta$  can be calculated by considering the effect of the aberration on Equation 5.1 [33, 114]. The small change in angular deflection allows the small angle approximation to be applied, giving for a single particle:

$$\tan(\delta\theta) \approx \delta\theta = \frac{x_0}{f} \frac{\Delta K}{K}. \quad (5.14)$$

For a particle bunch,  $x_0$  is replaced with  $x$  and the average over the bunch is taken. The top and bottom of the equation is multiplied by  $\sigma_x$  so that the averaged part is independent of the bunch dimensions:

$$\delta\theta = \frac{\sigma_x}{f} \left\langle \frac{x}{\sigma_x} \frac{\Delta K}{K} \right\rangle. \quad (5.15)$$

It is reported that using Monte Carlo methods to evaluate this expression gives a value of  $\left\langle \frac{x}{\sigma_x} \frac{\Delta K}{K} \right\rangle = 0.2$ . The expression for  $\delta\theta$  can be written in terms of emittance and the Twiss  $\beta$ :

$$\delta\theta = 0.2 \frac{\sqrt{\beta_0 \epsilon_0}}{f}. \quad (5.16)$$

The final emittance that results from the increase in divergence is given by [114]:

$$\epsilon = \sqrt{\epsilon_0^2 + \beta_0 \epsilon_0 \delta \theta^2} . \quad (5.17)$$

In the overdense regime, the spherical aberration for a Gaussian beam can be calculated by comparing the focusing field at  $r = \sigma_r$  from (5.12) with the value obtained by extrapolating the constant gradient at  $r \ll \sigma_r$  to  $r = \sigma_r$ . This gives a value for  $\Delta K/K$  of 0.21, similar to the value calculated by Rosenzweig and Chen. These results are valid for a Gaussian bunch distribution for which there is a deviation from linear focusing as a result of the bunch shape. It has been suggested that a flatter bunch shape, closer to a top hat distribution could be achieved using an octupole magnet upstream of the plasma lens [114]. The effect of an octupole is to provide non-uniform focusing in order to reshape the bunch, and higher order magnets can be used to achieve higher-order corrections to the bunch shape [115]. A uniform bunch shape would allow for more linear focusing compared to for a Gaussian bunch and hence lower spherical aberration. While the bunch shaping would introduce an emittance increase of its own this may be more controllable than the spherical aberration in a plasma. Shaping of an ion beam using an octupole magnet for the purposes of medical irradiation has been experimentally demonstrated [116].

In a passive plasma lens the longitudinal aberration is a major limit on the preservation of emittance. For a single bunch propagating in an initially uniform and unexcited plasma, the plasma has a finite response

time to the approaching bunch. The head of the bunch therefore travels through a uniform neutral medium and experiences no focusing force. Moving back along the bunch, the focusing force increases as the plasma responds. Depending on the length of the bunch in comparison to the plasma wavelength, the plasma electron density may reach a minimum within the bunch, and hence the focusing force reaches a maximum and then falls as the plasma electrons return to the axis. A realistic bunch will also have a variation in current density with longitudinal position which also leads to a variation in focusing strength. The result of the longitudinal aberration is that the transverse phase space of the bunch is smeared out, and the increase in phase space area corresponds to a growth in emittance. This is illustrated in Figure 5.3. The effect of the longitudinal aberration can be calculated by considering a bunch passing through a thin lens in which the focusing strength is a function of position within the bunch. In the overdense regime the plasma wakefield is linear and it is reasonable to assume that the focusing strength is proportional to  $\sin(z - ct)$ . This can be simulated independently of the other lens effects to determine the separate contributions of the aberrations and any other effects to the emittance growth.

## 5.4 Plasma focusing with VELA

With the intention of carrying out initial experiments in plasma focusing using the VELA beam, simulations were carried out to establish the degree of focusing that could be achieved using both the VELA and

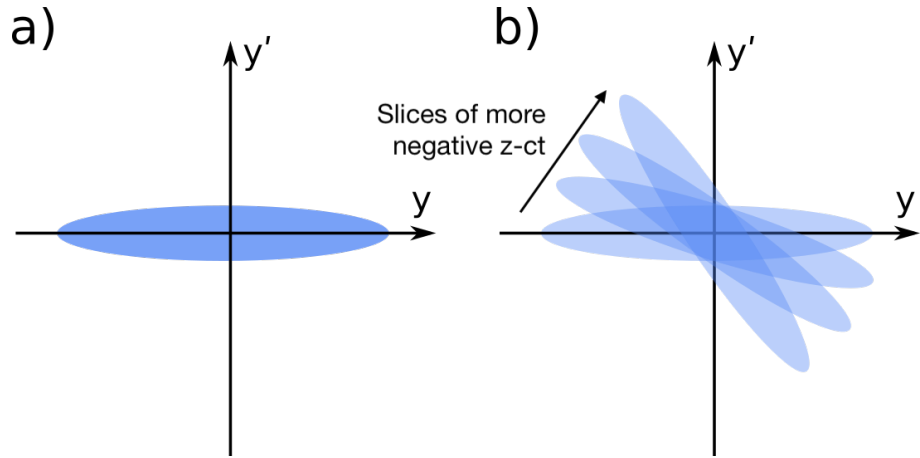


Figure 5.3: Illustration of the emittance increase that results from the longitudinal aberration. The initial phase space (a) is smeared out (b) as the degree of focusing and hence the rotation of the emittance ellipse depends on longitudinal position. The head of the bunch with  $z - ct = 0$  sees no focusing force, while slices of the bunch with increasingly negative  $z - ct$  see different focusing strengths.

CLARA Front End beams, and to investigate the effect of focusing on key beam quality parameters including emittance and energy spread. Bunch parameters generated by particle-tracking simulations for CLARA-FE and VELA, for 100 pC and 250 pC bunch charge, are shown in Table 5.1. Plasma focusing is considered to be an attractive area of study for the VELA and CLARA-FE accelerators. The relatively low energy of the beams allows the experiment to be compact compared to very high energy accelerators where the focal length would be much longer. The moderate bunch density and charge meanwhile ensures that the focusing strength is not so high that the bunch undergoes betatron oscillations within the plasma, which is contrary to the intended function of a plasma lens. Experiments with plasma lenses also provide an opportunity for developing experience in operating plasma sources in conjunction with

the accelerator facility. Emittance growth as a result of plasma focusing has not been extensively studied in the past, and results from VELA and CLARA-FE could help to verify theoretical predictions and validate simulation results.

Table 5.1: VELA and CLARA Front End (CFE) bunch parameters [117].

Accelerator	VELA		CFE	
Charge (pC)	100	250	100	250
Momentum (MeV/c)	4.8	4.8	55	55
RMS length $\sigma_z$ ( $\mu\text{m}$ )	2700	3300	45	270
RMS radius $\sigma_x$ ( $\mu\text{m}$ )	200	800	50	100
RMS radius $\sigma_y$ ( $\mu\text{m}$ )	300	250	200	100
Norm. emittance $x/y$ ( $\mu\text{m}$ )	2/2.75	6/7	4.5/4.5	15/6
Peak density $n_b$ ( $10^{17} \text{ m}^{-3}$ )	2.5	1.5	880	370
Peak current (A)	11.1	22.7	667	278

The focusing strength that can be achieved using an overdense plasma lens depends primarily on the bunch current. This makes the preferred modes VELA with 250 pC and CLARA-FE with 100 pC charge. The magnetic field gradient in the limit of small  $r$  can be estimated by applying Equation 5.13. This gives a magnetic field gradient of  $46 \text{ T m}^{-1}$  for VELA and a gradient of  $16.7 \text{ kT m}^{-1}$  for CLARA-FE. The much higher focusing gradient is attractive for demonstrating very strong focusing from a plasma lens, however the relatively low energy of the CLARA-FE beam means that the focal length for such focusing will be very short. As a result the measurement of bunch size and emittance downstream of the lens may be difficult due to the limited space available for diagnostic equipment. This makes the much weaker focusing with VELA more attractive as it is equally capable of demonstrating the effect of aberration.

tions and supporting study of plasma focusing without the drawbacks of the very high focusing strength of CLARA-FE. Due to the short plasma length required, a laser-ionized gas jet is an attractive source for plasma focusing experiments at low energies. For focusing of high energy beams a longer plasma lens may be required to achieve strong focusing and as such other plasma source technologies may be more suitable.

#### 5.4.1 Emittance growth

As stated previously, it has been calculated that for a rigid Gaussian beam and a thin plasma lens the deviation from linear focusing at  $r = \sigma_r$  is 0.21. However in practice the bunch is not rigid, especially for low energy bunches such as VELA/CLARA-FE. Preliminary simulations were carried out to compare the deviation in focusing strength to theoretical predictions. A transverse distribution of test particles was generated which did not deposit their charge into the simulation, thus being invisible to the plasma and beam. The particles do however experience the fields in the simulation. The energy of the particles was set to be very large in order that the focusing forces do not generate any significant divergence from their initial trajectory, enabling the transverse momentum gained by the particles to accurately measure the focusing force at different radii. Figure 5.4 shows the transverse phase space distribution of test particles after focusing showing the deviation from linear focusing for an overdense plasma. Measurements of the fractional deviation from linear focusing  $\Delta K/K$  gave values close to 0.14 over three plasma densi-

ties tested across the range used. This is smaller than the value predicted for an ideal Gaussian beam, likely as a result of the non-rigid bunch deviating from a Gaussian profile on focusing. For the VELA beam with a focal length of 10 cm the expected increase in divergence can be calculated from Equation 5.16 giving  $\delta\theta = 0.45$  mrad which when applied to Equation 5.17 gives an increase in emittance of  $4 \times 10^{-3}$  mm mrad which is negligible.

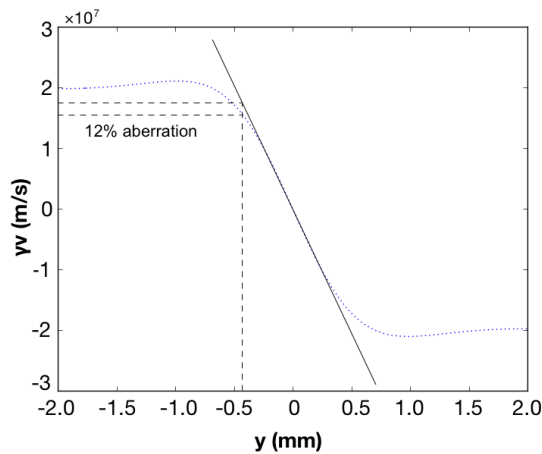


Figure 5.4: Transverse phase space distribution of test particles (blue points) after plasma focusing showing deviation from linearity due to the spherical aberration. The  $y$ -axis scale is the product of the transverse velocity and the relativistic  $\gamma$  factor.

The contribution due to the longitudinal aberration was estimated by particle tracking of a Gaussian bunch distribution through a lens with focusing strength a function of position in the bunch. For a lens with focusing strength  $K$  and length  $l$  small compared to its focal length, the effect of the lens on a particle with initial transverse position and momentum  $x_0$  and  $x'_0$  after propagating a distance  $s$  after the lens can be calculated by applying beam transfer matrices:

$$\begin{pmatrix} x \\ x' \end{pmatrix} = \begin{pmatrix} 1 & s \\ 0 & 1 \end{pmatrix} \begin{pmatrix} 1 & 0 \\ -Kl & 1 \end{pmatrix} \begin{pmatrix} x_0 \\ x'_0 \end{pmatrix} = \begin{pmatrix} x_0(1 - Kls) + sx'_0 \\ x'_0 - Klx_0 \end{pmatrix} \quad (5.18)$$

Using Python and Numpy [118], the beam transfer matrix was applied to a Gaussian particle distribution and the resulting increase in emittance was calculated. The variation in the focusing strength  $K$  was approximated as:

$$K(\zeta) = K_0 \sin(\zeta/2\pi\lambda_p) \exp(-\zeta^2/2\sigma_z^2) \quad (5.19)$$

where  $K_0$  is the maximum focusing strength. This expression takes into account the response time of the plasma and the variation in the Gaussian beam current. The maximum focusing strength of  $K = 2875 \text{ m}^{-2}$  was determined by the peak current. The emittance growth that resulted from the longitudinal aberration was measured for a range of 100 plasma densities from  $10^{18}$  to  $10^{22} \text{ m}^{-3}$  with equal spacing between the base-10 logarithm of the plasma density. The plasma densities correspond to a plasma wavelength ranging between 33 mm and 0.33 mm. For each density, 500 000 particles were tracked which was sufficient to eliminate fluctuations between runs. The variation in emittance growth with plasma density is shown in Figure 5.5. The emittance is seen to increase with plasma density at lower density values. This is a result of the plasma wavelength decreasing from substantially larger than the length of the bunch, where the variation in focusing strength over the bunch

is slow, to a plasma wavelength comparable to the bunch length where the variation in focusing strength is maximized. At higher densities, the emittance growth falls again as a smaller proportion of the bunch is subject to the maximum focusing strength. The emittance growth becomes constant at very high densities where there are multiple plasma periods across the bunch and the variation in focusing has little dependence on the plasma wavelength. The change in phase space for focusing with the longitudinal aberration is shown in Figure 5.6 for a plasma density of  $2.2 \times 10^{19} \text{ m}^{-3}$ , and after propagation 5 cm from the start of the plasma lens. This result can be compared with Figure 5.3 showing the smearing out of the distribution as predicted.

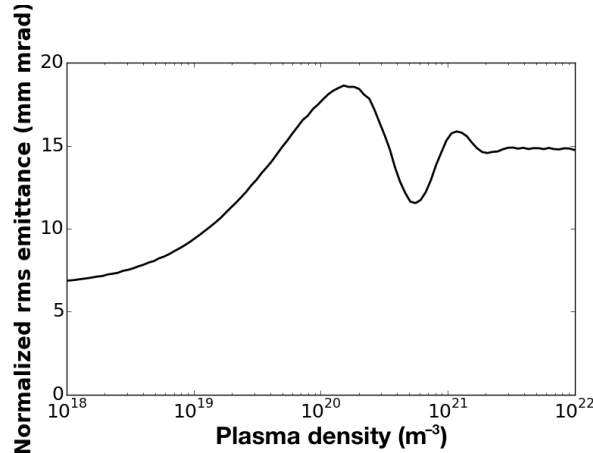


Figure 5.5: Variation of emittance growth due to the longitudinal aberration with plasma density over a large plasma density range.

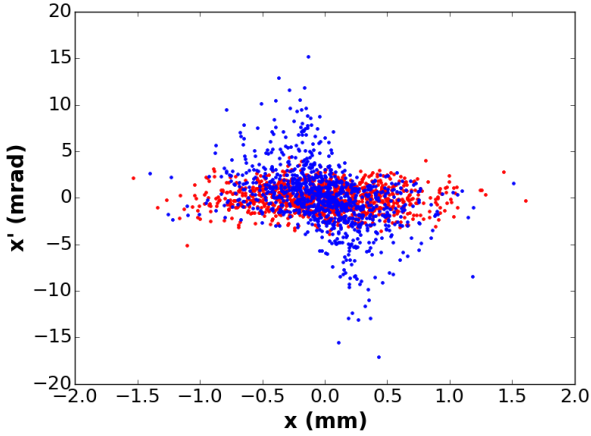


Figure 5.6: Phase space from particle tracking showing longitudinal aberration for a plasma density of  $2.2 \times 10^{19} \text{ m}^{-3}$ . Red points show the initial particle distribution and blue points show the distribution after 5 cm. To improve clarity this plot shows tracking of 1000 particles rather than the 500 000 actually used.

## 5.5 Simulation results

The predictions from theory and particle tracking were compared with two-dimensional particle-in-cell simulation results in which the electron bunch was allowed to propagate through the plasma and then beyond this focal length in vacuum. The PIC simulations thus were able to take into account aberrations and space charge effects. The two-dimensional nature of the simulations did require that in the case of asymmetrical transverse bunch size, the parameters were changed to symmetrical  $x$  and  $y$  dimensions while maintaining cross-sectional area. This is expected to be feasible for VELA and CLARA-FE [117].

The change in transverse phase space for the VELA bunch undergoing focusing by a plasma of density  $2.2 \times 10^{19} \text{ m}^{-3}$  is shown in Figure 5.7, which can be compared to the results from particle tracking (Figure 5.6).

The emittance growth that results from the longitudinal aberration can be seen in the smearing out of the phase space, with a small proportion of the particles undergoing no focusing. The deviation of the central axis of the tilted phase space distribution following focusing from a straight line indicates the focusing force is not linear in  $r$  as a result of the spherical aberration.

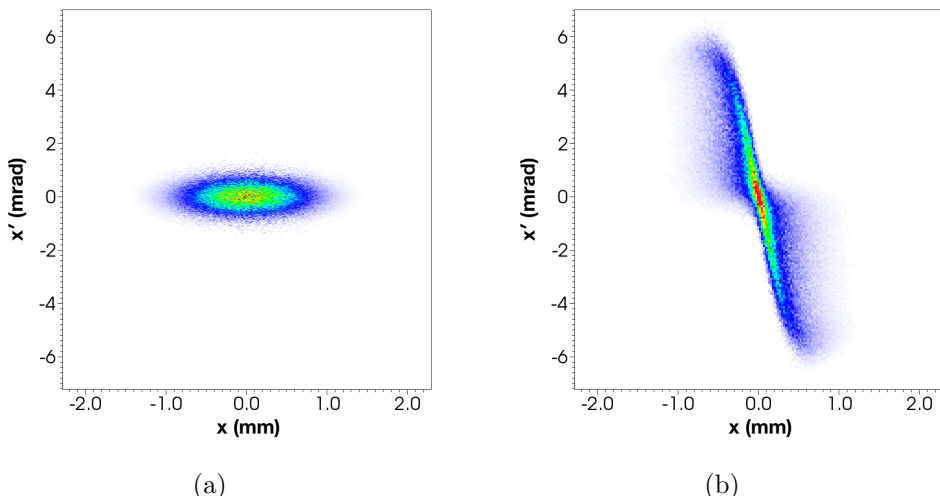


Figure 5.7: Transverse phase space for the VELA bunch before (a) and immediately after (b) focusing by a 1 cm plasma lens of density  $2.2 \times 10^{22} \text{ m}^{-3}$ . The qualitative effect of the spherical and longitudinal aberrations are apparent. The  $y$ -axis scale assumes the small angle approximation for  $\tan(x')$ .

The focusing field in the 2D simulation,  $E_y + c \times B_z$  and its relation to the plasma density is plotted in Figure 5.8. Outside the plasma the net force is close to zero while inside there is a large focusing field due to the neutralization of the bunch charge.

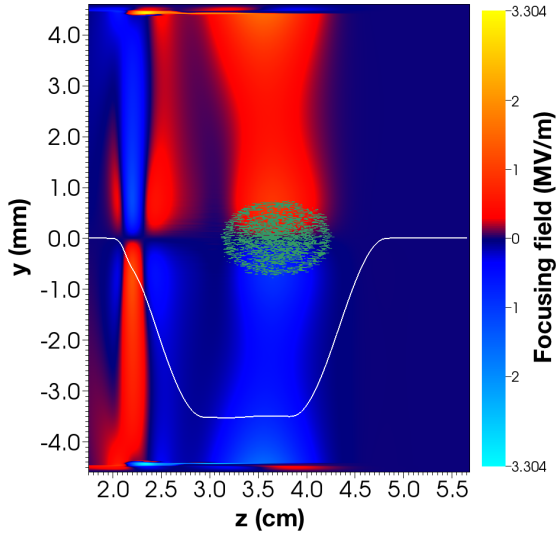


Figure 5.8: Pseudocolour plot of focusing field within an overdense plasma lens. The white curve shows the plasma density variation (zero at extreme  $z$ ); the broken green lines show contours of the bunch density, included for illustration of the bunch location.

### 5.5.1 Plasma density

The effect of different plasma densities on the emittance and focusing strength were studied. Due to the low density of the VELA bunch, the simulations were restricted to the overdense regime, in order to achieve a substantial focusing strength. Plasma density was varied between  $1 \times 10^{18} \text{ m}^{-3}$  and  $1.8 \times 10^{19} \text{ m}^{-3}$ . RMS bunch size was taken at a fixed position of  $z=20 \text{ cm}$  from the start of the simulation, with the plasma beginning at  $z=2.7 \text{ cm}$ . Figure 5.9 shows the variation in RMS bunch size and emittance with plasma density for the VELA beam with a plasma length of 9 mm. The focusing strength depends strongly on plasma density when the density is less than two orders of magnitude higher than the bunch density. For plasma densities greater than this, the focusing

strength is approximately constant. This is as expected for an overdense lens: as long as the plasma density is high enough to completely cancel the bunch charge, the focusing strength is dependent on the bunch density rather than the plasma density. The dependence of emittance growth on plasma density does not match expectations exactly. When the plasma density is very low and focusing is weakest, the emittance growth is also small as expected. However, emittance growth is largest when the plasma density is the lowest value that achieves the maximum focusing strength and falls as the density is increased contrary to the predicted increase in emittance with plasma density due to the longitudinal aberration. The overall variation in emittance growth is however small, which matches the expectation from Figure 5.5 over the relatively small plasma density range studied.

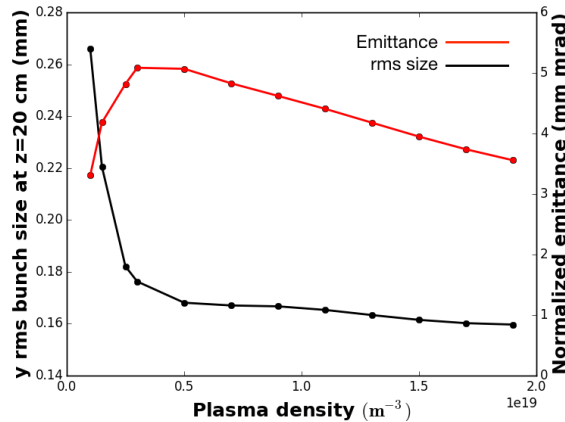


Figure 5.9: Plot showing the effect of plasma density change on emittance and rms transverse size at  $z=20\text{ cm}$ . Lines show linear interpolation.

The CLARA-FE bunch was tested with an underdense plasma lens. The variation in RMS size is shown in Figure 5.10. The focusing strength

for the higher current density is as expected much higher than for the VELA bunch. The plasma length was 1 cm and the focal length was 7 cm. The focusing strength can be calculated from the focal length giving a value of  $K=1429 \text{ m}^{-2}$  corresponding to a focusing gradient of  $262 \text{ T m}^{-1}$ .

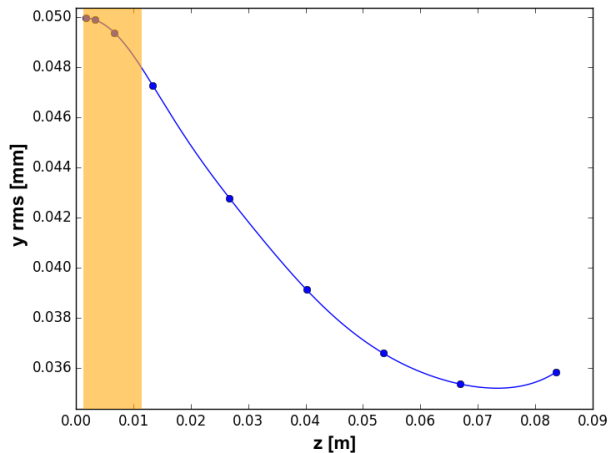


Figure 5.10: Variation in rms transverse size for the CLARA-FE bunch during and after interaction with an underdense plasma lens.

### 5.5.2 Plasma length

In studies of the effect of the length of the plasma lens on its focusing properties, the length of the plasma was varied between 1 mm and 13 mm. The limits on the plasma length were informed by the limits that could be achieved with a typical gas jet plasma source, and the requirement that a plasma lens have thickness much less than its focal length. Longer length plasmas could however be produced using other methods. Figure 5.11 shows the variation in RMS bunch size with propagation distance for different plasma lengths. The simulation results give the bunch size at a series of discrete dump locations. The focal length

was thus determined using spline interpolation of the data points, and locating the minimum in the interpolated curve. The focal length gives the focusing strength  $K$ , although this is an average value as  $K$  varies with position in the bunch as discussed earlier. Figure 5.12 shows a plot of inverse focal length against plasma length. The focusing strength of the plasma can be measured by taking the gradient of this plot, giving  $K = 200 \text{ m}^{-2}$ . This is equivalent focusing strength to a magnetic field gradient of  $3.33 \text{ T m}^{-1}$ . This compares with the predicted peak value of  $46 \text{ T m}^{-1}$ . Focal length is inversely proportional to plasma length for the shorter plasma lengths tested. For the longest lengths, the plot deviates from a linear relationship. Comparing Figures 5.11 and 5.12 shows that for the longer lengths, the focal length is no longer large compared to the thickness of the lens. The thin lens approximation is less valid in this situation and hence the divergence.

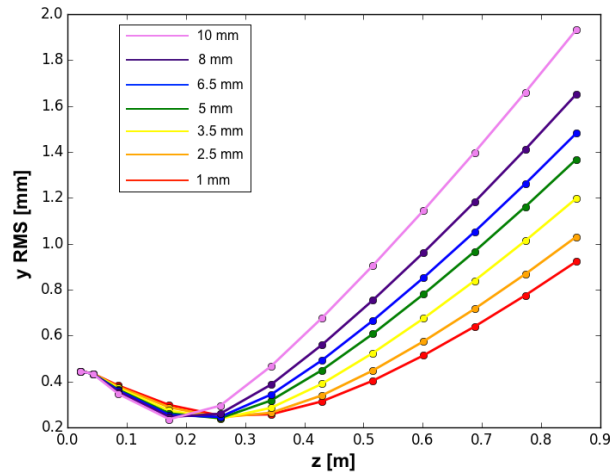


Figure 5.11: Variation of RMS transverse bunch size with propagation distance for a scan of plasma length. For clarity some plasma lengths that were simulated are omitted from this plot.

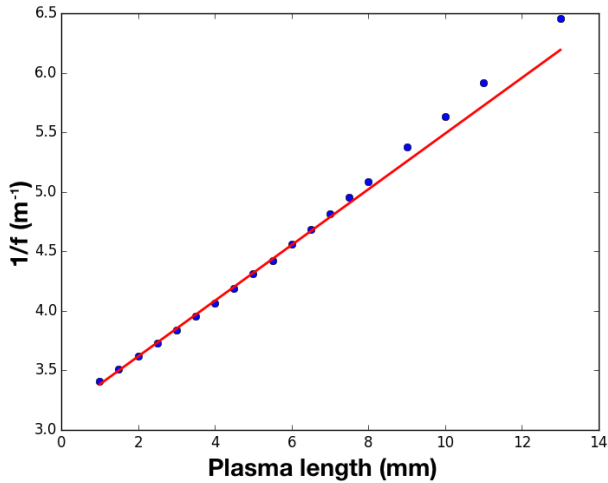


Figure 5.12: Plot of variation of inverse focal length with plasma length, with linear fit discarding the final points which clearly deviate from the straight line. The deviation for longer plasma lengths is due to the thin lens approximation becoming less applicable as plasma length increases. The gradient corresponds to an average focusing strength of  $200 \text{ m}^{-2}$ .

The effect of the plasma length on emittance growth is shown in Figure 5.13. Although the predictions from particle tracking are in reasonable agreement with PIC simulation results, there is a significant difference. The emittance growth from particle tracking does not take into account the contribution due to the spherical aberration. Although the spherical aberration contribution could be included, as the theoretical prediction of effect of the spherical aberration was not found to be in line with simulation results it was decided to leave the contributions separate.

Emittance growth is an inevitable feature of a passive plasma lens using a single bunch, as the longitudinal aberration cannot be avoided. As previously mentioned a passive plasma lens using a structured bunch can eliminate the longitudinal aberration but requires an a bunch shape

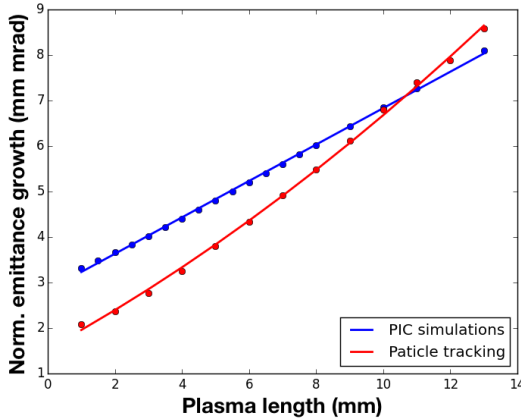


Figure 5.13: Emittance increase from particle tracking and particle-in-cell simulation for plasma length scan. The lines indicate a least-squares linear fit for the PIC results and a quadratic fit to the results from particle tracking.

that is unlikely to be achievable using VELA/CLARA-FE. Active plasma lenses can also avoid or significantly reduce longitudinal aberration, but the requirement for synchronization between the focused bunch and the external driver, as well as the overall complexity of the system, means that the reliability of such a system will be less than that of a passive lens. In high power accelerators, the consequences of a failure in focusing may be highly damaging to sensitive accelerator components such as cryogenic systems or detectors in a collider, so an active plasma lens would need to demonstrate a high degree of reliability before it could be considered. A passive plasma would need to be similarly reliable which may not be guaranteed if using a pre-formed plasma. A passive plasma lens using a plasma produced by beam field ionization on the other hand would be highly reliable as it would only rely on the presence of the neutral vapour.

### 5.5.3 Plasma lens experimental setup

It was intended to study the effect of plasma focusing of the VELA beam as well as deflection of the beam in a laser-ionized gas jet plasma source. The VELA experimental area consists of a large coffin vacuum chamber into which experiments can be installed. A gas jet nozzle and a Lanex scintillator screen were mounted on a moveable stage. The Lanex screen was used for alignment of the beam before being replaced by means of the moveable stage with the gas jet for experiments. The gas jet operated in a pulsed mode, synchronized with the laser. The laser was focused by an off-axis parabola upstream of the coffin. It was then aligned to co-propagate with the electron beam using a planar mirror with a hole. Diagnostics included a Lanex screen downstream of the plasma for detecting changes in the transverse size of the bunch and CCD cameras for imaging the plasma and the Lanex screens. An electron spectrometer was to be used to measure energy changes of the bunch. The experiment could not however be carried out due to the failure of the laser and the limited beam time that was available. This failure highlights one of drawbacks of components such as plasma lenses - the increased reliance on other complex systems such as lasers increases the risk of failure. In comparison a normal conducting quadrupole focusing element requires only a power supply, while a superconducting magnet additionally requires a cryogenic system. A passive plasma lens need not rely on laser ionization; it may use a discharge source or, for a very intense beam, field ionization. A plasma lens relying on field ionization would be

very reliable, while a discharge source may suffer from similar reliability limitations to a laser. The design of an active plasma lens would similarly need to achieve a high level of reliability if the lens was to be used in applications, as discussed earlier. Although the attempted experiment did not succeed in its aim of demonstrating plasma-beam interactions due to the failure of the laser, it was successfully demonstrated that a gas jet could be operated in the VELA coffin and experience was gained for future experiments. A schematic showing the experimental setup is shown in Figure 5.14.

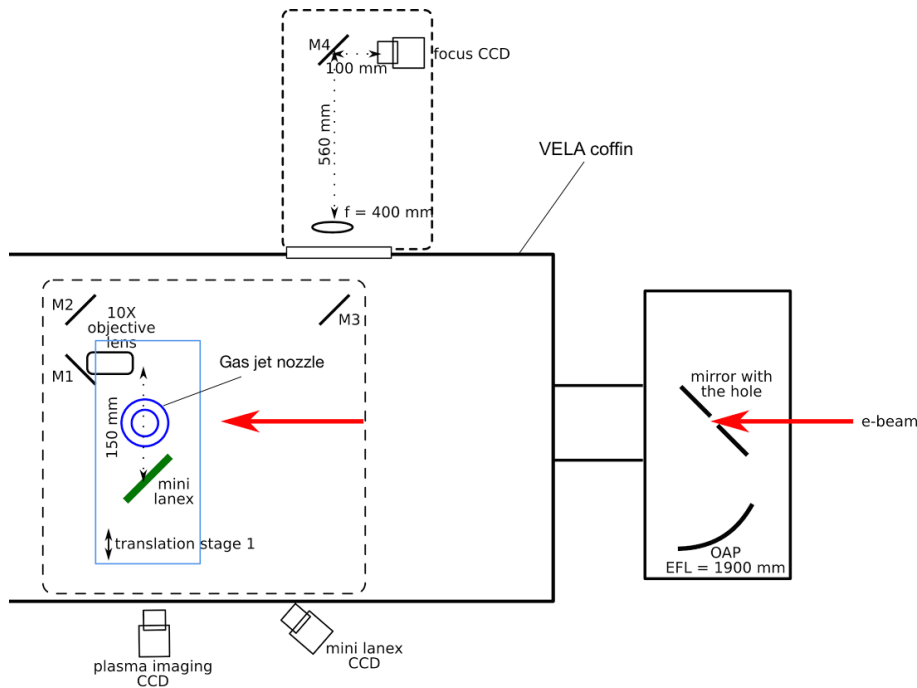


Figure 5.14: Schematic showing experimental setup for plasma experiments at VELA. Credit G. Manahan. Reproduced with permission. An electron spectrometer and Lanex screen and associated CCDs downstream of the plasma are omitted for reasons of space.

## 5.6 Summary

Simulations show that study of plasma lens effects using the VELA or CLARA-FE accelerators is possible, with focusing strength averaged over the bunch comparable to that seen in quadrupole magnets for VELA and considerably higher in CLARA-FE. The emittance growth associated with a plasma lens is one of its chief drawbacks, and the emittance growth due to the spherical and longitudinal aberrations was predicted and those results compared to simulation. Previous studies of plasma focusing have not investigated the dependence of emittance growth on plasma density and plasma length in detail. The effect of the longitudinal aberration was shown to be well predicted by particle tracking. The longitudinal aberration was also studied over a wide range of plasma densities, showing a periodic variation as plasma wavelength changes compared to bunch length. This effect has not been reported before. However, the effect of the spherical aberration shows a marked difference in the degree of deviation from linear focusing in simulations compared to theory, although the contribution of the spherical aberration to total emittance growth for the VELA beam is negligible. Three-dimensional PIC simulations could be carried out to investigate the effect of the spherical aberration more accurately. Experiments at Daresbury laboratory would allow both simulation and theory to be tested against real world results. Experiments would also be valuable in demonstrating a plasma source and developing experience of operating a plasma-based accelerator component in conjunction with the VELA/CLARA accelerators.

# Chapter 6

## Study of plasma beam dump

### 6.1 Challenges in high-energy beam dumps

A beam dump is crucial to the safe operation of a particle accelerator. Once a particle beam has served its purpose, it is necessary to dispose of it in such a way that its energy is dissipated without ionizing radiation or excessive heat posing a risk to people or the surrounding facility. It is also necessary to avoid the production of dangerous chemicals or the radioactivation of materials that can result from exposure to radiation. The conventional means of disposing of a particle beam is to have it impinge on a high density material - a solid or liquid - which will rapidly stop the beam's constituent particles. The Large Electron-Positron Collider (LEP) used a 2 m long aluminium dump to stop a 100 GeV electron beam [119] and the proposed water-based dump for the International Linear Collider (ILC) [9, 120] is designed to stop a 500 GeV beam in 11 m. The proposed design of the ILC beam dump consists of a cylindrical stainless

steel pressure vessel containing water and is based on the design used for the Stanford Linear Accelerator [121]. Water is pumped into the vessel via two inlet headers azimuthally with respect to the direction of beam propagation. The water in the vessel then flows in a vortex pattern and exits the vessel via a centrally located outlet header. The dump window is circular and occupies a small portion of the dump face plate. The beam is scanned over the window to manage localized heating and the window is additionally cooled by a separate water jet within the dump vessel. Once the beam has propagated through the water dump any remaining energy is absorbed by a three-inch-thick (76 mm) stainless steel end plate [120].

The beam dump must be capable of absorbing the high power of the beam (18 MW for the ILC) in a small volume, leading to high power density cooling requirements and high temperatures and pressures [120]. The ILC beam dump design would operate at 10 bar and at a maximum water temperature of 155 °C, while for safety the pressure vessel is designed to be capable of containing 20 bar. In the case of a water dump, decomposition generates hydrogen and oxygen gas which must be removed [9, 121]. The dump window design is challenging as it must be capable of admitting the beam to the water dump without excessive heating, necessitating a thin window, but it also must be able to withstand the high pressure inside the dump vessel [120]. In addition, structural materials may suffer radiation damage and lose strength, a concern for pressure vessels and windows [121, 122]. As a result the beam dump window must be replaced remotely during periodic maintenance [9]. Both

proton and electron beams lead to the production of radionuclides in the stopping material [123, 124]. In the case of an electron beam this radioactivation occurs due to photospallation caused by the bremsstrahlung photons. These considerations lead to a conventional beam dump being substantially larger than the length over which they are able to stop their beam may suggest. The proposed ILC dump will require a pumping station, water tower, catalytic hydrogen-oxygen recombiner, and deionizer sited above ground, connected via pipes to the dump location. A sump is also required to collect any radioactive water that may leak from the dump and ancillary equipment [120].

### 6.1.1 Noble gas beam dump

A beam dump that makes use of a much lower density material than a solid or liquid may be attractive. The low pressure of the dump in particular makes the requirements on the dump window much less demanding. One scheme that has been proposed is the noble gas beam dump, which consists of a long column of noble gas at atmospheric pressure surrounded by iron shielding surrounded in turn by a water cooling jacket [125, 126]. A diagram showing a cross-section of the noble gas beam dump is shown in Figure 6.1. Proposed dimensions are a diameter of 8 cm for the noble gas column and 1.2 m for the whole assembly. The beam propagates through the noble gas and particles are scattered at a low rate into the surrounding iron, where they rapidly lose their energy in a similar fashion to a conventional beam dump. Heat is transferred

through the iron by conduction into the water. The noble gas beam dump eliminates hydrogen production as the beam does not interact directly with that water. Tritium production is also reduced compared to a conventional beam dump, though radio-activation of the noble gas is still expected to occur. The dump operates at atmospheric pressure and low temperature compared to a conventional beam dump. This simplifies the beam window design as the strength requirement is greatly reduced. The major drawback of the noble gas dump is the very long length that would be required due to the low decelerating gradient. For a 400 GeV electron beam a gas column of 1000 m would be required. Other possible difficulties that have been identified include the potentially more difficulty maintenance in dealing with a radio-activated gas compared to a solid or liquid in a conventional dump, and the heating and ionization of the gas. It should be noted that the water-based dump proposed for the ILC will also generate radioactive gases in the form of tritium and radioisotopes of oxygen and nitrogen, so the problem of the gas is not unique to the gas dump. It is suggested that the gas dump could be used in conjunction with a simplified conventional beam dump in a hybrid dump scheme [126].

## 6.2 Plasma beam dump

A plasma beam dump promises to achieve decelerating gradients comparable to or greater than those achievable in conventional beam dumps while using a decelerating medium of lower density even than the noble

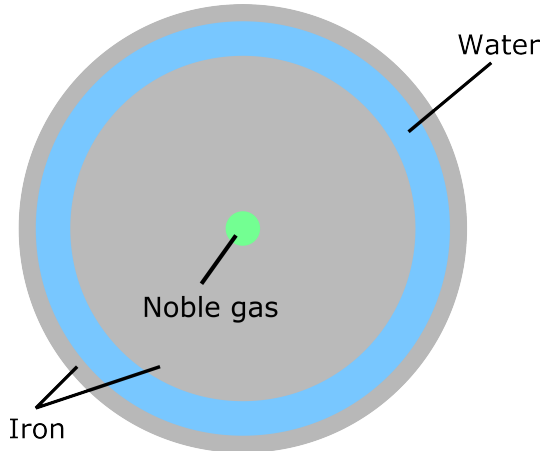


Figure 6.1: Diagram of the cross-section of the noble gas beam dump, with the direction of beam propagation perpendicular to the page. Based on a diagram in [125]; not to scale.

gas beam dump. This is achieved by making use of collective properties of the plasma: rather than rely on random interactions with the dump material, the particles in the plasma oscillate in coherently and can thus achieve a continuous high decelerating gradient even at a very low density. As the response of the plasma is collective it would be possible to recover energy electrically from the plasma [127], whereas in a conventional beam dump energy recovery is limited to low-grade heat. Recovery of electricity would also reduce the amount of heat generated and thus the cooling requirements on the plasma beam dump compared to a conventional dump. Plasma beam dumps have been proposed using a passive [127] or active [128] scheme.

In the passive scheme the plasma is excited by the electric field of the bunch that is to be decelerated. In the active scheme a laser pulse is used to excite the plasma and decelerate the bunch, the scheme operating as the inverse of a laser plasma accelerator. The active beam dump avoids

one the drawbacks of the passive dump: that in the passive dump there is a large variation in decelerating gradient with longitudinal position in the bunch. The head of the bunch sees no plasma wakefield and is hence not decelerated, while at some point along the bunch particles will experience a maximum decelerating gradient. This may be at the tail of the bunch if the entire bunch is located in front of the peak decelerating field, or it may be at some point in the middle of the bunch. The particles that see the maximum decelerating field lose energy more rapidly than other particles in the bunch. When the relativistic  $\beta$  of these particles becomes significantly less than one, the particles dephase with the rest of the bunch, and slip backwards relative to the wakefield. When they reach the accelerating region of the wakefield, they are re-accelerated. This leads to the rate of energy loss of the bunch dramatically decreasing after a saturation length  $L_{\text{sat}}$ , as a substantial proportion of the energy lost is reabsorbed. The saturation length for a beam of initial energy  $T_0$  is approximately the propagation length at which the maximum decelerating gradient  $E_{\text{dec}}$  decelerates a portion of the beam to non-relativistic velocity:

$$L_{\text{sat}} \approx \frac{T_0}{eE_{\text{dec}}}.$$
 (6.1)

In the active dump the wakefield is created by a preceding laser pulse and hence the whole of the bunch can be decelerated at once. Only once the beam has lost almost all of its initial energy does it slip into the accelerating phase of the wakefield and start to regain energy [128]. Particle-in-cell simulation studies of the active beam dump have shown

that the total energy of an electron bunch representative of that produced by laser wakefield acceleration can be reduced to 8% of its initial value. The drawbacks of the active dump are the additional cost and complexity that a laser represents and the requirement for synchronization between the laser and the particle bunch. The available laser pulse will also put a limit on the energy that can be absorbed by the beam dump whereas in a passive beam dump the energy absorption is only limited by the length of the dump and the continuing ability of the decelerated bunch to drive the plasma wakefield.

A plasma beam dump can be compared to a plasma accelerator. The active plasma beam dump is essentially a laser wakefield accelerator operating in reverse, and energy input comparable to that required for acceleration is required for deceleration. In the passive plasma beam dump on the other hand, no energy input is required other than that required to generate the plasma, if any. In a plasma wakefield accelerator, the behaviour of the drive bunch is not generally important as long as it can drive the required wakefield, while a high quality witness bunch is desired, typically with much smaller charge than the drive bunch. In the passive plasma beam dump, the behaviour of the bulk of particles in the drive bunch is of concern, but the bunch quality is not important as long as it can remain under control. The strong focusing forces of the plasma are therefore desirable in the passive plasma beam dump, whereas in a plasma wakefield accelerator the strong focusing is troublesome in extracting a high quality bunch from the plasma.

### 6.2.1 Plasma and conventional beam dump compared

The stopping power, the rate of loss of energy  $T$  with distance propagated, of a plasma beam dump can be compared with that of a conventional beam dump. A highly relativistic electron beam incident on a conventional beam dump loses energy by bremsstrahlung and ionization, and the stopping power depends on energy. The critical energy is the energy at which the contributions to stopping power for radiation and other factors are equal, and is approximated by  $T_c = (800 \text{ MeV})/(Z+1.2)$  where  $Z$  is the atomic number of the stopping material [129]. For high- $Z$  materials such as lead or copper, bremsstrahlung dominates at any relevant energy. For lower  $Z$  materials such as water, bremsstrahlung is dominant above a few hundred MeV. When considering a high-energy beam dump the per-particle energies of concern are typically GeV scale and thus it can be approximated that bremsstrahlung is the main cause of deceleration. The stopping power due to radiation is given by[127]:

$$-\frac{dT}{dx} = Z\alpha \frac{4e^4 n_e}{mc^2} (\gamma - 1) \ln \left( 183 Z^{-\frac{1}{3}} \right) \quad (6.2)$$

where  $\alpha$  is the fine structure constant,  $m$  is the incident particle mass,  $n_e$  is the electron density of the stopping material,  $e$  is the elementary charge,  $\gamma$  is the relativistic gamma factor and  $c$  is the speed of light, with all quantities in CGS units. This can be re-written as an engineering formula, with the logarithmic part treated as a constant as it changes by

less than a factor of two between hydrogen and uranium. The value of 4.09 corresponding to copper has been assumed. It is also convenient to use SI units for density and distance and gigaelectronvolts for energy:

$$-\frac{dT}{dx} [\text{GeV m}^{-1}] = 4.82 \times 10^{-34} Z n_e (\gamma - 1) . \quad (6.3)$$

As long as bremsstrahlung is dominant, the stopping power is linearly proportional to the kinetic energy of the incident particles,  $T = (\gamma - 1) mc^2$ . The initial stopping power for an electron bunch with energy 1 GeV in a copper beam dump is  $2.3 \text{ GeV m}^{-1}$ , and the stopping power falls as the energy of the bunch decreases. The stopping power of a plasma beam dump depends on the parameters of the bunch, but is limited by the relativistic wave-breaking field  $E_{\text{wb}}$ , which depends on the electron plasma frequency  $\omega_p$ :

$$E_{\text{wb}} = \frac{m_e c \omega_p}{e}, \quad (6.4)$$

The limit of the wave-breaking field for a plasma density of  $1 \times 10^{24} \text{ m}^{-3}$  can be compared with a copper beam dump for an electron beam of 1 GeV. Equation 6.2 gives an initial average decelerating gradient of  $5.1 \text{ GeV m}^{-1}$  compared with a wave-breaking field of  $96 \text{ GV m}^{-1}$ . The actual decelerating gradient that can be achieved in a plasma depends on the properties of the electron bunch. A short bunch with density higher than the plasma density can achieve a gradient approaching the wave-breaking limit, as has been demonstrated experimentally [130–133]. It is also noteworthy that the decelerating gradient for the plasma beam dump is independent of the mass of the particle being decelerated. This

is not the case for the conventional beam dump, where the stopping power is inversely proportional to the particle mass. Pair production of muons, with a mass 200 times that of the electron, can occur if the energy of bremsstrahlung photons is sufficiently high [134]. Muons are decelerated at the same rate as electrons in a plasma beam dump while in a conventional beam dump the stopping power is correspondingly lower and the muons can be considered to be effectively free. Energy loss in a plasma beam dump will also occur by bremsstrahlung, however it is reduced by a factor of the ratio of the densities of the plasma and the conventional dump i.e. several orders of magnitude. For a plasma density of  $1 \times 10^{24} \text{ m}^{-3}$  the stopping power is approximately  $30 \text{ keV m}^{-1}$  depending on the material which over a length of several metres is much less than the highly relativistic electron energies that are necessary for the plasma dump to function. Thus the energy loss due to bremsstrahlung in the plasma dump can be neglected.

The re-acceleration problem can be addressed by removing the low energy particles from the beam dump as they are decelerated. This prevents them from reaching the accelerating region and allows the dump to maintain a higher decelerating gradient for longer. It was proposed by Wu *et al.* [127] to achieve this by means of a series of thin foils placed in the path of the beam, with the foils starting after the saturation length with variable separation and thickness of  $0.1 \lambda_p$ . The foil is able to stop the low energy particles while the high energy portion of the bunch passes through. However, the foil in the plasma beam dump will be exposed to large electric fields, the high temperature plasma, and it will absorb some

energy from the high energy portion of the bunch. Given the previously calculated decelerating gradient in copper, an electron with energy 1 GeV incident on a 0.1 mm thick copper foil will lose on average 0.5 MeV as it passes through the foil. It should however be noted that this energy is radiated as x-rays and only a fraction will be absorbed by the foil. The extreme conditions that the foil is exposed to could lead to damage over the long time that the dump is expected to operate. It would thus be desirable to achieve similar removal of low energy particles from the accelerating phase of the wakefield without requiring that a fragile solid material be exposed to the plasma and the high energy beam.

### 6.3 Varying plasma density

A new method for addressing the re-acceleration problem in the passive plasma beam dump is presented here. This scheme uses an increasing plasma density in order to defocus low-energy particles and prevent their re-acceleration. This avoids the use of non-plasma materials and aims to offer better durability compared to the foil scheme.

The plasma wakefield has focusing and defocusing regions corresponding to low and high plasma electron densities respectively. The region where the plasma electron density is high defocuses the witness particles as the transverse electric field of the plasma overcomes the magnetic field of the bunch. The defocusing region of the wakefield therefore lies behind the accelerating region. If the low-energy portion of the bunch in a passive plasma beam dump can be forced to pass through the de-

focusing region, it will be rapidly removed from the axis and will no longer be available for re-acceleration. If the accelerating gradient is low enough, the particles may pass through the accelerating region and into the defocusing region before they gain enough energy to become highly relativistic and stop slipping relative to the wakefield. Since a high decelerating, and therefore accelerating gradient is desired in a plasma beam dump this is unlikely to be the case. It is instead necessary to shift the plasma wakefield relative to the bunch in order to pass the low-energy particles into the defocusing region. This can be achieved by increasing the plasma density and therefore shortening the plasma wavelength. The position of the particles in the accelerating region of the wakefield can then be changed to be located in the defocusing region. This is illustrated in Figure 6.2. Doubling the plasma density decreases the plasma wavelength by a factor of  $\sqrt{2}$  and allows the low-energy part of the bunch to be defocused.

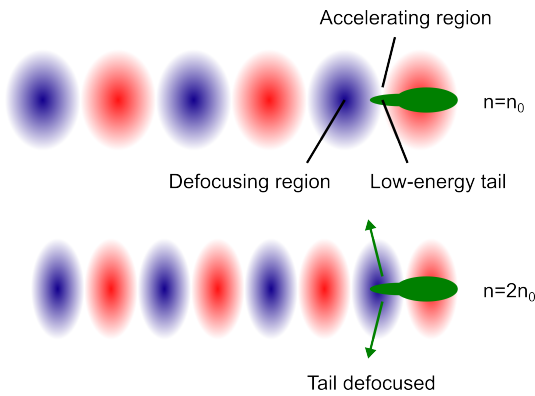


Figure 6.2: Diagram showing how an increase in plasma wavelength can shift particles from the accelerating region of the plasma wakefield into a defocusing region. Blue indicates regions of high electron density and red regions of low density.

The plasma density may be increased gradually or in a series of steps. In the case of a stepped density increase, once a significant population of decelerated particles have entered the accelerating region, the density is increased, shifting these particles into the defocusing region and removing them. The energy of the defocused particles must still be sufficiently low that they can be easily absorbed by the walls or end of the beam dump since they will not be decelerated further by any significant amount in the very low density plasma. If the plasma density is increased gradually, it is necessary for the density increase to be sufficiently fast such that the decelerated particles pass through the accelerating region and into the defocusing region before they gain an excessive amount of energy. The functional form of the density increase should also give a roughly constant rate of plasma wavelength change with distance propagated by the bunch. It is not obvious how a stepped plasma density profile would be generated in practice; although a density step has been produced for laser wakefield acceleration in 100  $\mu\text{m}$ -scale gas jet plasma sources [135] by the use of a razor blade producing a shock front in the gas flow, such a scheme is unlikely to be applicable to the much longer plasma required for a plasma beam dump. A gradient plasma density change may be easier to realize using a gas flow from a high density region to a lower density counter to the direction of propagation of the beam. The functional form that such a gas density would take is not considered here; it is assumed that simple linear and quadratic forms would be the most likely to be achievable. Figure 6.3 shows the change in plasma density and plasma wavelength with longitudinal position for stepped

and linear and quadratic gradient plasma profiles. The rate of change of plasma wavelength is approximately constant for a quadratic density gradient, while for a linear density gradient the rate of change of the plasma wavelength decreases with propagation distance. The stepped plasma density scheme also follows the trend of the linear density increase for constant step size. A step size that increases quadratically would allow for a more consistent change in plasma wavelength with each step, but this was not implemented in simulations as the wavelength change with each step was considered to be sufficient for the density change used here. For larger density increases, the difference between quadratic and linear density profiles, both for the stepped and gradient cases, would be more pronounced [136].

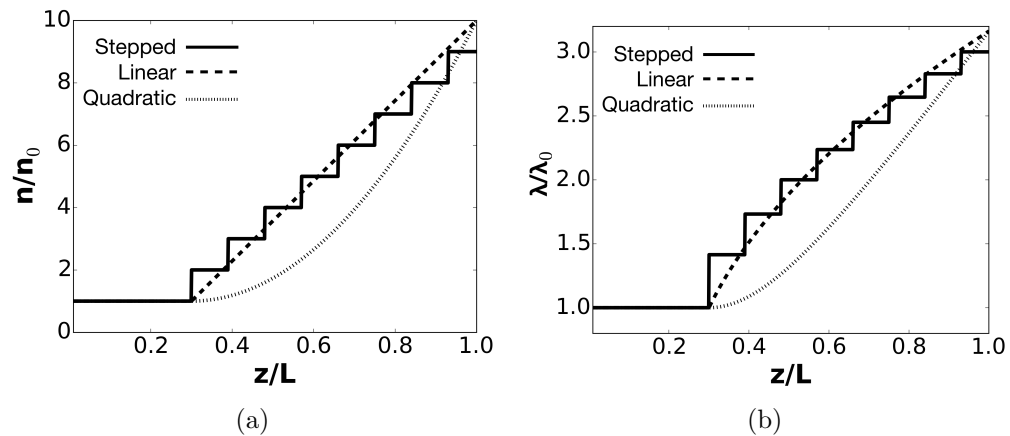


Figure 6.3: Diagrams showing stepped and gradient plasma density profiles (a) and the corresponding change in plasma wavelength that results (b).

The rate of change with position of the plasma wavelength can be calculated for a given plasma profile, by taking the derivative of  $\lambda_p$  with respect to  $z$ . For a linearly increasing plasma density from initial density

$n_i$  to a final density  $n_f$  over a length  $l$ :

$$\frac{d\lambda}{dz} = \frac{\pi c e^2 n_f}{\varepsilon_0 l m_e} \left[ \frac{e^2 n_i \left(1 + \frac{n_f z}{n_i l}\right)}{\varepsilon_0 m_e} \right]^{-\frac{3}{2}}. \quad (6.5)$$

In the linear regime, the defocusing region is located  $\lambda_p/4$  behind the maximum decelerating region. The propagation distance  $\Delta z$  over which the plasma wavelength changes by 1/4 can be estimated assuming that the rate of change of plasma wavelength is constant, and the energy gain  $\Delta T$  is the average accelerating field  $E_{acc}$  multiplied by the propagation distance.

$$\Delta T = E_{acc} \Delta z = E_{acc} \frac{\lambda_0}{4} \left( \frac{d\lambda}{dz} \right)^{-1}, \quad (6.6)$$

where  $\lambda_0$  is the initial plasma wavelength at a given position  $z$ . The more rapid the change in plasma density, the less energy will be gained by the decelerated particles, however the density has to remain low enough to be achievable, and to generate a high decelerating field. Figure 6.4 shows a plot of  $\Delta z$  for linear and quadratic profiles. The singularity in the quadratic energy gain is a result of the assumption that the rate of plasma wavelength change is constant for each data point, and this is zero at  $z = 0$ . In practice when the rate of plasma wavelength change is small this assumption is not valid and the singularity will not occur. The plot shows that the quadratic density profile maintains smaller  $\Delta z$  over a larger distance compared to the linear profile.

The practicalities of achieving a varying plasma density have not been investigated in depth. Stepped plasma densities have been achieved in

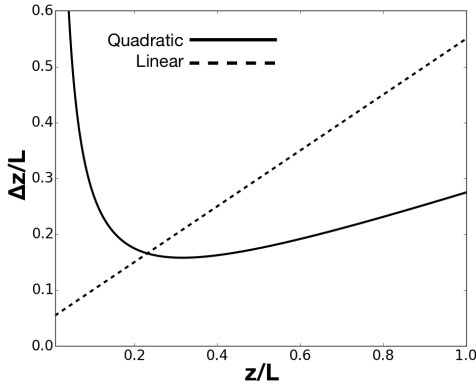


Figure 6.4: Length  $\Delta z$  over which a low-energy particle is accelerated before passing into defocusing region as a function of propagation distance  $z$  for linear and quadratic plasma density increases over a distance  $L$ .

beam- and laser-driven plasma wakefield acceleration experiments using a gas jet source [137, 138] where the plasma is of millimetre length, but this technique is not applicable to plasmas of metre-scale length. Maintaining a plasma density for a large distance either side of a step is likely to be difficult. A possibility is to use separate plasma cells with different density, but this would introduce materials into the path of the beam. A gap between plasmas may also lead to additional de-phasing between the high- and low-energy portions of the bunch. A gradient plasma density profile could be achieved by differential pumping; gradient gas density from differential pumping was suggested as a means of improving the performance of the noble gas dump [126] and this may be applicable to a plasma source. However, the large density change required for a plasma beam dump may still be difficult to achieve.

### 6.3.1 Energy recovery from a plasma beam dump

One of the most attractive features of the plasma beam dump is that the energy that is transferred to the plasma remains in a concentrated, low entropy form in the oscillations of the plasma electrons rather than being dissipated immediately as heat. This makes it in principle possible to recover the energy as electricity [127]. Since the plasma oscillations are damped by collisions between the plasma particles, removing energy before it is converted to heat may be necessary to control the temperature of the plasma beam dump. A simple method of energy recovery from the plasma would be a pickup circuit that passes through the plasma in which the large oscillating electric field produces a current [127]. The electrons in the plasma oscillate in the radial direction, so the magnetic field of the oscillating plasma electrons is in the azimuthal direction. The magnetic field could induce a current in a metallic wire running parallel to the path of the beam. The radio frequency current may then transferred to an external circuit and converted to usable electricity via a rectifier and inverter. This concept has not however been studied in detail and it is not known if the efficiency or other practical considerations such as material durability in a plasma would make such a scheme viable. In a conventional dump, some energy may be recovered as hot water, but this may be of limited use in an accelerator facility, and conversion to electricity is unlikely to be practical due to the relatively low temperature of the output.

## 6.4 Simulation results

In order to validate the varying plasma density beam dump concept, particle-in-cell simulations were carried out. The aim of these simulations was to verify that the method of removing low-energy particles from the axis by having them pass into the defocusing region is viable. The simulations also aimed to measure the effectiveness of the plasma beam dump using a bunch with parameters representative of those available from laser wakefield acceleration. The bunch parameters used were for a 250 MeV electron bunch with rms radius 20  $\mu\text{m}$  and length 7.5  $\mu\text{m}$ . The bunch charge was 100 pC. This gives a total bunch energy of 0.025 J which is realistic for a laser wakefield accelerated bunch. The bunch parameters were fixed for these simulations as it is known that higher gradients can be achieved with shorter, denser or higher charge bunches, and the dependence of the performance of the beam dump on the characteristics of the plasma structure was the subject under study. The initial plasma density was  $2 \times 10^{23} \text{ m}^{-3}$  corresponding to a plasma wavelength of 75  $\mu\text{m}$ .

A comparison of the case of a uniform plasma beam dump, a stepped density profile with different step lengths, and linear and quadratic gradient profiles was made. A plot of the total bunch energy with distance propagated is shown in Figure 6.5. As expected, the constant density profile was least effective, and the energy loss decreased substantially after approximately 12 cm. The largest overall energy loss was achieved with a quadratic density increase, though its performance was only slightly

better than the linear gradient profile. It is notable that the linear profile energy loss tails off in comparison with the quadratic profile at the end of the plasma, which may reflect the decrease in the rate of plasma wavelength change that occurs in the linear profile but not the quadratic profile. The stepped profiles performed worse than the gradient profiles for all step lengths tested. The different step lengths gave nearly identical energy loss over the full length of the plasma despite the energy of the beam differing significantly at intermediate distances. Even in the uniform bunch case the plasma beam dump is capable of absorbing approximately half of the bunch energy before saturation. A uniform plasma beam dump could be used as a preceding stage to a conventional beam dump to reduce cooling requirements and radio-activation in the conventional dump. The conventional beam dump would still have to be capable of stopping particles with the initial energy of the beam however, as the plasma beam dump does not reduce the peak energy of the bunch.

The average decelerating gradient for the bunch with different plasma density schemes is shown in Table 6.1. In comparison to the average gradient, the initial decelerating gradient before saturation was approximately  $1.4 \text{ GeV m}^{-1}$ . The peak decelerating field in the vicinity of the bunch is approximately  $3 \text{ GV m}^{-1}$ , while the maximum field in the plasma is  $4.7 \text{ GV m}^{-1}$ . Thus the average decelerating gradient is 16% of the maximum field. The plasma and beam density, and the transverse and longitudinal electric fields are plotted in Figure 6.6. Comparing the longitudinal and transverse field plots it can be seen that the accelerating

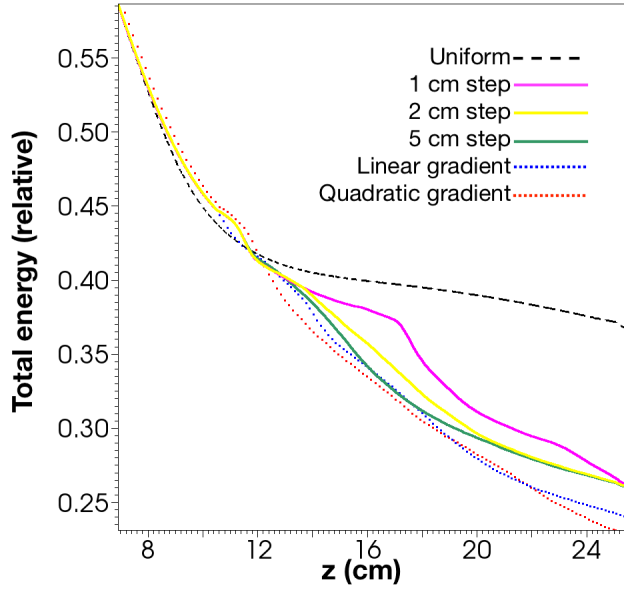


Figure 6.5: Plot of total bunch energy as a fraction of initial energy against propagation distance. Prior to  $z \approx 10$  cm all plasma profiles are uniform and the loss of energy is the same, so this portion of the plot is omitted.

region (blue in Figure 6.6b) contains both a focusing region at the forward end and a defocusing region at the back. The shift of the wakefield relative to the bunch caused by increasing plasma density allows particles in the accelerating region to be shifted into the defocusing region and removed from the axis and thus prevented from undergoing further acceleration.

The detailed effect of the plasma density change can be observed by studying the longitudinal phase space of the bunch (Figure 6.7). This shows the re-acceleration that limits energy loss in the uniform plasma case, while in the linear gradient case after the same propagation distance, the re-accelerated portion of the bunch is absent. The reason for the loss of the decelerated particles can be seen in the transverse

Table 6.1: Average decelerating gradients for different plasma beam dump profiles.

Profile	Energy loss (%)	Gradient ( $\text{MeV m}^{-1}$ )
Uniform	63	630
1 cm step	73.5	735
2 cm step	74	740
5 cm step	74	740
Linear	75.5	755
Quadratic	77	770

coordinate-energy space (Figure 6.8, in which gradient case shows the defocusing of the low energy particles. In contrast the uniform case shows no defocusing and hence allows re-acceleration. The loss of low energy particles can be more clearly seen in the evolution of the longitudinal phase space over the full length of the plasma (Figure 6.9). Initially the bunch is non-uniformly decelerated (Figure 6.9a,b), and the lowest energy portion of the bunch passes into the accelerating region of the wakefield (Figure 6.9c). After this the change in the plasma wavelength causes the loss of the low energy particles and re-acceleration is prevented for the remainder of the plasma length (Figure 6.9d-f).

The effectiveness of the plasma density schemes can be assessed by measuring the amount of charge re-accelerated. This was done by calculating the charge of particles in the region  $z - ct < 30 \mu\text{m}$  with energy greater than 30 MeV. This region is initially free of charge, and the energy threshold includes particles that are re-accelerated while excluding particles that pass through the region without gaining significant energy. Figure 6.10 gives a comparison between the charge in this region of lon-

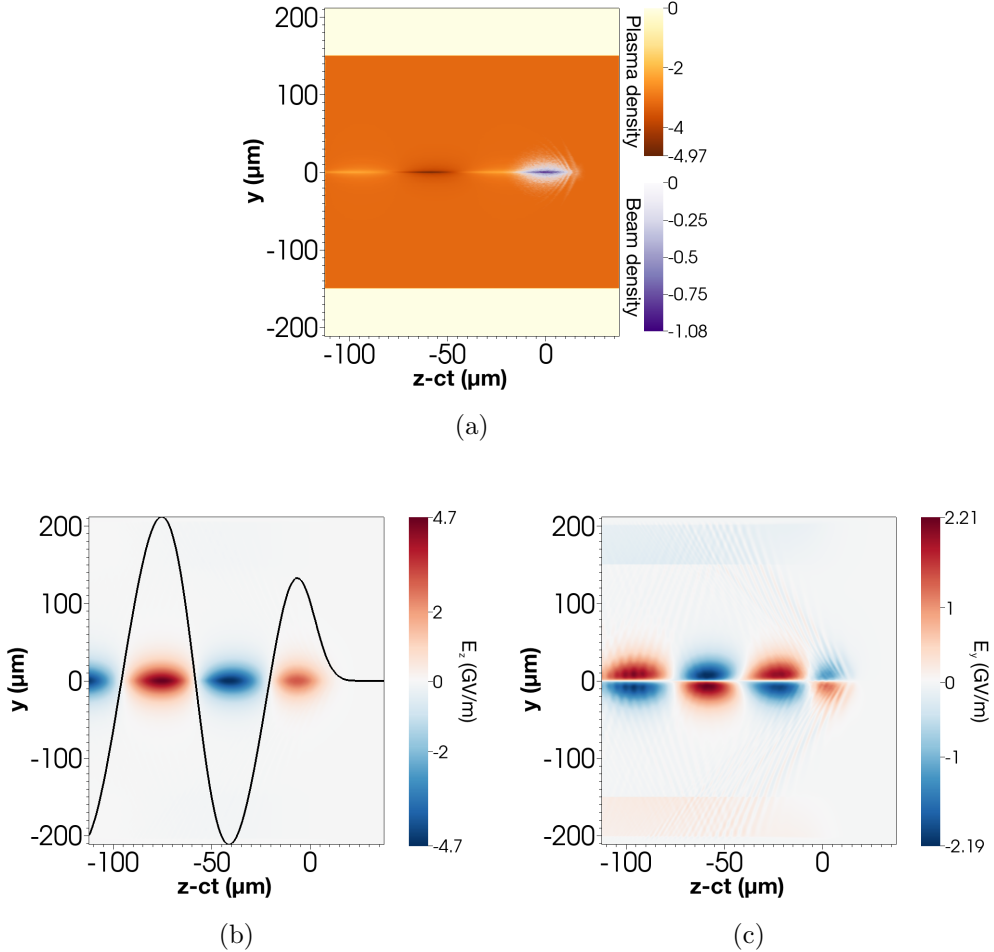


Figure 6.6: Plasma and beam density, and longitudinal and transverse electric fields for the plasma beam dump in the initial region of uniform plasma density.

itudinal phase space for the linear and quadratic ramps. The change in the charge present in this region differs significantly between the different profiles despite the similar overall performance in terms of energy loss of the bunch as a whole that is seen in Figure 6.5. The rationale for using a quadratic density profile in place of a linear ramp is that the quadratic profile maintains a more constant rate of plasma wavelength

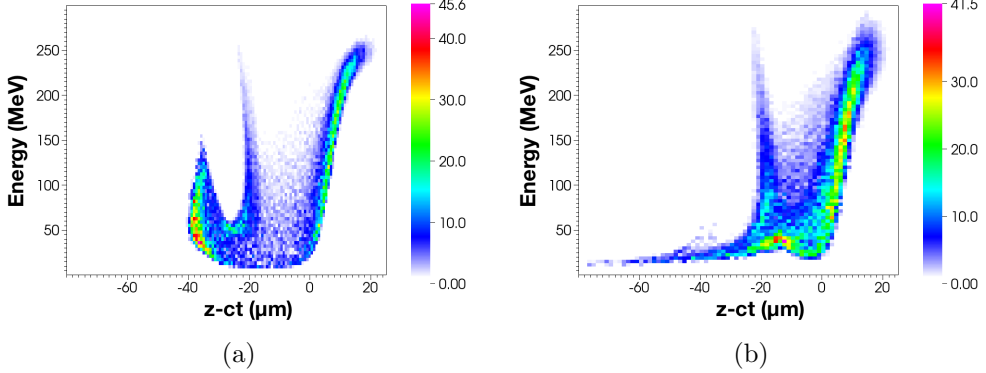


Figure 6.7: Longitudinal phase space at  $z=16.3$  cm for uniform (a) and linear gradient (b) plasma profiles.

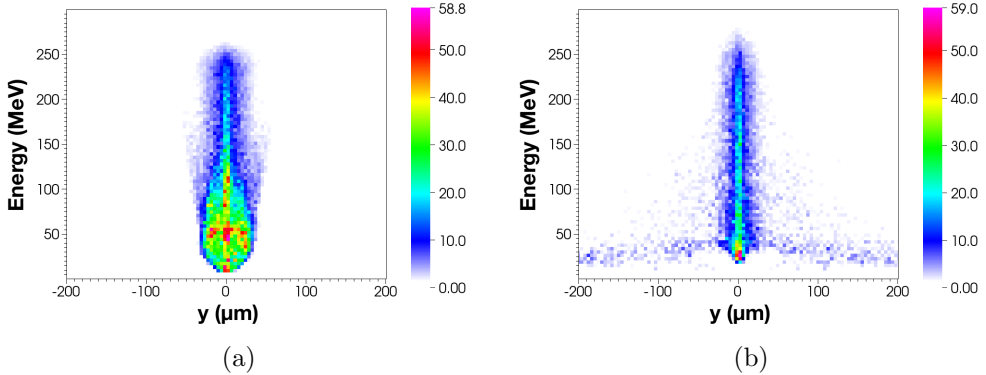


Figure 6.8: Transverse coordinate-energy plot at  $z=16.3$  cm for uniform (a) and linear gradient (b) plasma profiles.

change at the expense of a slower initial change. However, the simulation results show that the re-accelerated charge in fact falls more quickly for the quadratic case and there is relatively little difference as propagation distance increases. This indicates that a slow initial increase in plasma density may be more effective than a rapid one, which may also explain the somewhat lower performance of the stepped profiles compared to the continuously varying density.

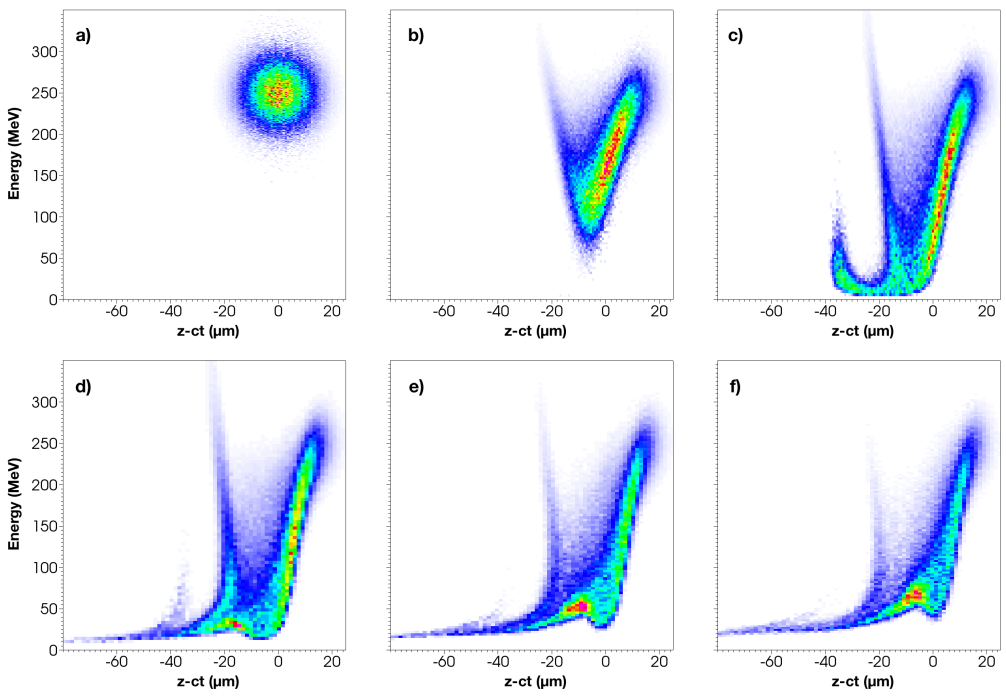


Figure 6.9: Evolution of longitudinal phase space for a linear gradient plasma beam dump. Plots are for a) 0, b) 5, c) 10, d) 15, e) 20 and f) 25 cm.

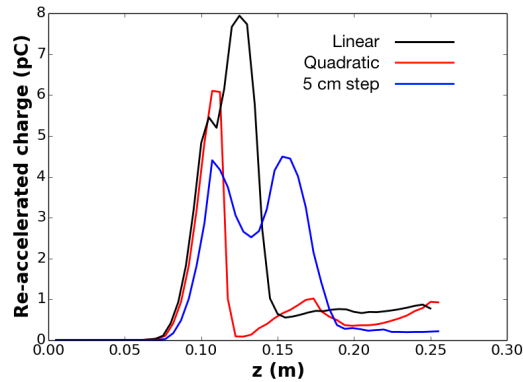


Figure 6.10: Charge of particles with energy  $> 30$  MeV and  $z - ct > -30$  μm for linear and quadratic gradient, and 5 cm step length plasma profiles.

The energy spectrum of a bunch that has passed through a plasma beam dump is important as unlike in a conventional beam dump, the

deceleration of the bunch is not uniform. The spectrum for the case of a linear plasma density increase is shown in Figure 6.11. The peak energy of the bunch is unchanged after passage through the plasma beam dump: this is as expected as the small proportion of particles at the extreme front of the bunch experience no decelerating field. The intensity at this energy however is greatly decreased, and the intensity at the initial central energy of the bunch is decreased by a factor of ten. The energy corresponding to the peak intensity of the decelerated bunch is to approximately 75 MeV.

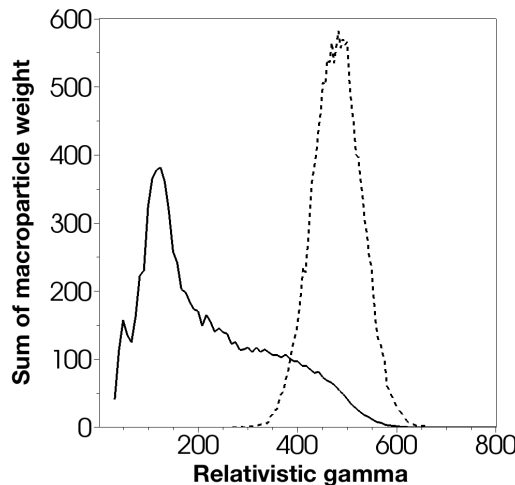


Figure 6.11: Energy spectrum before and after a 25 cm plasma beam dump with a linear plasma gradient profile.

## 6.5 Summary

The plasma beam dump differs from a conventional beam dump in that deceleration occurs as a collective excitation of the plasma rather than

stochastic interaction between the beam and a dense material. This allows a very low density medium to decelerate a beam at a comparable rate to that of a material of density several orders of magnitude higher. The low density of the plasma beam dump is attractive due to the reduction in radio-activation and the potential for the production of hazardous chemicals. The plasma beam dump also offers the possibility for more efficient energy recovery than is possible with a conventional dump.

A plasma beam dump does however suffer from the limitation of being unable to decelerate the extreme head of the bunch and thus a small portion of particles maintain the initial bunch energy. There is also a limit to the energy that can be absorbed by the plasma dump as it relies on a relativistic and cohesive bunch to provide the large decelerating gradient. Thus it would be necessary for a high-energy plasma beam dump to operate in conjunction with a conventional beam dump to absorb the remaining energy. The conventional dump would need to be of equivalent length to one which would absorb the full energy of the beam (e.g. 11 m for the ILC) however since the conventional dump would only routinely absorb a fraction of the initial bunch energy the requirements on cooling and dealing with the undesirable products of the beam-solid/liquid interaction would be dramatically reduced. It would also be desirable for the conventional dump component to be capable of absorbing the full-energy bunch in the case of a failure of the plasma dump component, which may be a concern especially when using a transient plasma source.

The varying plasma density scheme described in this chapter is an effective means of reducing the re-acceleration of particles which have lost

almost all of their energy to the plasma. The scheme's major advantage over the previously proposed use of metallic foils is to avoid the introduction of non-plasma materials into the beam dump and thus improve the durability of the device. There may be some difficulties in implementing a varying plasma density scheme because of the large density change that would be required. The realization of the varying density plasma dump scheme is a topic for future research.

# Chapter 7

## Conclusion

Plasma accelerator technology has seen extensive research over the last few decades as it offers dramatic improvements in certain aspects of accelerator performance. Laser- and beam-driven plasma wakefield acceleration can achieve accelerating gradients three orders of magnitude higher than are typically achieved in conventional RF accelerators. The focusing gradients that can be achieved in plasma lenses are similarly large compared to conventional focusing elements. A plasma beam dump offers comparable or better beam stopping capability to a conventional dump while being several orders of magnitude lower in density.

However, the capabilities of plasmas are also accompanied by challenges. It has proven difficult to simultaneously achieve high energy, beam quality and luminosity in plasma wakefield acceleration. Plasma lenses are prone to aberrations that increase emittance. Saturation occurs in the passive plasma beam dump, and it is incapable of decelerating the bunch head. Recent experiments in plasma acceleration have made

significant progress towards the former, but the latter two cases have seen little recent experimental investigation. This thesis presents results of investigations into plasma wakefield acceleration, plasma lensing and a passive plasma beam dump using theory and particle-in-cell simulation. The aim of these investigations was to demonstrate the viability of experimental study of these phenomena using existing and planned accelerators at Daresbury Laboratory and elsewhere.

Simulations of plasma wakefield acceleration using the planned 250 MeV CLARA beam show that wakefields in the  $\text{GV m}^{-1}$  range can be driven in the weakly nonlinear regime. Simulations of a ramped drive bunch with otherwise comparable parameters to the CLARA beam showed that a transformer ratio greater than six could be achieved. This would allow continuous acceleration over a length of 4.8 m and potentially acceleration of the witness bunch to an energy of 1.3 GeV. Acceleration using the CLARA-FE beam has also been studied showing that acceleration is also possible in the linear regime, albeit at a gradient only somewhat larger than is commonly achieved in RF acceleration. These CLARA-FE experiments would nonetheless be useful for testing plasma sources and developing experience in their operation in conjunction with the existing accelerator. Such experiments would be valuable as a precursor to experiments using the full CLARA beam which is able to access a wider range of bunch parameters and hence plasma regimes. The evidence obtained on the viability of plasma wakefield acceleration using a ramped drive bunch provides motivation to investigate the possibility of generating such bunch distributions in CLARA.

Focusing using a passive plasma lens was also studied in simulations, and an experiment was planned but could not be carried out due to external technical factors. It was demonstrated that an experimental study of plasma lensing at the VELA experimental area is viable. Modest focusing gradients can be achieved using the VELA beam and significantly higher gradients can be achieved using CLARA-FE. There was some disagreement between theory and simulation results in the study of the spherical aberration, making an experimental test of this effect desirable. Further simulation studies of the spherical aberration including 3D simulations would also be valuable in determining the source of the disagreement. The longitudinal aberration was studied using particle tracking and particle-in-cell simulation, and results were found to be in reasonable agreement. Experimental studies of plasma lensing are likely to be viable using a wide range of accelerators. Detailed emittance measurements could be carried out to determine the relative effects of longitudinal and spherical aberrations.

Simulations of the passive plasma beam dump were carried out using parameters suitable for a modest laser wakefield accelerator. A new scheme to address the problem of re-acceleration of the de-phased portion of the bunch was studied, in which the plasma density is increased in order to de-focus the low-energy particles and remove them from the accelerating region. This scheme is considered to have an advantage over the previously proposed method of using foils to scatter low-energy particles as it relies on a purely plasma-based structure and avoids the introduction of solid material into the path of the beam, and exposure

to the plasma. It would be desirable in the future to compare the foil scheme to the varying plasma density in terms of performance, but this was not possible with the software available. In order for an experimental test of the density varying scheme to be carried out it would be necessary to determine the best way of achieving the required density change in a practical plasma source. Simulations would need to be carried out to determine the energy loss that can be achieved in a realistic plasma source given that it will likely have limitations compared to the idealized plasma structure considered here.

# Appendix A

## Parameters for simulations presented in this thesis

Table A.1 summarizes parameters of simulations used in this thesis, and provides the plasma wavelength for comparison. Parameters shown are plasma density  $n_e$ , plasma wavelength  $\lambda_p$ , longitudinal and transverse RMS drive bunch size ( $\sigma_x$  and  $\sigma_r$ ), resolution in cells per RMS bunch size ( $R_x$  and  $R_r$ ), extent in multiples of RMS bunch size ( $R_x$  and  $R_r$ ) and grid interval ( $\Delta x$  and  $\Delta r$ ), and approximate total number of cells  $N$ . For the ramped drive bunch,  $\sigma_x$  is the well-defined bunch length rather than RMS length. Although this thesis uses  $z$  as the longitudinal coordinate, VSim uses  $x$  by default, and so these simulation parameters also use  $x$  for consistency. For simulations which used a range of parameters, the extremes are shown for comparison.

Table A.1: Parameters for simulations presented in this thesis

Simulation	$n_e$ [m $^{-3}$ ]	$\lambda_p$ [mm]	$\sigma_r$ [ $\mu\text{m}$ ]	$\sigma_x$ [ $\mu\text{m}$ ]	$R_x$	$R_r$	$X_x$	$X_r$	$\Delta x$ [ $\mu\text{m}$ ]	$\Delta r$ [ $\mu\text{m}$ ]	$N$
CLARA-PWFA	$3 \times 10^{21}$	0.17	75	20	60	16	20	20	3.75	2.5	64 000
VELA lens	$3 \times 10^{17}$ $9 \times 10^{18}$	61 11	3300	445	45	90	73	12	20	4.9	$3.6 \times 10^6$
CLARA-FE Gauss	$1 \times 10^{22}$	0.34	45	100	8	16	12	25	5.6	6.3	38 265
CLARA-FE ASTRA	$1 \times 10^{22}$	0.34	120	39	16	50	24	20	7.5	0.78	384 000
CLARA-FE 3D	$1 \times 10^{22}$	0.34	120	39	31	10	24	20	3.9	3.9	$2.95 \times 10^7$
Ramped drive	$5 \times 10^{21}$	0.47	472 944	50	160 320	32	10	16	2.95	1.56 $1.64 \times 10^6$	821 000
Plasma dump	$2 \times 10^{23}$ $2 \times 10^{24}$	0.074 0.023	7.5	20	16	40	20	20	0.46	0.19	687 000

# List of publications

## Journal publications

1. **K. Hanahoe**, G. Xia, M. Islam, Y. Li, O. Mete-Apsimon, B. Hidding, J. Smith, “Simulation study of a passive plasma beam dump using varying plasma density”, *Phys. Plasmas*, vol. 24, 023120, 2017.
2. Y. Li, G. Xia, K. V. Lotov, A. P. Sosedkin, **K. Hanahoe**, O. Mete-Apsimon, “High-quality electron generation in a proton-drive hollow plasma wakefield accelerator”, *Phys. Plasmas*, accepted, 2017.
3. Y. Wei, S. Jamison, G. Xia, **K. Hanahoe**, Y. Li, J. Smith, C. P. Welsch, “Beam quality study for a grating-based dielectric laser-driven accelerator”, *Phys. Plasmas*, vol. 24, 023102, 2017.
4. **K. Hanahoe**, O. Mete, G. Xia, D. Angal-Kalinin, J. Jones, J. Smith, “Simulation study of plasma lens experiments at Daresbury Laboratory”, *Plasma Phys. Control. Fusion*, vol. 58, 034002, 2016.
5. G. Xia, Y. Nie, O. Mete, **K. Hanahoe**, M. Dover, M. Wigram, J. Wright, J. Zhang, J. Smith, T. Pacey, Y. Li, Y. Wei, C. Welsch, “Plasma wakefield acceleration at CLARA facility in Daresbury Laboratory”, *Nucl. Instrum. Meth. Phys. Res. Sect. A*, vol. 829, pp. 43-49, 2016.
6. O. Mete, M. Labiche, G. Xia, **K. Hanahoe**, “GEANT4 Simulations for beam emittance in a linear collider based on plasma wakefield acceleration”, *Phys. Plasmas*, vol. 22, 083101, 2015.

7. O. Mete, G. Xia, **K. Hanahoe**, M. Dover, M. Wigram, J. Wright, J. Zhang, J. Smith, “Design studies and commissioning plans for plasma acceleration research station experimental program”, *Phys. Plasmas*, vol. 22, 103117, 2015.
8. G. Xia, D. Angal-Kalinin, J. Clarke, J. Smith, E. Cormier-Michel, J. Jones, P. Williams, J. Mckenzie, B. Militsyn, **K. Hanahoe**, O. Mete, A. Aimidula, C. Welsch, “A plasma wakefield acceleration experiment using CLARA beam”, *Nucl. Instrum. Meth. Phys. Res. Sect. A*, vol. 740 pp. 165-172, 2014.

## Conference publications

1. Y. Li, G. Xia, **K. Hanahoe**, T. Pacey, O. Mete, “Proton-driven electron acceleration in a hollow plasma”, *Proc. IPAC16*, (Busan, Korea), TUPMY025, 2016.
2. Y. Wei, C. P. Welsch, S. Jamison, G. Xia, **K. Hanahoe**, Y. Li, J. Smith, “Beam dynamics studies into grating-based dielectric laser-driven accelerators”, *Proc. IPAC16*, (Busan, Korea), TUPOY027, 2016.
3. O. Mete, G. Burt, **K. Hanahoe**, G. Xia, J. Smith, B. Hidding, “iIMPACT, undulator based multi bunch plasma wakefield accelerator”, *Proc. IPAC16*, (Busan, Korea), WEPMY025, 2016.
4. T. Pacey, O. Mete, **K. Hanahoe**, G. Xia, “A gas-filled capillary based plasma source for wakefield experiment”, *Proc. IPAC16*, (Busan, Korea), WEPMY026, 2016.
5. **K. Hanahoe**, R. Appleby, B. Kyle, Y. Li, T. Pacey, G. Xia, O. Mete, B. Hidding, J. Smith, “Feasibility study of plasma wakefield acceleration at the CLARA front-end facility”, *Proc. IPAC16*, (Busan, Korea), WEPMY027, 2016.
6. O. Mete, **K. Hanahoe**, G. Xia, M. Dover, M. Wigram, J. Wright, J. Zhang, J. Smith, “Design Studies and Commissioning Plans for PARS Experimental Program”, *Proc. IPAC15*, (Richmond, VA, USA), WEPWA048, 2015.
7. O. Mete, **K. Hanahoe**, G. Xia and M. Labiche, “Emittance Growth in a Plasma Wakefield Accelerator”, *Proc. IPAC15*, (Richmond, VA, USA), WEPWA047, 2015.

8. **K. Hanahoe**, O. Mete, G. Xia, D. Angal-Kalinin, J. Jones, J. Smith, “Particle-in-cell Simulations of a Plasma Lens at Daresbury Laboratory”, *Proc. IPAC15*, (Richmond, VA, USA), MOPJE084, 2015.
9. Y. Wei, C. Welsch, G. Xia, J. Smith, **K. Hanahoe**, O. Mete, “Investigations into Dielectric Laser-driven Accelerators using the CST and VSIM Simulation Codes”, *Proc. IPAC15*, (Richmond, VA, USA), WEPWA051, 2015.
10. Y. Wei, G. Xia, J. Smith, **K. Hanahoe**, O. Mete, S. Jamison, C. Welsch, “Numerical study of a multi-stage dielectric laser-driven accelerator”, *Physics Procedia*, vol. 77, pp. 50-57, 2015.
11. O. Mete, **K. Hanahoe**, G. Xia, M. Labiche, O. Karamyshev, Y. Wei, C. Welsch, M. Wing, “Emittance growth due to multiple Coulomb scattering in a linear collider based on plasma wakefield acceleration”, *Proc. IPAC14*, (Dresden, Germany), TUPRO074, 2014.
12. **K. Hanahoe**, O. Mete, G. Xia, D. Angal-Kalinin, J. Clarke, S. P. Jamison, J. Jones, J. W. McKenzie, B. L. Militsyn, P. Williams, J. Smith, B. Hidding, “Plasma wakefield acceleration at CLARA PARS”, *Proc. IPAC14*, (Dresden, Germany), TUPME081, 2014.
13. G. Xia, J. Clarke, D. Angal-Kalinin, J. Smith, P. Williams, J. Jones, **K. Hanahoe**, “A proposed plasma acceleration research station at CLARA facility”, *Proc. IPAC13*, (Shanghai, China), pp.1280-1282, TUPEA064, 2013.

# Bibliography

- [1] T. W. Aitken, B. S. Halliday, W. T. Johnstone, C. W. Jones, T. Joy, M. C. Morris, N. R. S. Tait, and R. G. P. Voss, *The Nuclear Structure Facility at Daresbury*, 1974.
- [2] B. J. Holzer, “Introduction to particle accelerators and their limitations”, in *Proc. of the CERN Accelerator School: Plasma Wake Acceleration*, (CERN, Geneva, Switzerland), 2016, pp. 29–50.
- [3] S. Geer, “Muon colliders and neutrino factories”, *Annu. Rev. Nucl. Part. Sci.*, vol. 59, pp. 347–365, 2009.
- [4] W. D. Kilpatrick, “Criterion for vacuum sparking designed to include both rf and dc”, *Rev. Sci. Instrum.*, vol. 28, pp. 824–826, 1957.
- [5] “IEEE standard letter designations for radar-frequency bands”, IEEE Aerospace and Electronic Systems Society, New York, NY, USA, Tech. Rep. IEEE Std 521-2002, 2003.
- [6] J. T. Seeman, “The Stanford Linear Collider”, Stanford Linear Accelerator Center, Stanford, CA, USA, Tech. Rep. SLAC-PUB-5607, 1991.
- [7] T. Behnke *et al.*, “ILC Technical Design Report vol. 1 - Executive Summary”, Linear Collider Collaboration, Batavia, IL, USA, Tech. Rep. ILC-REPORT-2013-040, 2010.
- [8] M. Aicheler, P. Burrows, M. Draper, T. Garvey, P. Lebrun, K. Peach, N. Phinney, H. Schmickler, D. Schulte, and N. Toge, “A multi-TeV collider based on CLIC technology: CLIC conceptual design report”, CERN, Geneva, Switzerland, Tech. Rep. CERN-2012-007, 2012.
- [9] C. Adolphson *et al.*, “ILC Technical Design Report vol. 3, Part II - Baseline Design”, Linear Collider Collaboration, Batavia, IL, USA, Tech. Rep. ILC-REPORT-2013-040, 2010.

- [10] M. E. Hill, C. Adolphsen, W. Baumgartner, R. S. Callin, X. E. Lin, M. Seidel, T. Slaton, and D. H. Whittum, “High-gradient millimeter-wave accelerator on a planar dielectric structure”, *Phys. Rev. Lett.*, vol. 87, 094801, 2001.
- [11] D. Wang, S. Antipov, C. Jing, J. G. Power, M. Conde, E. Wisniewski, W. Liu, J. Qiu, G. Ha, V. Dolgashev, C. Tang, and W. Gai, “Interaction of an ultrarelativistic electron bunch train with a W-band accelerating structure: High power and high gradient”, *Phys. Rev. Lett.*, vol. 116, 054801, 2016.
- [12] E. Fermi, “On the origin of cosmic radiation”, *Phys. Rev.*, vol. 75, pp. 1169–1174, 1949.
- [13] E. M. McMillan, “The origin of cosmic rays”, *Phys. Rev.*, vol. 79, pp. 498–501, 1950.
- [14] T. Tajima and J. M. Dawson, “Laser electron accelerator”, *Phys. Rev. Lett.*, vol. 43, pp. 267–270, 1979.
- [15] P. Maine, D. Strickland, P. Bado, M. Pessot, and G. Mourou, “Generation of ultrahigh peak power pulses by chirped pulse amplification”, *IEEE J. Quantum Electron.*, vol. 24, pp. 398–403, 1988.
- [16] K. Nakajima, D. Fisher, T. Kawakubo, H. Nakanishi, A. Ogata, Y. Kato, Y. Kitagawa, R. Kodama, K. Mima, H. Shiraga, K. Suzuki, K. Yamakawa, T. Zhang, Y. Sakawa, T. Shoji, Y. Nishida, N. Yugama, M. Downer, and T. Tajima, “Observation of ultrahigh gradient electron acceleration by a self-modulated intense short laser pulse”, *Phys. Rev. Lett.*, vol. 74, pp. 4428–4431, 1995.
- [17] A. Modena, Z. Najmudin, A. E. Dangor, C. E. Clayton, K. A. Marsh, C. Joshi, V. Malka, C. B. Darrow, C. Danson, D. Neely, and F. N. Walsh, “Electron acceleration from the breaking of relativistic plasma waves”, *Nature*, vol. 377, pp. 606–608, 1995.
- [18] S. P. D. Mangles, C. D. Murphy, Z. Najmudin, A. G. R. Thomas, J. L. Collier, A. E. Dangor, E. J. Divali, P. S. Foster, J. G. Gallacher, C. G. Hooker, D. A. Jaroszynski, A. J. Langley, W. B. Mori, P. A. Norreys, F. S. Tsung, R. Viskup, B. R. Walton, and K. Krushelnick, “Monoenergetic beams of relativistic electrons from intense laser-plasma interactions”, *Nature*, vol. 431, pp. 535–538, 2004.

- [19] C. G. R. Geddes, C. Toth, J. van Tilborg, E. Esarey, C. B. Schroeder, D. Bruhwiler, C. Nieter, J. Cary, and W. P. Leemans, “High-quality electron beams from a laser wakefield accelerator using plasma channel guiding”, *Nature*, vol. 431, pp. 538–541, 2004.
- [20] J. Faure, Y. Glinec, A. Pukhov, S. Kiselev, S. Gordienko, E. Lefebvre, J. P. Rousseau, F. Burgy, and V. Malka, “A laser-plasma accelerator producing monoenergetic electron beams”, *Nature*, vol. 431, pp. 541–544, 2004.
- [21] P. A. Walker, “Horizon 2020 EuPraxia design study”, in *Proc. IPAC2017*, (Copenhagen, Denmark), 2017, pp. 1265–1268.
- [22] S. P. D. Mangles, A. G. R. Thomas, O. Lundh, F. Lindau, M. C. Kaluza, A. Persson, C.-G. Wahlström, K. Krushelnick, and Z. Najmudin, “On the stability of laser wakefield accelerators in the monoenergetic regime”, *Phys. Plasmas*, vol. 14, 056702, 2007.
- [23] J. Osterhoff, A. Popp, Z. Major, B. Marx, T. P. Rowlands-Rees, M. Fuchs, M. Geissler, R. Hörlein, B. Hidding, S. Becker, E. A. Peralta, U. Schramm, F. Grüner, D. Habs, F. Krausz, S. M. Hooker, and K. S., “Generation of stable, low-divergence electron beams by laser-wakefield acceleration in a steady-state-flow gas cell”, *Phys. Rev. Lett.*, vol. 101, 085002, 2008.
- [24] W. P. Leemans, B. Nagler, A. J. Gonsalves, C. Tóth, K. Nakamura, C. G. R. Geddes, E. Esarey, C. B. Scroeder, and S. M. Hooker, “GeV electron beams from a centimetre-scale accelerator”, *Nature Phys.*, vol. 2, pp. 696–699, 2006.
- [25] W. P. Leemans, A. J. Gonsalves, H. S. Mao, K. Nakamura, C. Benedetti, C. B. Scroeder, C. Tóth, J. Daniels, D. E. Mittelberger, S. S. Bulanov, J. L. Vay, C. G. R. Geddes, and E. Esarey, “Multi-GeV electron beams from capillary-discharge-guided subpetawatt laser pulses in the self-trapping regime”, *Phys. Rev. Lett.*, vol. 113, 245002, 2014.
- [26] B. Cros, “Laser-driven plasma wakefield: Propagation effects”, in *Proc. of the CERN Accelerator School: Plasma Wake Acceleration*, (CERN, Geneva, Switzerland), 2016, pp. 207–230.
- [27] A. Pukhov and I. Kostyukov, “Control of laser-wakefield acceleration by the plasma-density profile”, *Phys. Rev. E*, vol. 77, 025401(R), 2008.

- [28] S. Steinke, J. van Tilborg, C. Benedetti, C. G. R. Geddes, C. B. Schroeder, J. Daniels, K. K. Swanson, A. J. Gonsalves, K. Nakamura, N. H. Matlis, B. H. Shaw, E. Esarey, and W. P. Leemans, “Multistage coupling of independent laser-plasma accelerators”, *Nature*, vol. 530, pp. 190–193, 2016.
- [29] M. Roth and M. Schollmeier, “Ion acceleration - target normal sheath acceleration”, in *Proc. of the CERN Accelerator School: Plasma Wake Acceleration*, (CERN, Geneva, Switzerland), 2016, pp. 231–270.
- [30] L. Yin, B. J. Albright, B. M. Hegelich, and J. C. Fernández, “GeV laser ion acceleration from ultrathin targets: The laser break-out afterburner”, *Las. and Part. Beams*, vol. 24, pp. 291–298, 2006.
- [31] I. Jong Kim, K. Hong Pae, I. Woo Choi, C. L. Lee, H. Taek Kim, H. Singhal, J. H. Sung, S. Ku Lee, H. Woon Lee, P. V. Nickles, T. M. Jeong, C. Min Kim, and C. Hee Nam, “Radiation pressure acceleration of protons to 93 MeV with circularly polarized petawatt laser pulses”, *Phys. Plasmas*, vol. 23, 070701, 2016.
- [32] P. Chen, J. M. Dawson, R. W. Huff, and T. Katsouleas, “Acceleration of electrons by the interaction of a bunched electron beam with a plasma”, *Phys. Rev. Lett.*, vol. 54, pp. 693–696, 1985.
- [33] J. B. Rosenzweig, D. B. Cline, B. Cole, H. Figueroa, W. Gai, R. Konecny, J. Norem, P. Shoessow, and J. Simpson, “Experimental observation of plasma wake-field acceleration”, *Phys. Rev. Lett.*, vol. 61, pp. 98–101, 1988.
- [34] N. Barov, J. B. Rosenzweig, M. E. Conde, W. Gai, and J. G. Power, “Observation of plasma wakefield acceleration in the underdense regime”, *Phys. Rev. S. T. Accel. Beams*, vol. 3, 011301, 2000.
- [35] M. Hogan, R. Assmann, F. J. Decker, R. Iverson, P. Raimondi, S. Rokni, R. H. Siemann, D. Walz, D. Whittum, B. Blue, C. E. Clayton, E. Dodd, R. Hemker, C. Joshi, K. A. Marsh, W. B. Mori, S. Wang, T. Katsouleas, S. Lee, P. Muggli, P. Catravas, S. Chattopadhyay, E. Esarey, and W. P. Leemans, “E-157: A 1.4-m-long plasma wakefield acceleration experiment using a 30 GeV electron beam from the Stanford Linear Accelerator Center linac”, *Phys. Plasmas*, vol. 7, pp. 2241–2248, 2000.

- [36] P. Muggli, B. E. Blue, C. E. Clayton, S. Deng, F. J. Decker, M. J. Hogan, C. Huang, R. Iverson, C. Joshi, T. C. Katsouleas, S. Lee, W. Lu, K. A. Marsh, W. B. Mori, C. L. O'Connell, P. Raimondi, R. Siemann, and D. Walz, "Meter-scale plasma-wakefield accelerator driven by a matched electron beam", *Phys. Rev. Lett.*, vol. 93, 014802, 2004.
- [37] B. E. Blue, C. E. Clayton, C. L. O'Connel, F. J. Decker, M. J. Hogan, C. Huang, R. Iverson, C. Joshi, T. C. Katsouleas, W. Lu, K. A. Marsh, W. B. Mori, P. Muggli, R. Siemann, and D. Walz, "Plasma-wakefield acceleration of an intense positron beam", *Phys. Rev. Lett.*, vol. 90, 214801, 2003.
- [38] B. E. Blue, "Plasma wakefield acceleration of an intense positron beam", University of California, Los Angeles, Los Angeles, CA, USA, 2003.
- [39] C. E. Clayton, B. E. Blue, E. S. Dodd, C. Joshi, K. A. Marsh, W. B. Mori, S. Wang, P. Catravas, S. Chattopadhyay, E. Esarey, W. P. Leemans, R. Assmann, F. J. Decker, M. J. Hogan, R. Iverson, P. Raimondi, R. H. Siemann, D. Walz, T. Katsouleas, S. Lee, and P. Muggli, "Transverse envelope dynamics of a 28.5-GeV electron beam in a long plasma", *Phys. Rev. Lett.*, vol. 88, 154801, 2002.
- [40] I. Blumenfeld, C. E. Clayton, F. J. Decker, M. J. Hogan, C. Huang, R. Ischebeck, R. Iverson, C. Joshi, T. Katsouleas, N. Kirby, W. Lu, K. A. Marsh, W. B. Mori, P. Muggli, E. Oz, R. H. Siemann, D. Walz, and M. Zhou, "Energy doubling of 42 GeV electrons in metre-scale plasma wakefield accelerator", *Nature*, vol. 445, pp. 741–744, 2010.
- [41] M. Hogan, T. O. Raubenheimer, A. Seryi, T. Katsouleas, C. Huang, W. Lu, W. An, K. A. Marsh, W. B. Mori, C. C. E., and C. Joshi, "Plasma wakefield acceleration experiments at FACET", *New J. Phys.*, vol. 12, 055030, 2010.
- [42] M. Litos, E. Adli, W. An, C. I. Clarke, C. E. Clayton, S. Corde, J. P. Delahaye, R. J. England, A. S. Fisher, J. Frederico, S. Gessner, S. Z. Green, M. J. Hogan, C. Joshi, W. Lu, K. A. Marsh, W. B. Mori, P. Muggli, N. Vafaei-Najafabadi, D. Walz, G. White, Z. Wu, V. Yakimenko, and G. Yocky, "High-efficiency acceleration of an electron beam in a plasma wakefield accelerator", *Nature*, vol. 515, pp. 92–95, 2014.

- [43] S. Corde, E. Adli, J. M. Allen, W. An, C. I. Clarke, C. E. Clayton, J. P. Delahaye, J. Frederico, S. Gessner, S. Z. Green, M. J. Hogan, C. Joshi, N. Lipkowitz, M. Litos, W. Lu, K. A. Marsh, W. B. Mori, M. Schmeltz, N. Vafaei-Najafabadi, D. Walz, V. Yakimenko, and G. Yocky, “Multi-gigaelectronvolt acceleration of positrons in a self-loaded plasma wakefield”, *Nature*, vol. 524, pp. 442–445, 2015.
- [44] A. Aschikhin, C. Behrens, S. Bohlen, J. Dale, N. Delbos, L. di Lucchio, E. Elsen, J. H. Erbe, M. Felber, B. Foster, L. Goldberg, J. Grebenyuk, J. N. Gruse, B. Hidding, Z. Hu, S. Karstensen, A. Knetsch, O. Kononenko, V. Libov, K. Ludwig, A. R. Maier, A. Martinez de la Ossa, T. Mehrling, C. A. J. Palmer, F. Pannek, L. Schaper, H. Schlarb, B. Schmidt, S. Schreiber, J. P. Schwinkendorf, H. Steel, M. Streeter, G. Tauscher, V. Wacker, S. Weichert, S. Wunderlich, J. Zemella, and J. Osterhoff, “The FLASHForward facility at DESY”, *Nucl. Instrum. Meth. Phys. Res. Sect. A*, vol. 806, pp. 175–183, 2015.
- [45] B. Hidding, G. Pretzler, J. B. Rosenzweig, T. Königstein, D. Schiller, and D. L. Bruhwiler, “Ultracold electron bunch generation via plasma photocathode emission and acceleration in a beam-driven plasma blowout”, *Phys. Rev. Lett.*, vol. 108, 035001, 2012.
- [46] B. Hidding, G. G. Manahan, T. Heinemann, P. Scherkl, F. Habib, D. Ullmann, A. Beaton, A. Sutherland, A. Knetsch, O. Karger, G. Wittig, B. O’Shea, V. Yakimenko, M. Hogan, S. Green, C. Clarke, S. Gessner, J. B. Rosenzweig, A. Deng, M. Litos, D. L Bruhwiler, J. Smith, J. R. Cary, R. Zgadzaj, M. C. Downer, C. Lindstrom, E. Adli, and G. Andonian, “First measurements of Trojan Horse injection in a plasma wakefield accelerator”, in *Proc. IPAC2017*, (Copenhagen, Denmark), 2017, pp. 1252–1257.
- [47] R. D’Arcy, A. Aschikhin, C. Behrens, S. Bohlen, J. Dale, L. Di Lucchio, M. Felber, B. Foster, L. Goldberg, J. N. Gruse, Z. Hu, G. Indorg, A. Knetsch, O. Kononenko, V. Libov, S. Karstensen, K. Ludwig, A. Martinez de la Ossa, F. Marutzky, T. Mehrling, P. Niknejadi, C. A. J. Palmer, P. Pourmoussavi, M. Quast, P. Winkler, J. H. Röckermann, B. Sheeran, M. J. V. Streeter, G. Tauscher, J. Thesinga, V. Wacker, S. Weichert, S. Wesch, S. Wunderlich, J. Zemalla, and J. Osterhoff, “FLASHForward - future-oriented wakefield accelerator research and development”, in *Proc. IPAC2017*, (Copenhagen, Denmark), 2017, pp. 1692–1695.

- [48] O. S. Brüning, P. Collier, P. Lebrun, S. Myers, R. Ostojic, J. Poole, and P. Proudlock, “LHC Design Report”, CERN, Geneva, Switzerland, Tech. Rep. CERN-2004-003-V-1, 2004.
- [49] A. Caldwell, K. Lotov, A. Pukhov, and F. Simon, “Proton-driven plasma wakefield acceleration”, *Nat. Phys.*, vol. 5, pp. 363–367, 2009.
- [50] A. Caldwell, K. Lotov, A. Pukhov, and G. Xia, “Plasma wakefield excitation with a 24 GeV proton beam”, *Plasma Phys. Control. Fusion*, vol. 53, 014003, 2011.
- [51] “AWAKE Design Report”, CERN, Geneva, Switzerland, Tech. Rep. SPSC-TDR-003, 2013.
- [52] J. Viera, Y. Fang, W. B. Mori, L. O. Silva, and P. Muggli, “Transverse self-modulation of ultra-relativistic lepton beams in the plasma wakefield accelerator”, *Phys. Plasmas*, vol. 19, 063105, 2012.
- [53] E. Adli, V. K. Berglyd Olson, C. A. Lindstrøm, P. Muggli, O. Reimann, J. M. Viera, L. D. Amorim, C. I. Clarke, S. J. Gessner, S. Z. Green, M. J. Hogan, M. D. Litos, B. D. O’Shea, V. Yakimenko, C. Clayton, K. A. Marsh, W. B. Mori, C. Joshi, N. Vafaei-Najafabadi, and O. Williams, “Progress of plasma wakefield self-modulation experiments at FACET”, *Nucl. Instrum. Meth. Phys. Res. Sect. A*, vol. 829, pp. 334–338, 2016.
- [54] O. Lishilin, M. Gross, R. Brinkmann, J. Engel, G. F., G. Koss, M. Krasilnikov, A. Martinez de la Ossa, T. Mehrling, J. Osterhoff, P. G., S. Phillip, Y. Renier, D. Richter, C. Schroeder, S. R., and F. Stephan, “First results of the plasma wakefield acceleration experiment at PITZ”, *Nucl. Instrum. Meth. Phys. Res. Sect. A*, vol. 829, pp. 37–42, 2016.
- [55] E. Öz and P. Muggli, “A novel Rb vapor plasma source for plasma wakefield accelerators”, *Nucl. Instrum. Methods Phys. Res. Sect. A*, vol. 740, pp. 197–202, 2014.
- [56] E. Öz, F. Batsch, and P. Muggli, “An accurate Rb density measurement for a plasma wakefield accelerator experiment using a novel Rb reservoir”, *Nucl. Instrum. Methods Phys. Res. Sect. A*, vol. 829, pp. 321–325, 2016.
- [57] E. Gschwendtner, “AWAKE, a particle-driven plasma wakefield acceleration experiment”, in *Proc. of the CERN Accelerator School: Plasma Wake Acceleration*, (CERN, Geneva, Switzerland), 2016, pp. 271–288.

- [58] S. Hills, *AWAKE: Making waves in accelerator technology*, CERN press release, 2016. [Online]. Available: [cds.cern.ch/record/2240017](https://cds.cern.ch/record/2240017).
- [59] E. Gschwendtner, “Starting up the AWAKE experiment at CERN”, in *Proc. IPAC2017*, (Copenhagen, Denmark), 2017, pp. 1261–1264.
- [60] R. Fitzpatrick, *Introduction to plasma physics*, Lecture notes, 1998.
- [61] C. K. Birdsall and A. B. Langdon, *Plasma physics via computer simulation*. New York, NY, USA: McGraw-Hill, 1985.
- [62] W. Lu, C. Huang, M. Zhou, W. Mori, and T. Katsouleas, “Non-linear theory for relativistic plasma wakefields in the blowout regime”, *Phys. Rev. Lett.*, vol. 96, p. 165 002, 2006.
- [63] W. Lu, “Nonlinear plasma wakefield theory and optimum scaling for laser wakefield accelerator (LWFA) in the blowout regime”, University of California, Los Angeles, CA, USA, 2006.
- [64] R. Bingham and R. Trines, “Introduction to plasma accelerators: the basics”, in *Proc. of the CERN Accelerator School: Plasma Wake Acceleration*, (CERN, Geneva, Switzerland), 2016, pp. 67–77.
- [65] V. Malka, “Review of laser wakefield accelerators”, in *Proc. IPAC2013*, (Shanghai, P. R. China), 2013, pp. 11–15.
- [66] T. Katsouleas, S. Wilks, P. Chen, J. M. Dawson, and J. J. Su, “Beam loading in plasma accelerators”, *Part. Accel.*, vol. 22, pp. 81–99, 1987.
- [67] W. Lu, C. Huang, W. B. Mori, and T. Katsouleas, “Limits of linear plasma wakefield theory for electron or positron beams”, *Phys. Plasmas*, vol. 12, p. 063 101, 2005.
- [68] A. D. Polyanin, *Handbook of linear partial differential equations for engineers and scientists*, First. Chapman & Hall/CRC, 2002.
- [69] W. K. H. Panofsky and W. A. Wenzel, “Some considerations concerning the transverse deflection of charged particles in radio-frequency fields”, *Rev. Sci. Instrum.*, vol. 27, p. 967, 1956.
- [70] S. Vaganian and H. Henke, “The Panofsky-Wenzel theorem and general relations for the wake potential”, *Part. Accel.*, vol. 48, pp. 239–242, 1994.

- [71] R. D. Ruth, A. W. Chao, P. L. Morton, and W. P. B., “A plasma wake field accelerator”, Stanford Linear Accelerator Center, Stanford, CA, USA, Tech. Rep. SLAC-PUB-3374, 1984.
- [72] A. Macchi, “An introduction to ultraintense laser-plasma interactions”, 2011.
- [73] R. W. Hockney and J. W. Eastwood, *Computer simulation using particles*. Bristol, UK and New York, NY, USA: Adam Hilger, 1988.
- [74] C. Nieter and J. R. Cary, “VORPAL: A versatile plasma simulation code”, *J. Comput. Phys.*, vol. 196, pp. 448–473, 2003.
- [75] K. Yee, “Numerical solution of initial boundary value problems involving Maxwell’s equations in isotropic media”, *IEEE Trans. Antennas and Propagation*, vol. 14, pp. 302–307, 1966.
- [76] R. Courant, K. Friedrichs, and H. Lewy, “On the partial differential equations of mathematical physics”, *IBM J. Res. Dev.*, vol. 11, pp. 215–234, 1967 [1928].
- [77] L. N Trefethen, *Finite difference and spectral methods for ordinary and partial differential equations*. 1996, Unpublished text. [Online]. Available: <http://people.maths.ox.ac.uk/trefethen/pdetext.html>.
- [78] A. Pukhov, “Particle-in-cell codes for plasma-based particle acceleration”, in *Proc. of the CERN Accelerator School: Plasma Wake Acceleration*, (CERN, Geneva, Switzerland), 2016.
- [79] *VSim*. Boulder, CO, USA: Tech-X Corporation, 2015.
- [80] *VSim Documentation*. Boulder, CO, USA: Tech-X Corporation, 2012-2017.
- [81] J. A. Clarke, D. Angal-Kalinin, N. Bliss, R. Buckley, R. Cash, P. Corlett, L. Cowie, G. Cox, G. P. Diakun, D. J. Dunning, B. D. Fell, A. Gallagher, P. Goudket, A. R. Goulden, D. M. P. Holland, S. P. Jamison, J. K. Jones, A. S. Kalinin, W. Liggins, L. Ma, K. B. Marinov, B. Martlew, P. A. McIntosh, J. W. McKenzie, K. J. Middleman, B. L. Militsyn, A. J. Moss, B. D. Muratori, M. D. Roper, R. Santer, Y. Saveliev, E. Snedded, R. J. Smith, S. L. Smith, M. Surman, T. Thakker, N. R. Thompson, R. Valizadeh, A. E. Wheelhouse, P. H. Williams, R. Bartolini, I. Martin, R. Barlow, A. Kolano, G. Burt, S. Chattopadhyay, D. Newton, A. Wolski, R. B. Appleby, H. L. Owen, M. Serluca, G. Xia, S.

- Boogert, A. Lyapin, L. Campbell, B. W. J. McNeil, and V. V. Paramonov, “CLARA conceptual design report”, *J. Inst.*, vol. 9, T05001, 2014.
- [82] G. Xia, D. Angal-Kalinin, J. Clarke, J. Smith, E. Cormier-Michel, J. Jones, P. H. Williams, J. W. Mckenzie, B. L. Militsyn, K. Hanahoe, O. Mete, A. Aimidula, and C. P. Welsch, “A plasma wakefield acceleration experiment using CLARA beam”, *Nucl. Instrum. Meth. Phys. Res. Sect. A*, vol. 740, pp. 165–172, 2014.
  - [83] M. V. Ammosov, N. B. Delone, and V. P. Krainov, “Tunnel ionization of complex atoms and of atomic ions in an alternating electromagnetic field”, *Sov. Phys. JETP*, vol. 64, pp. 1191–1194, 1986.
  - [84] J. E. Sansonetti, W. C. Martin, and S. L. Young, *Handbook of Basic Atomic Spectroscopic Data (version 1.1.3)*. Gaithersburg, MD, USA: National Institute of Standards and Technology, 2005.
  - [85] G. Mainfray and C. Manus, “Multiphoton ionization of atoms”, *Rep. Prog. Phys.*, vol. 54, pp. 1333–1372, 1991.
  - [86] L. F. Berzak, S. E. Dorfman, and S. P. Smith, Lawrence Berkeley National Laboratory, Berkeley, CA, USA, Tech. Rep.
  - [87] T. Pacey, O. Mete Apsimon, K. Hanahoe, and G. Xia, “A gas-filled capillary based plasma source for wakefield experiments”, in *Proc. IPAC2016*, (Busan, Korea), 2016, pp. 2613–2616.
  - [88] K. Floetmann, *ASTRA: A space charge tracking algorithm*, Version 3.2, DESY, Hamburg, Germany, 2017.
  - [89] B. Kyle, Private communication, 2016.
  - [90] K. L. F. Bane, P. B. Wilson, and T. Weiland, “Wake fields and wake field acceleration”, *AIP Conf. Proc.*, vol. 127, pp. 875–928, 1985.
  - [91] K. L. F. Bane, P. Chen, and P. B. Wilson, “On colinear wakefield acceleration”, *IEEE Trans. Nuc. Sci.*, vol. NS-32, pp. 3524–3526, 1985.
  - [92] R. J. England, J. B. Rosenzweig, and G. Travish, “Generation and measurement of relativistic electron bunches characterized by a linearly ramped current profile”, *Phys. Rev. Lett.*, vol. 100, 214802, 2008.

- [93] P. Piot, C. Behrens, C. Gerth, M. Dohlus, F. Lemery, D. Mihalcea, S. P., and M. Vogt, “Generation and characterization of electron bunches with ramped current profiles in a dual-frequency superconducting linear accelerator”, *Phys. Rev. Lett.*, vol. 108, 034801, 2012.
- [94] K. V. Lotov, “Efficient operating mode of the plasma wakefield accelerator”, *Phys. Plasmas*, vol. 12, 053105, 2005.
- [95] S. van der Meer, “Improving the power efficiency of the plasma wakefield accelerator”, European Organization for Nuclear Research, Geneva, Switzerland, Tech. Rep. CLIC Note No. 3 (CERN/PS/85-65), 1985.
- [96] B. Parker, M. Anerella, J. Escallier, M. Harrison, P. He, A. Jain, A. Marone, K. C. Wu, T. Markiewicz, T. Maruyama, Y. Nosochkov, and A. Seryi, “Compact superconducting final focus magnet options for the ILC”, *Proc. 2005 Part. Accel. Conf.*, p. 1568, 2005.
- [97] D. Brandt, H. Burkhardt, M. Lamont, S. Myers, and J. Wenninger, *Rep. Prog. Phys.*, vol. 63, pp. 939–1000, 2000.
- [98] V. Kumar, “Understanding the focusing of charged particle beams in a solenoid magnetic field”, *Am. J. Phys.*, vol. 77, p. 737, 2009.
- [99] M. Reiser, *Theory and design of charged particle beams*, Second, updated and expanded edition. Weinheim, Baden-Württemberg, Germany: Wiley-VCH, 2008.
- [100] C. Thaury, E. Guillaume, D. A., R. Lehe, A. Lifschitz, K. Ta Phuoc, J. Gautier, J.-P. Goddet, A. Tafzi, A. Flacco, F. Tissandier, S. Sebban, R. A., and V. Malka, “Demonstration of relativistic electron beam focusing by a laser-plasma lens”, *Nat. Comm.*, vol. 6, p. 6860, 2015.
- [101] E. Boggasch, A. Tauschwitz, H. Wahl, K. G. Dietrich, D. H. H. Hoffmann, W. Laux, M. Stetter, and R. Tkotz, “Plasma lens fine focusing of heavy-ion beams”, *Appl. Phys. Lett.*, vol. 60, pp. 2475–2477, 1991.
- [102] E. Boggasch, J. Jacoby, H. Wahl, K. G. Dietrich, D. H. H. Hoffmann, W. Laux, M. Elfers, C. R. Haas, V. P. Dubenkov, and A. A. Golubev, “Z-pinch plasma lens focusing of heavy-ion beams”, *Phys. Rev. Lett.*, vol. 66, pp. 1705–1708, 1992.
- [103] P. Chen, K. Oide, A. M. Sessler, and S. S. Yu, “Plasma-based adiabatic focuser”, *Phys. Rev. Lett.*, vol. 64, pp. 1231–1234, 1990.

- [104] A. Weidemann, P. Chen, and C. K. Ng, “Plasma lens backgrounds at a future linear collider”, Stanford Linear Accelerator Center, Stanford, CA, USA, Tech. Rep. SLAC-PUB-9207, 2002.
- [105] A. Ogata, “Plasma lens and wake experiments in Japan”, *AIP Conf. Proc.*, vol. 279, p. 420, 1993.
- [106] H. Nakanishi, Y. Yoshida, T. Ueda, T. Kozawa, H. Shibata, K. Nakajima, T. Kurihara, N. Yagami, Y. Nishida, T. Kobayashi, A. Enomoto, O. T., H. Kobayashi, B. S. Newberger, S. Tagawa, K. Miya, and A. Ogata, “Direct observation of plasma-lens effect”, *Phys. Rev. Lett.*, vol. 66, pp. 1870–1873, 1991.
- [107] J. B. Rosenzweig, P. Schoessow, B. Cole, C. Ho, W. Gai, R. Konecny, S. Mttingwa, J. Norem, M. Rosing, and J. Simpson, “Demonstration of electron beam self-focusing in plasma wake fields”, *Phys. Fluids B: Plasma Physics*, vol. 2, pp. 1376–1383, 1990.
- [108] J. G. Davis, “Plasma lenses for relativistic electron beams”, PhD thesis, University of California, Los Angeles, USA, 1996.
- [109] R. Govil, S. J. Wheeler, and W. P. Leemans, “Experimental observation of electron beam focusing through plasma lenses”, *Proc. IEEE Part. Accel. Conf.*, vol. 1, pp. 654–656, 1998.
- [110] M. C. Thompson, H. Badakov, J. B. Rosenzweig, G. Travish, N. Barov, P. Piot, R. Fliller, G. M. Kazakevich, J. Santucci, J. Li, and R. Tikhoplav, “Observations of low-aberration plasma lens focusing of relativistic electron beams at the underdense threshold”, *Phys. Plasmas*, vol. 17, 073105, 2010.
- [111] S. Kuschel, D. Hollatz, T. Heinemann, O. Karger, M. B. Schwab, D. Ullmann, A. Knetsch, A. Seidel, C. Rödel, M. Yeung, M. Leier, A. Blinne, H. Ding, T. Kurz, D. J. Corvan, A. Sävert, S. Karsch, M. C. Kaluza, B. Hidding, and M. Zepf, “Demonstration of passive plasma lensing of a laser wakefield accelerated electron bunch”, *Phys. Rev. S.T. Accel. Beams*, vol. 19, 071301, 2016.
- [112] *Mathematica version 10.0*. Champagne, IL, USA: Wolfram Research inc., 2014.
- [113] K. Hanahoe, O. Mete, G. Xia, D. Angal-Kalinin, J. Jones, and J. Smith, “Simulation studies of plasma lens experiments at Daresbury Laboratory”, *Plas. Phys. Control. Fusion*, vol. 58, 034002, 2016.

- [114] J. Rosenzweig and P. Chen, “Beam optics of a self-focusing plasma lens”, *Phys. Rev. D*, vol. 39, p. 2039, 1989.
- [115] B. Sherrill, J. Bailey, E. Kashy, and C. Leakeas, “Use of multipole magnetic fields for making uniform irradiations”, *Nucl. Instrum. Meth. Phys. Res. Sect. B*, vol. B40/41, pp. 1004–1007, 1989.
- [116] E. Urakabe, Y. Fujita, K. Hiramoto, M. Inoue, Y. Iwashita, M. Kanazawa, A. Morita, M. Nishi, T. Norimine, A. Noda, K. Noda, H. Ogawa, T. Shirai, M. Torikoshi, M. Umezawa, and S. Yamada, “Beam-profile control using an octupole magnet”, *Jpn. J. Appl. Phys.*, vol. 38, pp. 6145–6149, 1999.
- [117] J. Jones, “Multi-user station experimental station beam dynamics examples”, Private communication, 2014.
- [118] E. Jones, T. Oliphant, P. Peterson, *et al.*, *SciPy: Open source scientific tools for Python*, 2001–. [Online]. Available: <http://www.scipy.org/>.
- [119] E. Carlier, U. Jansson, R. Jung, V. Mertens, S. Péraire, M. Ross, G. Schröder, G. R. Stevenson, E. B. Vossenberg, E. Weisse, and J. M. Zazula, “The LEP beam dumping system”, in *Proc. 4th European Part. Accel. Conf.*, (London, United Kingdom), 1994, p. 2494.
- [120] P. Satyamurthy, P. Rai, V. Tiwari, K. Kulkarni, J. Amann, R. G. Arnold, D. Walz, A. Seryi, T. Davenne, O. Caretta, C. Densham, and R. Appleby, “Design of an 18 MW vortex flow water beam dump for 500 GeV electrons/positrons of an international linear collider”, *Nucl. Instrum. Meth. Phys. Res. Sect. A*, vol. 679, pp. 67–81, 2012.
- [121] D. R. Walz, J. Jurow, and E. L. Garwin, “Water cooled beam dumps and collimators for the Stanford Linear Accelerator”, *IEEE Trans. Nuc. Sci*, vol. 12, pp. 867–871, 1965.
- [122] K. Nordlund, A. Sand, F. Granberg, S. J. Zinkle, R. Stoller, R. S. Averback, T. Suzudo, L. Malerba, F. Banhart, W. J. Weber, F. Willaime, S. Dudarev, and D. Simeone, “Primary radiation damage in materials”, OECD-NEA, Paris, France, Tech. Rep. NEA/NSC/DOC(2015)9, 2015.

- [123] D Schumann, J. Neuhausen, J. Eikenberg, M. Rüthi, M. Wohlmuther, P. W. Kubik, H. A. Synal, V. Alfimov, G. Korschinek, G. Rugel, and T. Faestermann, “Radiochemical analysis of a copper beam dump irradiated with high-energetic protons”, *Radiochim. Acta*, vol. 97, pp. 123–131, 2009.
- [124] A. Leuschner and K. Tesch, “The residual radioactivity of a water-copper beam dump for the TESLA test facility”, Deutsches Elektronen-Synchrotron, Hamburg, Germany, Tech. Rep. DESY D3-92, 1998.
- [125] A. Leuschner, *Another crazy idea of an LC dump compared to the water dump design*, LC-ABD dump meetings, Sep. 2005.
- [126] R. Appleby, J. R. J. Bennet, T. Broome, C. Densham, and H. Vincke, “The charged beam dumps for the International Linear Collider”, in *Proc. 10th European Part. Accel. Conf.*, (Edinburgh, United Kingdom), 2006, pp. 736–737.
- [127] H. C. Wu, T. Tajima, D. Habs, A. W. Chao, and J. Meyer-ter-Vehn, “Collective deceleration: Toward a compact beam dump”, *Phys. Rev. ST Accel. Beams*, vol. 13, 101303, 2010.
- [128] A. Bonatto, C. B. Schroeder, J. L. Vay, C. G. R. Geddes, C. Benedetti, E. Esarey, and W. P. Leemans, “Passive and active plasma deceleration for the compact disposal of electron beams”, *Phys. Plasmas*, vol. 22, 083106, 2015.
- [129] Particle Data Group, “Experimental methods and colliders”, *Phys. Lett. B*, vol. 667, pp. 261–315, 2008, ISSN: 0370-2693.
- [130] M. Hogan, T. O. Raubenheimer, A. Seryi, T. Katsouleas, C. Huang, W. Lu, W. An, K. A. Marsh, W. B. Mori, C. C. E., and C. Joshi, “Plasma wakefield acceleration experiments at FACET”, *New J. Phys.*, vol. 12, 055030, 2010.
- [131] I. Blumenfeld, C. E. Clayton, F. J. Decker, M. J. Hogan, C. Huang, R. Ischebeck, R. Iverson, C. Joshi, T. Katsouleas, N. Kirby, W. Lu, K. A. Marsh, W. B. Mori, P. Muggli, E. Oz, R. H. Siemann, D. Walz, and M. Zhou, “Energy doubling of 42 GeV electrons in metre-scale plasma wakefield accelerator”, *Nature*, vol. 445, pp. 741–744, 2010.
- [132] M. Litos, E. Adli, W. An, C. I. Clarke, C. E. Clayton, S. Corde, J. P. Delahaye, R. J. England, A. S. Fisher, J. Frederico, S. Gessner, S. Z. Green, M. J. Hogan, C. Joshi, W. Lu, K. A. Marsh, W. B. Mori, P. Muggli, N. Vafaei-Najafabadi, D. Walz, G. White, Z. Wu, V. Yakimenko, and G. Yocky, “High-efficiency acceleration

- of an electron beam in a plasma wakefield accelerator”, *Nature*, vol. 515, pp. 92–95, 2014.
- [133] S Corde, E. Adli, J. M. Allen, W. An, C. I. Clarke, C. E. Clayton, J. P. Delahaye, J. Frederico, S. Gessner, S. Z. Green, M. J. Hogan, C. Joshi, N. Lipkowitz, M. Litos, W. Lu, K. A. Marsh, W. B. Mori, M. Schmeltz, N. Vafaei-Najafabadi, D. Walz, V. Yakimenko, and G. Yocky, “Multi-gigaelectronvolt acceleration of positrons in a self-loaded plasma wakefield”, *Nature*, vol. 524, pp. 442–445, 2015.
  - [134] W. P. Swanson, “Radiological safety aspects of the operation of electron linear accelerators”, International Atomic Energy Agency, Vienna, Austria, Tech. Rep. 188, 1979.
  - [135] K. Schmid, A. Buck, C. M. S. Sears, J. M. Mikhailova, R. Tautz, D. Hermann, M. Geissler, F. Krausz, and L. Veisz, “Density-transition based electron injector for laser driven wakefield accelerators”, *Phys. Rev. S.T. Accel. Beams*, vol. 13, 091301, 2010.
  - [136] K. Hanahoe, G. Xia, M. Islam, Y. Li, O. Mete-Apsimon, B. Hidding, and J. Smith, “Simulation study of a passive plasma beam dump using varying plasma density”, *Phys. Plasmas*, vol. 24, 023120, 2017.
  - [137] J. Grebenyuk, A. Martinez de la Ossa, T. Mehrling, and J. Osterhoff, “Beam-driven plasma-based acceleration of electrons with density down-ramp injection at FLASHForward”, *Nucl. Instrum. Meth. Phys. Res. Sect. A*, vol. 740, pp. 246–249, 2014.
  - [138] M. Hansson, B. Aurand, X. Davoine, H. Ekerfelt, K. Svensson, A. Persson, C. G. Wahlström, and O. Lundh, “Down-ramp injection and independently controlled acceleration of electrons in a tailored laser wakefield accelerator”, *Phys. Rev. S.T. Accel. Beams*, vol. 18, 071303, 2015.